NOTICE

The quality of this microfiche is heavily dependent upon the quality of the original thesis submitted for microfilming. Every effort has been made to ensure the highest quality of reproduction possible.

If pages are missing, contact the university which granted the degree.

Some pages may have indistinct print especially if the original pages were typed with a poor typewriter ribbon or if the university sent us a poor photocopy.

Previously copyrighted materials (journal articles, published tests, etc.) are not filmed.

Reproduction in full or in part of this film is governed by the Canadian Copyright Act, R.S.C. 1970, c. C-30. Please read the authorization forms which accompany this thesis.

THIS DISSERTATION
HAS BEEN MICROFILMED
EXACTLY AS RECEIVED

AVIS

La qualité de cette microfiche dépend grandement de la qualité de la thèse soumise au microfilmage. Nous avons tout fait pour assurer une qualité supérieure de reproduction.

S'il manque des pages, veuillez communiquer avec l'université qui a conféré le grade.

La qualité d'impression de certaines pages peut laisser à désirer, surtout si les pages originales ont été dactylographiées à l'aide d'un ruban usé ou si l'université nous a fait parvenir une photocopie de mauvaise qualité.

Les documents qui font déjà l'objet d'un droit d'auteur (articles de revue, examens publiés, etc.) ne sont pas microfilmés.

La reproduction, même partielle, de ce microfilm est soumise à la Loi canadienne sur le droit d'auteur, SRC 1970, c. C-30. Veuillez prendre connaissance des formules d'autorisation qui accompagnent cette thèse.

LA THÈSE A ÉTÉ
MICROFILMÉE TELLE QUE
NOUS L'AVONS REÇUE

MECHANICAL PROPERTIES OF FRESH CONCRETE

by

Angelos Alexandridis

Submitted in partial fulfillment of the
requirement for the degree of
Master of Applied Science

Department of Civil Engineering
University of Ottawa
Ottawa, Canada

April 1979

ABSTRACT

This study deals with the mechanical properties of fresh concrete in the nonflow condition as they pertain to its shear strength behaviour.

The shear strength characteristics of fresh concrete have been studied through the use of a triaxial compression apparatus. Tests were performed on fresh concrete cylinders 4 inches in diameter and 8 inches high at 70^0F (21^0C) and 38^0F (4^0C) for set times ranging from 40 minutes to 160 minutes. The test results were subsequently analyzed by the shear strength theories of Mohr Coulomb and Rowe and expressed as two strength parameters corresponding to the internal friction and the cohesion components of shear strength for each set time - temperature combination. The angle of internal friction was found to be a constant property of the mix and lay in the range of 37^0 to 41^0 for a 10% failure strain and 34^0 to 39^0 for a 20% failure strain when analyzed by the Mohr Coulomb theory. Rowe's analysis gave friction angles of 18^0 to 21^0 for a 10% failure strain and 19^0 to 23^0 for a 20% failure strain. Both theories indicated that the cohesion of fresh concrete is initially zero and increases with set time causing the fresh concrete to stiffen with time.

In addition to shear testing, the coefficient of lateral pressure at rest (K_0) was evaluated by loading cylindrical concrete specimens restrained against lateral expansion by a plexiglass cylinder. The specimens were allowed to drain freely from the top. Tests were carried out at temperatures of 70^0F (21^0C) and 38^0F (4^0C) for set times of 40 Minutes to 160 minutes. K_0 was found to be variable and highly dependent on set time. Initially K_0 approached unity. With set time K_0 decreased significantly, this decrease being of a smaller order at the colder temperature because of the hydration process being retarded.

ACKNOWLEDGEMENTS

The author wishes to express his sincere appreciation to the following individuals:

To proffesor N. J. Gardner for his continuous encouragement and helpful advice as supervisor of this thesis.

To Mr. Dick Moore and Mr. William Watson for their helpful assistance in setting up the testing apparatus.

To Mr. Undriadi Benggawan and Mr. Amjid Quereshi for their friendship throughout his graduate studies.

To his parents for their support and understanding.

TABLE OF CONTENTS

Chapter		Page
I.	INTRODUCTION	1
	1.1 Plain Concrete	1
	1.2 Development of Lateral Pressure in Formwork	3
	1.3 Lateral Pressure Exerted by Particulate Systems	8
	1.4 Workability of Fresh Concrete	18
	1.5 Scope of the Investigation	19
II.	THEORY	21
	2.1 Stress in a Particulate System	21
	2.2 Resolution of Principle Stresses	22
	2.3 Stress Points	22
	2.4 Shear Strength	23
	2.5 Measurement of Shear Strength	24
	2.6 Shear Strength Theories	27
III.	LITERATURE REVIEW	36
IV.	EXPERIMENTAL PROCEDURE AND TEST RESULTS	42
	4.1 Choice of Testing Procedure	42
	4.2 Concrete Mix Characteristics	44
	4.3 Testing Procedures	44
	4.4 Experimental Results	54
V.	ANALYSIS OF EXPERIMENTAL DATA	79
	5.1 Choice of Shear Strength Theories	79
	5.2 Choice of Failure Criteria	80
	5.3 Mohr Coulomb Analysis	81
	5.4 Rowe's Analysis	82
VI.	DISCUSSION	96
	6.1 Discussion of Test Results	96
	6.2 Application of Test Results to Formwork Pressures	100

Chapter Page

VII. CONCLUSIONS AND RECOMMENDATIONS 104

7.1 Conclusions 104

7.2 Recommendations 105

REFERENCES 106

ADDITIONAL REFERENCES 107

TRIAXIAL COMPRESSION DATA 108

UNCONFINED COMPRESSION DATA 149

LIST OF FIGURES

Figure		Page
1.1	Stages in the Development of Lateral Pressure in Formwork	5
1.2	Conditions of Lateral Pressure in a Dry Cohesionless Deposit	9
1.3	Coulomb's Theory for Active Lateral Pressure in a Cohesionless Deposit	13
2.1	Shear Testing of Particulate Masses	25
2.2	The Shearing of a Non Cohesive Continuum	29
2.3	The Stressing of a System by Two Normal Forces	31
2.4	The Body Centred Cubic Packing	32
3.1	L'Hermite's Load Deformation Curve	36
4.1	Grain Size Distribution	45
4.2	Triaxial Compression Set Up	46
4.3	(a) Vacuum Being Aplied to the Membrane	48
	(b) A Test Sample During its Setting Period	48
4.4	(a) Entire Triaxial Assembly Prior to Testing	50
	(b) Samples After Having Been Tested	50
4.5	Typical Triaxial Test Data Sheet	51
4.6	Unconfined Compression Test Samples During its Setting Period and Prior to Testing	53
4.7	Typical K_0 Test Data Sheet	55
4.8	K_0 Apparatus Prior to and During the Testing Procedure	56
4.10 A	Stress Difference Versus Axial Strain for $70^{\circ}F$ and 160 Min. Set	59
4.10 B	Pore Pressure Versus Axial Strain for $70^{0}F$ and 160 Min. Set	60
4.11 A	Stress Difference Versus Axial Strain for $70^{0}F$ and 120 Min. Set	61
4.11 B	Pore Pressure Versus Axial Strain for $70^{0}F$ and 120 Min. Set	62

Figure		Page
4.12 A	Stress Difference Versus Axial Strain for 70°F and 80 Min. Set	63
4.12 B	Pore Pressure Versus Axial Strain for 70°F and 80 Min. Set	64
4.13 A	Stress Difference Versus Axial Strain for 70°F and 40 Min. Set	65
4.13 B	Pore Pressure Versus Axial Strain for 70°F and 40 Min. Set	66
4.14 A	Stress Difference Versus Axial Strain for 38°F and 160 Min. Set	67
4.14 B	Pore Pressure Versus Axial Strain for 38°F and 160 Min. Set	68
4.15 A	Stress Difference Versus Axial Strain for 38°F and 120 Min. Set	69
4.15 B	Pore Pressure Versus Axial Strain for 38°F and 120 Min. Set	70
4.16 A	Stress Difference Versus Axial Strain for 38°F and 80 Min. Set	71
4.16 B	Pore Pressure Versus Axial Strain for 38°F and 80 Min. Set	72
4.17 A	Stress Difference Versus Axial Strain for 38°F and 40 Min. Set	73
4.17 B	Pore Pressure Versus Axial Strain for 38°F and 40 Min. Set	74
4.18 A	Compressive Stress Versus Axial Strain at 70°F	75
4.18 B	Compressive Stress Versus Axial Strain at 38°F	76
4.19 A	K_0 Versus Effective Vertical Stress at 70°F	77
4.19 B	K_0 Versus Effective Vertical Stress at 38°F	78
5.1	p' - q' Plot for 70°F and 10% Failure Strain	84
5.2	p' - q' Plot for 38°F and 10% Failure Strain	85
5.3	p' - q' Plot for 70°F and 20% Failure Strain	86

Figure		Page
5.4	p' - q' Plot for 38^0F and 20% Failure Strain . . .	87
5.5	Cohesion Versus Set Time From Coulomb's Analysis . .	88
5.7	σ_1'/ν' Versus σ_3' for 70^0F and 10% Failure Strain . .	90
5.8	σ_1'/ν' Versus σ_3' for 38^0F and 10% Failure Strain . .	91
5.9	σ_1'/ν' Versus σ_3' for 70^0F and 20% Failure Strain . .	92
5.10	σ_1'/ν' Versus σ_3' for 38^0F and 20% Failure Strain . .	93
5.11	Cohesion Versus Set Time From Rowe's Analysis . . .	94

LIST OF TABLES

Table		Page
3.2	L'Hermite's Test Results	37
3.3	Ritchie's Test Results	39
3.4	Olsen's Test Results	40
4.9	Summary of Tests Performed	57
5.6	Results of Mohr Coulomb Analysis	89
5.12	Results of Rowe's Analysis	95

List of Abbreviations and Symbols

A'	q' intercept in a p' - q' plane.
C	cohesion from a Mohr Coulomb analysis.
C_u	cohesion from Rowe's analysis.
C', C_u'	cohesion with respect to effective stresses.
F	Fahrenheit.
H	height of concrete pour.
in	inch.
K_A	coefficient of active lateral pressure.
K_0	coefficient of lateral pressure at rest.
K_p	coefficient of passive lateral pressure.
Kg	kilogram force.
Kgf/cm^2	kilogram force per square centimetre.
KN/M^2	kilonewtons per square metre.
LB/IN^2	pounds per square inch.
Min	minute.
ml	millilitre.
P_V	vertical pressure at a point.
P_H	horizontal pressure at a point.
P_{HA}	active horizontal pressure.
P_{HP}	passive horizontal pressure.
qu	drained unconfined compressive strength.
S	second.
tan ϕ	coefficient of friction.
tan' ϕ	coefficient of friction with respect to post peak strength.
u	pore pressure.
Z	depth to a given point.
α'	slope of a line in a p' - q' plane.
γ	weight density of fresh concrete.
θ	inclination of a plane to the principle stress plane.
ν'	instantaneous Poisson's ratio.
σ^*	standard deviation.

σ_1	major principle stress.
σ_3	minor principle stress.
σ'_1, σ'_3	effective principle stresses.
σ_n	normal stress on a shear plane.
σ_θ	normal stress on a plane inclined at angle θ to the major principle stress plane.
τ	shear strength.
τ_θ	shear stress on a plane inclined at angle θ to the major principle stress plane.
φ	angle of internal friction from Mohr Coulomb analysis.
φ_μ	angle of internal friction from Rowe's analysis.
φ', φ'_μ	effective angles of internal friction.
$+\infty$	positive infinity.

CHAPTER I

INTRODUCTION

1.1 Plain Concrete

Concrete is the name given to a prepared mixture of cement, fine aggregate, coarse aggregate and water. Cement has the property that in the presence of water it bonds to the inert aggregate in the concrete and grows crystals which interlock, converting the particulate aggregates into a particulate solid. These ingredients are mixed in predetermined proportions so that certain desired physical properties such as compressive strength, workability, durability and permeability are achieved. In studying the behaviour of plain concrete it is useful to distinguish between two conditions or state; that, when water is freshly added to the solids and the cured or hardened state of concrete.

When fresh concrete is first mixed, it possesses in addition to viscosity significant shear strength so that when it is poured from its mixing-container into a form it does not fully take the shape of the form unless it is tamped or vibrated. However, when removed from its container, fresh concrete is unable to maintain any shape of its own and will slump. The properties of fresh concrete therefore, lie between those of a liquid and those of a solid substance. For this reason, concrete is initially referred to as being a plastic material.

Fresh concrete may be visualized as particles of inert aggregate which are held or suspended in a deformable matrix of cement paste and air bubbles. The paste matrix itself is composed of water and grains of cement.

Given enough time and the proper environmental conditions, the cement paste matrix is converted by means of a physicochemical process between the cement grains and the water into a rocklike mass of particles. This process is called hydration. The hardened particulate material which replaces the original cement grains is called cement gel and it occupies the space in the mixture originally occupied by the cement grains and the water. Consequently, with the passage of time concrete loses its plasticity and becomes a solid.

To date, a significant amount of research has been carried out dealing with the physical properties of plain concrete. However, this research has been predominantly aimed at understanding the mechanical properties of concrete in the hardened state. Although of immense value to the architect and the design engineer, the results of such research are of little importance to the constructor who must deal with concrete in its fresh state.

Problems pertaining to the pumpability, workability, placing of fresh concrete and the lateral pressures developed in formwork are examples in which little is understood of how fresh concrete behaves. Engineers who need to undertake calculations for the solution of such problems must resort to empirical formulae, charts and tables. Such a procedure however, may lead to gross inaccuracies when applied to concretes whose mix proportions and conditions at mixing differ significantly from those corresponding to the concrete for which the procedure was derived. Consequently, a more fundamental understanding of the mechanical behaviour of fresh concrete is necessary.

To undertake a study of the physical behaviour of fresh concrete, it is first necessary to isolate the factors which may influence it.

It is then desirable to express the physical behaviour in terms of certain parameters having physical units and which can be measured by some test device when the influencing factors are kept constant under laboratory conditions.

To determine what factors influence the mechanical behaviour of fresh concrete and what parameters may be used to describe this behaviour, it is useful to look at the development of lateral pressures in formwork and the workability of fresh concrete.

1.2 Development of Lateral Pressure in Formwork

The formwork for concrete structures represents a very important part of concrete construction, both in terms of the service it provides and its cost. Formwork frequently costs more than the concrete and in some cases more than the concrete and the reinforcing steel combined. In order that formwork be safe as well as economical, it is important that estimation of the lateral pressures exerted by fresh concrete on the forms be made as accurately as possible.

If fresh concrete poured into a form behaved like a fluid possessing no shear strength, then the pressure distribution observed would be hydrostatic and the lateral pressure would increase linearly with depth reaching a maximum value at the bottom of the form equal to γH where

γ = density of the mix

H = height of the pour.

However, fresh concrete in formwork does not behave as a liquid but in many ways similar to soil behind a retaining wall.

Fresh concrete like soil is a particulate system composed of

particles weakly bonded together and submerged in a liquid medium. It possesses shear strength as a result of the:

(1) Frictional resistance and interlocking between the aggregate and the cement particles and

(2) The bonding together of the aggregate particles by the cement during hydration.

The former component of shear strength is termed internal friction and requires strain to be mobilized. The latter component is termed cohesion. True cohesion results from cement hydration and therefore depends on the time since addition of water to the mix and the temperature at which the mix is allowed to hydrate.

During a pour, the lateral pressure exerted on the vertical faces of the formwork for a given head of concrete is a function of the shrinkage and the shear strength properties of the mix, and the lateral strains resulting from yielding of the form boards. The changes in lateral pressure with respect to a hydrostatic pressure distribution may be depicted in stages (see figure 1.1), each stage representing an increase in concrete head:

stage (1); At a small head of concrete, the lateral pressure distribution is hydrostatic; the fresh concrete possessing negligible shear strength in terms of internal friction or cohesion.

stage (2); As the head of concrete increases, both the vertical and lateral pressures increase causing the form walls to yield laterally. This deformation partially mobilizes the internal friction of the mix. Cohesion also develops with time as the cement paste

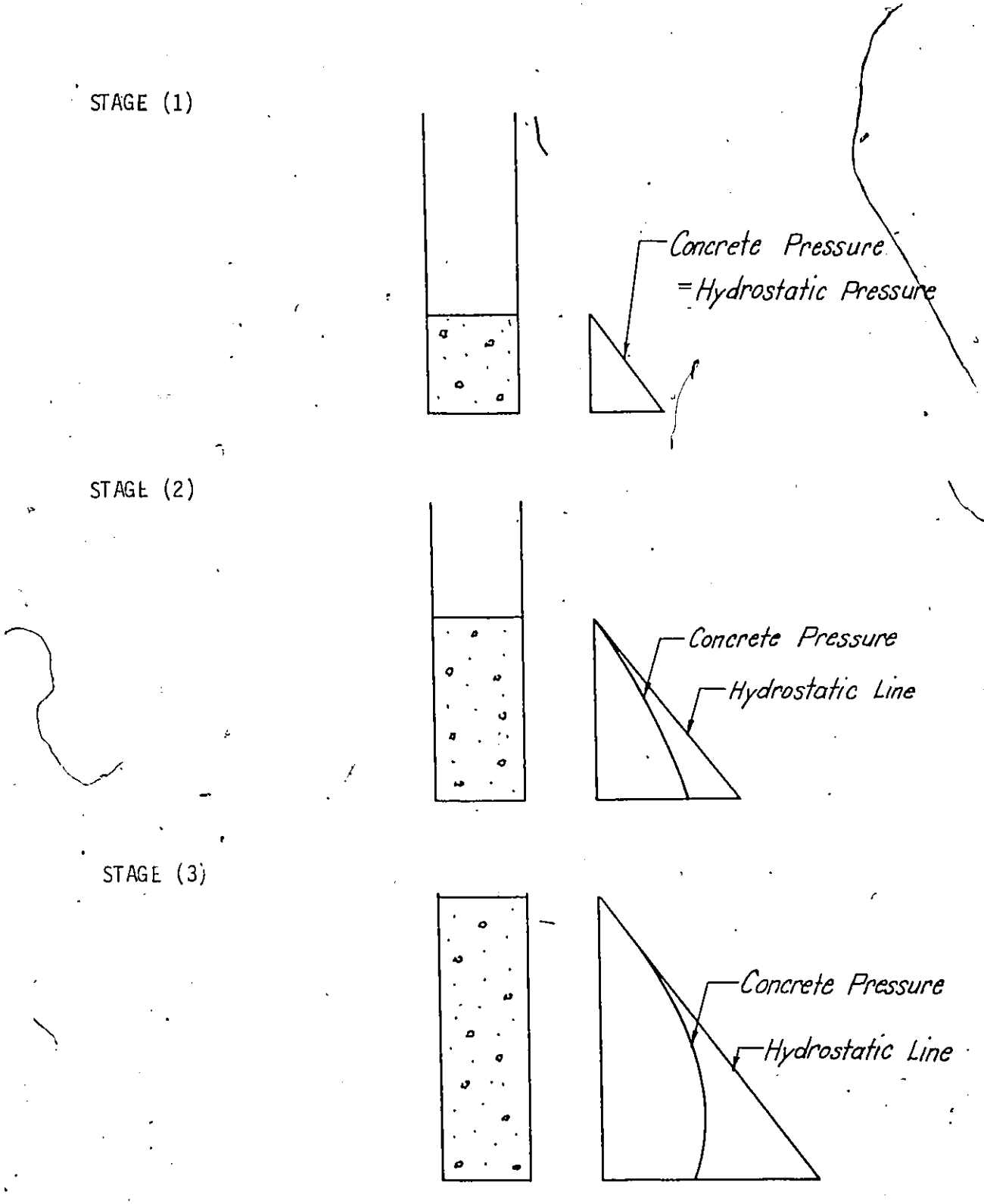

Fig. 1.1. Stages in the development of lateral pressure in formwork.

hydrates and begins to bond the aggregate into a solid mass. The concrete in the lower portion of the form therefore, possesses significant shear strength and resists lateral expansion. In addition to the development of shear strength, the fresh concrete shrinks and settles in the form as a result of the expulsion of water through form leakage, water being absorbed by the aggregate and water combining with the cement during hydration. This settlement creates shear stresses between the concrete and the form walls which support the overlying concrete. Therefore, there is a decreasing rate of increase in vertical load on the lower concrete with depth. The result of the development of shear strength and the settlement of the fresh concrete in the formwork is a pressure distribution which deviates from and is less than a hydrostatic distribution.

stage (3); As the concrete head continues to increase, the shear strength and the rigidity of the concrete in the lower portion of the form continues to increase and the rate of increase in lateral pressure with depth decreases until a point of maximum lateral pressure is reached. With greater depth the pressure will then decrease. This decrease in pressure results from the shrinkage of the fresh concrete in the form which creates shrinkage strains. The decrease in lateral pressure as a result of these shrinkage strains, exceeds the increase in pressure due to an increasing concrete head, the result being a decreasing lateral pressure.

In addition to lateral deformation, time and shrinkage, other factors influence the pressures developed in formwork. These factors have been discussed by many authors (Ref. 1, 7, 9). Rodin, summarized and discussed the factors most likely to affect lateral pressure. These are:

(1) Rate of filling the forms; the higher the rate of pour, the greater will be the maximum pressure and the depth at which it occurs.

(2) Method of placing the concrete; vibration, and ramming to a lesser degree, destroys any development of shear strength in the vicinity of the disturbance and results in pressures approaching the hydrostatic line.

(3) Proportions of the concrete mix; the richer the mix, the greater is the value of the maximum pressure because of the increased lubricating action of the cement paste.

(4) Consistency of the concrete; for a particular mix, the higher the water/cement ratio or slump, the smaller is the deviation of the lateral pressure from a hydrostatic distribution resulting from a reduction in the strength of the mortar and causing the concrete to behave more like a fluid.

(5) Temperature of the concrete; there is a significant rise in the maximum pressure with a decrease in temperature which is likely due to the lower rate of hardening of the cement.

(6) Size and shape of the form; the smaller the width of the form, the lower are the concrete pressures because of the relatively greater effect of shear stresses between the concrete and the form walls. Similarly, the presence of reinforcing steel tends

to reduce the lateral pressure.

1.3 Lateral Pressure Exerted by Particulate Systems

To more fully understand the mechanism for the development of lateral pressure by fresh concrete on formwork and the factors influencing the lateral pressure, it is advantageous to look at presently accepted theories for evaluating the lateral pressures exerted by particulate masses.

In the following discussion it is assumed that the shear strength of a particulate system may be represented by the Mohr Coulomb strength parameters C and $\emptyset$ (see chapter 2), corresponding to the cohesion and internal friction components of shear strength respectively. The equations which are presented correspond to a dry system.

For a saturated system where the water in the voids exerts no seepage pressure, the dry unit weight of the particles must be replaced with the submerged unit weight. The pressures developed by the particulate system and the water must then be determined separately and subsequently summed to give the resultant pressure.

Rankine's Theory. - For an arbitrarily chosen point A in a dry cohesionless deposit (see figure 1.2 (a)), the vertical pressure is given by $P_V = \gamma z$ where γ is the unit weight of the material and z is the depth to the point A. The horizontal pressure is directly proportional to the vertical pressure and is given by $P_H = K_o \gamma Z$. In soil mechanics, Ko is known as the coefficient of earth pressure at rest. It may be determined for cohesive as well as non cohesive particulate masses. In general, the value of Ko lies between 0 and 1.0. Terzaghi gives Ko = 0.4 for loose sands

(a) AT REST CONDITION

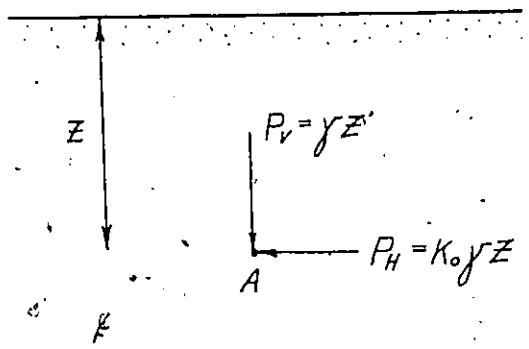

(b) ACTIVE CONDITION

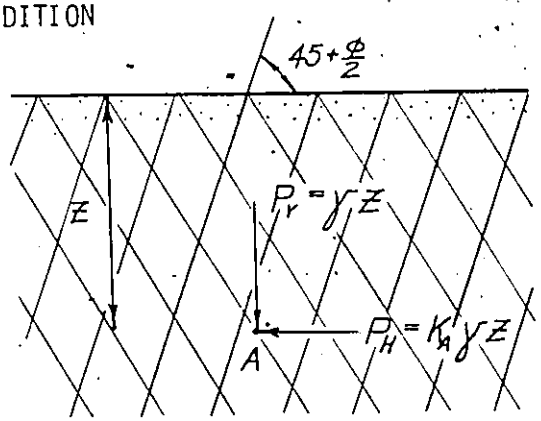

(c) PASSIVE CONDITION

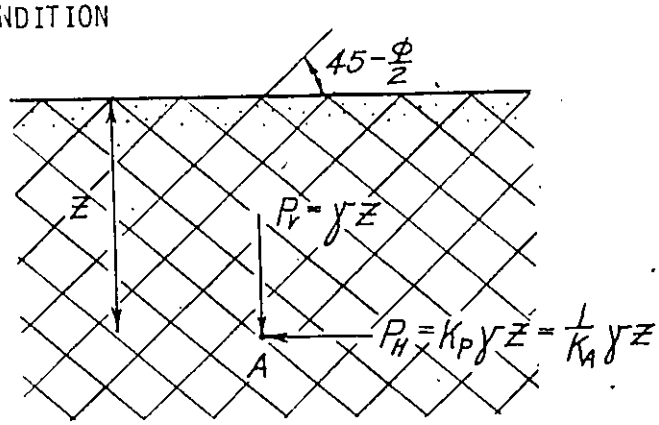

Fig. 1.2. Conditions of lateral pressure in a dry cohesionless deposit.

and Ko = 0.5 for dense sands.

If by some process such as the yielding of a retaining wall the deposit is stretched horizontally (figure 1.2 (b)), the horizontal pressure P_H decreases as the internal friction of the deposit is mobilized. The vertical pressure Pv however, remains equal to γz. As the stretching is continued, failure takes place within the deposit along two sets of planes inclined at $(45 + \frac{\phi}{2})$ to the horizontal. Once failure has occurred, the horizontal pressure does not experience any further decreases with stretching. This state of minimum lateral pressure is known as the Active Rankine State. The active lateral pressure is given by $P_{H_A} = \tan^2 (45 - \frac{\phi}{2})\gamma z = K_A \gamma z$. The value K_A is known as the coefficient of active earth pressure and its value generally lies between 0 and Ko.

If the deposit is compressed instead of being stretched horizontally (figure 1.2 (c)), failure will eventually occur along two sets of planes inclined at $(45 - \frac{\phi}{2})$ to the horizontal. The horizontal pressure increases to a maximum value when failure is reached. This condition of maximum lateral pressure is known as the Passive Rankine State and the lateral pressure P_{HP} associated with it is given by $P_{HP} = \tan^2 (45 + \frac{\phi}{2})\gamma z = K_p \gamma Z$. The value K_p is known as the coefficient of passive earth pressure and its value generally lies between Ko and + ∞.

The magnitude of strain necessary to produce the passive state is several times larger than that required to produce the active state. Also, the state of stress associated with Rankine's theory requires that there be no shearing stresses on vertical planes. Since the backs of walls in reality are rough and shearing stresses may develop, the Rankine theory can provide only an approximation to the actual lateral pressure.

Lateral Pressure of Cohesive Particulate Systems. - Rankine's theory can be expanded to include the effects of cohesion on lateral pressure. The relation between the principle stress values in the active or the passive failure states is given by

$$\frac{\sigma_1' - \sigma_3'}{2} = 2C \cos \phi + (\sigma_1' + \sigma_3') \sin \phi$$

where σ_1' and σ_3' denote the major and minor principle stresses respectively and C and ϕ denote the cohesion and internal friction respectively.

For the active case, σ_1' denotes the vertical pressure $P_v = \gamma z$ (see Fig. 1.2(b)) and σ_3' denotes the corresponding lateral pressure P_{H_A}. Substituting P_v and P_{H_A} and reducing the above expression, the active lateral pressure with depth z is

$$P_{H_A} = \gamma z K_A - 2C(K_A)^{\frac{1}{2}} \qquad (1.3.1)$$

For the passive case σ_3' denotes the vertical pressure $P_v = \gamma z$ (see Fig. 1.2(c)) and σ_1' the lateral pressure P_{H_P}. Substituting P_v and P_{H_P}, the passive lateral pressure with depth z is

$$P_{H_P} = \frac{\gamma z}{K_A} + \frac{2C}{(K_A)^{\frac{1}{2}}} \qquad (1.3.2)$$

It can be seen that cohesion tends to decrease the lateral pressure in the active failure state and increase the lateral pressure in the passive failure state. In the case of active lateral pressure in a cohesive system, small values of depth z yield nagative values for P_{H_A}, while large values of depth z yield positive values for P_{H_A}. Setting $P_{H_A} = 0$ and solving (1.3.1) for z, one gets

$$z_o = \frac{2C}{\gamma (K_A)^{\frac{1}{2}}}$$

Here, z_o is the depth at which transition from negative to positive values

of lateral pressure takes place. Twice the value z_o corresponds to the height for which a cohesive material can remain standing up vertically with no lateral support to assist it.

Coulomb's Theory. - The back of every wall is to some degree rough giving rise to wall shear forces. Under such conditions, the validity of Rankine's theory is not fully met. This results in appreciable error. Much of this error however, can be avoided by making use of Coulomb's theory which involves a simplifying assumption as to the shape of the surface of sliding at failure. The error associated with this assumption is generally small compared to that associated with the use of Rankine's theory and may be neglected. When the boundary conditions for the validity of Rankine's theory are satisfied, the two theories lead to identical results.

The surface of sliding behind a retaining wall in reality is slightly curved. To simplify computations, Coulomb assumed it to be plane. The forces acting on such a sliding wedge in a dry cohesionless deposit at the instant of failure are shown in figure 1.3 together with the resultant triangle of forces corresponding to the active case.

The failure wedge behind a retaining wall is in equilibrium under its weight W, the resultant force P from the retaining wall and the reaction F along the surface of sliding. The reaction F is inclined at angle $\emptyset$ as shown because frictional resistance is assumed to be fully developed along the surface of sliding. Similarly, the force P is inclined at an angle δ to the normal to the back of the wall due to frictional resistance between the wall and the material being retained at failure. Since the weight W is known and the direction of all three forces

(a) FAILURE WEDGE

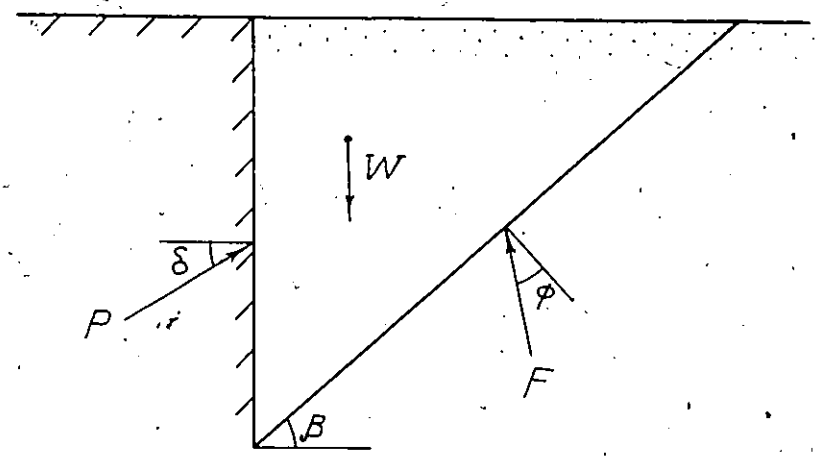

(b) FORCE POLYGON

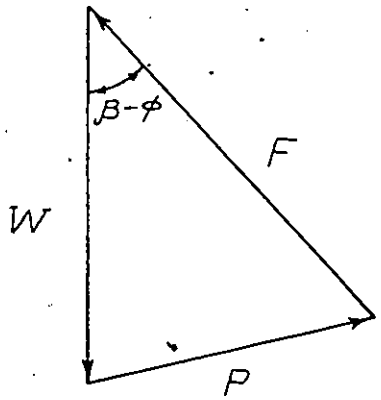

Fig. 1.3. Coulomb's theory for active lateral pressure in a cohesionless deposit.

may be determined knowing the angle of internal friction of the material, the force P can be scaled from the triangle of forces.

Since the sliding surface initially assumed may not be the real surface of sliding, similar computations must be done for other arbitrarily selected sliding surfaces until the greatest value of force P is found.

Pressures Developed in Silos. - As was previously mentioned, fresh concrete exerts vertical forces on form walls in addition to lateral pressure as a result of friction developing between the concrete and the form walls. The nature of these vertical shear forces can be better understood by looking at similar vertical forces which are developed in silos used to store various materials such as grains, coal and cement.

The term silo is used to denote the type of container whose dimensions are such that the plane of rupture does not pass out of the material filling the container before it intersects the side wall. Much of the weight of the material filling a silo is supported on the side walls by friction and the load actually supported by the container bottom is but a small proportion of the weight above it. Material stored in a silo applies lateral and vertical forces through friction to the side walls, vertical forces to horizontal bottoms and both normal and frictional forces to inclined surfaces. The static values of these forces generally increase during the withdrawal of material from the silo.

Janssen (Ref. 2), investigated and proposed a method for computing the vertical pressures on the walls of silos based on the vertical equilibrium of a thin horizontal lamina of the material in the silo. No assumption was made as to whether the material is in a state of failure or not. Jansen's formula along with his notation is as follows:

A = Internal area of a horizontal section through the silo

U = Perimeter of the same section

P_V = Vertical pressure

P_H = Horizontal pressure

ϕ' = Angle of internal friction of the stored material on the silo walls

μ' = Coefficient of friction tan ϕ'

W = Weight density of the stored material

e = Base of the natural logarithm

The total vertical weight on a horizontal plane through the stored material at depth h is

$$P = P_V A = A \frac{WA}{UK\mu'} \left(1 - e^{\frac{-UK\mu' h}{A}}\right)$$

The value of $K = P_H/P_V$, may be determined experimentally along with μ' corresponding to the material being stored and the finished surface of the silo. For instance, Janssen found that for wheat in a concrete silo K = 0.60 and Jamieson gives μ' = 0.4 to 0.425 depending on the concrete finish. Since no assumption was made as to the state of failure of the material, the value K does not necessarily equal $\tan^2(45 - \frac{\phi}{2})$ as would be the case with a wall under active pressure. If this were the case, then $K = \tan^2(45 - \frac{28}{2}) = 0.36$. This is significantly smaller than 0.60. This implies that material stored in a silo is not necessarily in a state of failure and the ratio of the principle stresses, $K = P_H/P_V$, may vary between $\tan^2(45 - \frac{\phi}{2})$ and $\tan^2(45 + \frac{\phi}{2})$ depending on whether the lateral pressure considered is active, passive or somewhere in between.

Based on the discussion of the lateral pressures exerted by particulate masses and the vertical shear forces existing in silos, it may be concluded that the lateral pressure exerted by fresh concrete on formwork lies between the two extreme pressures defined by the passive and active

states of plastic equilibrium. However, since it is highly unlikely in normal practice to find form walls moving inwards so as to compress the fresh concrete, the following hypothesis can be made:

(1) The maximum lateral pressure developed in formwork corresponds to the at rest condition as a result of infinitely rigid form boards, and

(2) The minimum lateral pressure developed in formwork corresponds to the active state of plastic equilibrium as a result of highly flexible form boards.

The theories and equations which have been presented on the lateral pressure of particulate systems have the following characteristics which may differ from those of fresh concrete in formwork:

(1) The parameters representing shear resistance are C (cohesion) and Ø (internal friction) corresponding to the Mohr Coulomb theory of shear strength. However, the Mohr Coulomb theory is strictly applicable to a continuum and caution must be exercised when applying it to a dilatant particulate system such as fresh concrete.

(2) The shear strength parameters appearing in the pressure equations have values which when determined by some appropriate test procedure remain constant with respect to time and temperature. Concrete however, differs in that its shear strength as a result of hydration goes from a low to a substantially high value as fluid to a solid. Hydration, being a chemical reaction has a rate of completion which is both time and temperature dependent.

(3) In evaluating the lateral pressure or the vertical shear forces on form walls, it was assumed that the particulate system was in a state of active or passive failure i. e. along any failure plane a condition of maximum shearing resistance existed. For concrete in formwork, this is not necessarily the case where lateral deformations as a result of rigid form boards or vertical deformations as a result of insufficient settlement may not be sufficient to fully mobilize the internal fictional resistance of the mix.

(4) Fresh concrete being largely composed of aggregate is a permeable material. The possibility of water seeping through cracks and joints in formwork must therefore be considered since the lateral pressure would be reduced as a result of seepage pressures existing rather than hydrostatic pressures. In such a case it is necessary to evaluate the total lateral pressure by summing that portion exerted by seeping water and that portion exerted by the solid particles. This implies that shearing resistance must be represented in the form of effective strength parameters.

(5) Concrete is not a unique material but is a term used to denote a large variety of materials composed of varying proportions of water, cement and aggregate. The physical behaviour of fresh concrete is not necessarily the same for all mix proportions. Therefore, a set of shear strength parameters

applying to one particular mix will not necessarily apply to a different kind of mix although the factors influencing the shear resistance of one mix may be expected to influence those of another mix in a similar manner.

1.4 Workability of Fresh Concrete

The quality and strength of cured concrete for a particular mix proportion is largely affected by the degree of compaction in the fresh state. Whether compaction is achieved by ramming or vibration, the process consists of eliminating entrapped air from the concrete so as to achieve as close a packing of aggregate and cement particles as is possible. In addition, it is important that the concrete mix can be easily transported, placed and finished without segregation. Workability is a general term used to describe the ease of placement and compaction offered by a particular concrete mix.

The mixing and placing of fresh concrete may be visualized as a continuous shearing process where particles of cement and aggregate move and interact with each other in the form of friction and interlock after the initial cohesion of the cement paste has been overcome. The workability of fresh concrete mix therefore, is a function of the work which must be done in overcoming this shearing resistance. In more formal terms, workability may be defined as the work required to overcome the friction between individual particles in the concrete so as to achieve full compaction.

A second term often used to describe the state of fresh concrete is consistency. This refers to the ease with which fresh concrete will flow

and is sometimes taken to mean the degree of wetness. In general, it may be stated that a wet concrete is more workable than a dry one, but, concretes of different mix proportions having the same consistency may vary in their respective workabilities.

In measuring the rheological properties of fresh concrete, various test procedures and forms of apparatus have evolved such as slump, compaction factor, flow test, remoulding test, vebe test and the ball penetration test. However, these tests do not express the quality of workability in terms of physical units. This implies that whatever quality is being measured, it is not independent of the apparatus by which it is measured. Instead, it is purely comparative in nature to the results obtained by others using the same apparatus.

1.5 Scope of the Investigation

The determination of the lateral pressure distribution and the corresponding maximum lateral pressure of fresh concrete on formwork along with a more satisfactory method of measuring the workability of fresh concrete necessitates a basic understanding of its shear strength behaviour in the non flow condition.

In this investigation, an attempt will be made to measure the shear strength properties of fresh concrete and the variation of shear strength with set time and temperature for a given mix. An attempt will also be made to evaluate the coefficient of lateral pressure at rest (Ko) so as to make possible the determination of the maximum as well as the minimum lateral pressures for the mix. It is hoped that this will lead to a better understanding of the development of lateral pressures in formwork and the work-

ability of fresh concrete. It is further hoped that the information obtained will be of value in the development of theoretical techniques for lateral pressure and workability calculations which would be of wider application compared to the present empirical techniques.

CHAPTER II

THEORY

2.1 Stress in a Particulate System

Fresh concrete may be thought of as a particulate system - a system composed of particles which are not strongly bonded together like the grains of a solid yet neither free to move like the elements of a fluid, which are submerged in a liquid medium. A system such as this may transmit forces through three types of region:

(1) Through the voids (pore pressure).

(2) Through particle contact points (effective stresses).

(3) Through the cross-sections of the particles.

It has been shown by Terzaghi that for a particulate system the total stress on any plane not cutting across any particle is given with sufficient accuracy by the following equation

$$\sigma = \sigma' + U$$

where σ' = effective stress

U = pore pressure.

The above equation is based on the assumption that the ratio $(A_c/A)^2$ is much smaller than unity where A_c denotes the area of contact points on the plane and A denotes the total area of the plane. σ' effectively controls the mechanical behaviour of a particulate system and hence its name.

The pore pressure U developed in a particulate system which has been stressed is given by Skempton's equation

$$\triangle U = B\left[\Delta\sigma_3 + A\ (\Delta\sigma_1 - \Delta\sigma_3)\right]$$

where $\triangle$ denotes a change.

σ_1, σ_3 denote major and minor principle stresses respectively.

A, B denote pore pressure parameters.

For a saturated system B = 1.0.

2.2 Resolution of Principle Stresses

Given a major and minor principle stress σ_1, and σ_3, the normal and shear stress combination on any plane inclined at angle θ to the major principle stress plane may be evaluated using the following two equations:

$$\sigma_\theta = \frac{\sigma_1 + \sigma_3}{2} + \frac{\sigma_1 - \sigma_3}{2} \cos 2\theta$$

$$\tau_\theta = \frac{\sigma_1 - \sigma_3}{2} \sin 2\theta$$

where σ_θ = normal stress on the plane inclined at angle θ

τ_θ = shear stress on the plane inclined at angle θ

The above two equations represent points on a circle in a rectangular coordinate system where the abscissa is normal stress and shear stress is the ordinate. Such a circle is termed a Mohr Stress Circle and allows the evaluation of σ_θ and τ_θ in a graphical manner.

2.3 Stress Points

A given Mohr circle represents only one state of stress. In order to trace a series of stresses imposed upon a material, numerous circles would

have to be drawn which becomes cumbersome. A more satisfactory way of showing these stresses is to plot a series of stress points on a p - q plane, each point representing a state of stress. To do this, we define the ordinate as $q = (\sigma_1 - \sigma_3)/2$ and the abscissa as $p = (\sigma_1 + \sigma_3)/2$ or in terms of effective stresses $p' = (\sigma_1' + \sigma_3')/2$.

2.4 Shear Strength

The shear strength of fresh concrete may be defined as the maximum resistance offered against shear stress. Shear strength can be considered to have three components:

(1) Structural resistance to displacement because of particle interlocking.

(2) Frictional resistance to movement between particles at their points of contact, and

(3) Cohesion (adhesion) between the surface of particles.

Two kinds of cohesion may be distinguished:

(1) True cohesion arising from the shear strength of a cementing agent between particles, and

(2) Apparent cohesion attributed to moisture surface tension between particles. It can be interpreted as internal friction induced by capillary pressure.

The shear strength of coarse particled materials is due mainly to the interlocking of their particles and intergranular friction, where as fine grained materials exhibit shear strength in the form of internal friction and cohesion.

2.5 Measurement of Shear Strength

There are basically four methods in which specimens may be tested to evaluate their shear strength (Ref. 10); direct shear, triaxial compression, torsion and vane or cylindrical shear.

Direct Shear Test. - The direct shear test (see figure 2.1(a)), makes use of a rectangular or cylindrical specimen incased in a split box. A normal force is applied to the box top and subsequently a shear force, forces the top of the box across the bottom causing the soil to shear along a plane predetermined by the split between the top of the box and the bottom. The normal load is ordinarily applied by a rigid plate that is free to move vertically as the soil deforms. The bottom of the box and the sides are rigid so that no lateral deformation takes place. The top and bottom of the box frequently have porous stones to permit drainage.

The direct shear test has extensively been used because the equipment is simple to operate, thin specimens permit rapid consolidation under normal load and the rigid box makes it possible to measure the volume changes which accompany shear.

Major drawbacks in the use of the direct shear test are the indeterminacy of the stresses on the box sides and the non-uniformity of shear strains leading to results which are difficult to interpret. In addition, drainage control is difficult.

a) DIRECT SHEAR

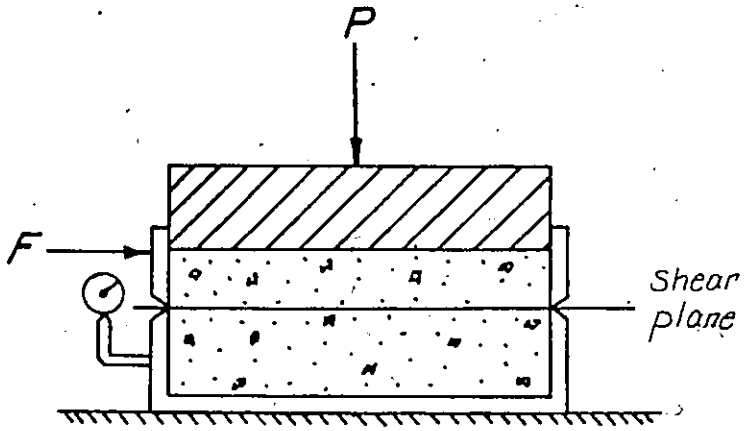

b) TORSION SHEAR

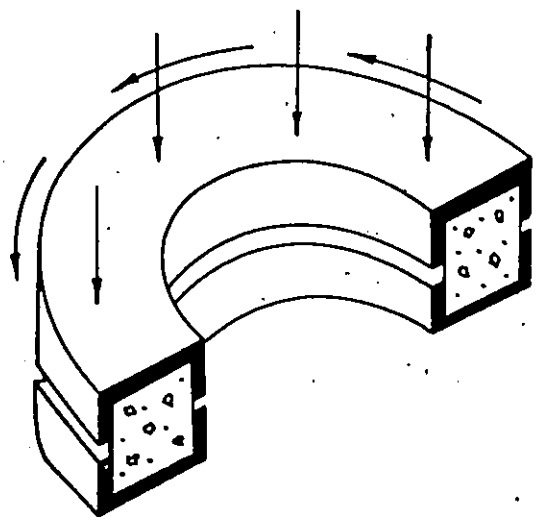

Torsion Direct Shear

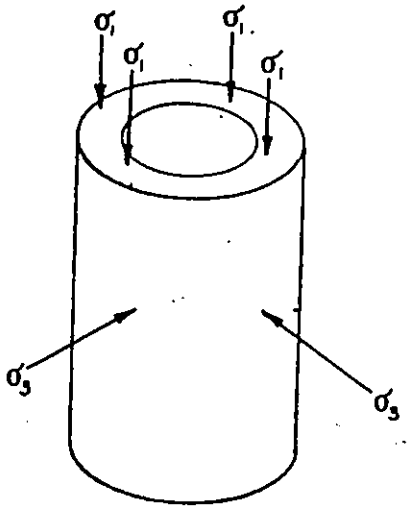

Torsion Triaxial Shear

Fig. 2.1. Shear testing of particulate masses.

Triaxial Compression Test. - In a triaxial test a cylindrical specimen is initially subjected to an equal all around pressure and then failed through application of an axial load. The specimen is enclosed by a rubber membrane which is sealed at the bottom to a pedestal and the top to a metal cap. The entire assemblage is contained in a chamber into which air or water is allowed to enter at any desired pressure. This pressure acts on the sides and top of the specimen through the rubber membrane and cap. Additional axial load may be applied to the specimen by means of a piston passing through the top of the chamber and resting on the metal cap. Porous stone is placed on the bottom of the sample and is connected to the outside of the chamber by tubing. This allows the pressure of the water in the sample to be measured if drainage is not allowed. Alternatively, if drainage is allowed, the quantity of water passing into or out of the sample can be monitored.

The triaxial test predominates in research because of its versatility. The principle stresses can be controlled to simulate field conditions. Pore pressure measurement is possible. Also, for non homogeneous specimens, the specimen is allowed to develop its own failure plane rather than it being predetermined by the apparatus as in the direct shear test. However, the non uniformity of stresses and strains and the inability to measure or control the lateral strains accurately are disadvantages which incidentally are also common to other shear tests.

Torsion Test. - In torsion testing, a cylindrical or annular specimen is first subjected to a normal and then a torsional stress until failure is produced.

In the torsional direct shear test (see fig. 2.1(b)), a ring shaped specimen is confined within an annular box and a normal force is applied to the plane surface of the box. Torsion is then applied causing the specimen to shear along a ring shaped surface parallel to the plane surfaces of the specimen. The shear strains in torsion vary with the distance from the centre of rotation.

In the triaxial cylinder test (figure 2.1(b)), a hollow cylindrical specimen is subjected to internal and external pressures and an axial load. This is followed by torsional loading which leads to failure. The hollow cylinder minimizes the non uniformity of torsional strain inherent in the simple torsion test. Pore pressures however, are indeterminate.

Vane Shear Test. - The vane shear device consists of four thin blades on a rod. The rod is forced into the material to be tested and a torque is applied until failure occurs along a cylindrical surface defined by the vanes. The torque causing such a failure is a measure of the shear strength.

Unlike the other methods of shear testing, the stresses in the vane shear test are defined by the state of stress already existing in the material. This method of testing is well adapted to determining the in-situ strength of a material with a minimum of disturbance. However, it offers little indication or control over the drainage conditions or principle stresses existing in the material.

2.6 Shear Strength Theories

Mohr Coulomb Theory. - A free body diagram of a non cohesive continuum tending to be sheared by a shear stress V along a plane A - A is shown in

figure 2.2(a). A section of the system has been taken along the shear plane A - A and the portion removed is replaced by normal and shear stresses N and V respectively. The resultant stress of N and V is denoted R. Angle α in the resultant triangle of forces is termed the angle of obliquity. As the shear stress V is increased to a maximum value τ and the normal stress N is kept constant, a stage will be reached when sliding is imminent. Angle α will correspondingly increase to a maximum value ϕ. Considering the triangle of forces at the brink of failure we may write

$$\tau = N \tan \phi \qquad (2.6.1)$$

where $\tan \phi$ = coefficient of friction.

The Mohr stress circle for the system is drawn in figure 2.2(b) at the instant of failure. The maximum shearing resistance is developed when the angle α equals the limiting value ϕ i.e. α is maximized. Therefore, line OD becomes tangent to the stress circle inclined at angle ϕ to the abscissa. Such a line is referred to as a Mohr Coulomb Failure Envelope.

It should be noted that many materials exhibit shear resistance when the normal stress on the shear plane considered is zero. Therefore (2.6.1) may be generalized and put in the form

$$\tau = C + \sigma_n \tan \phi \qquad (2.6.2)$$

where τ = shear resistance

C = cohesion

σ_n = normal stress on the shear plane

$\tan \phi$ = coefficient of friction.

Equation (2.6.2) is known as Coulomb's Equation. The result is that the failure envelope will now have a cohesive intercept on the C ordinate.

(a) FREE BODY DIAGRAM

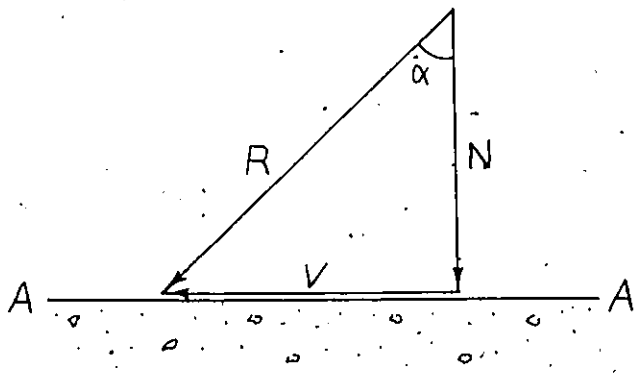

(b) MOHR STRESS CIRCLE

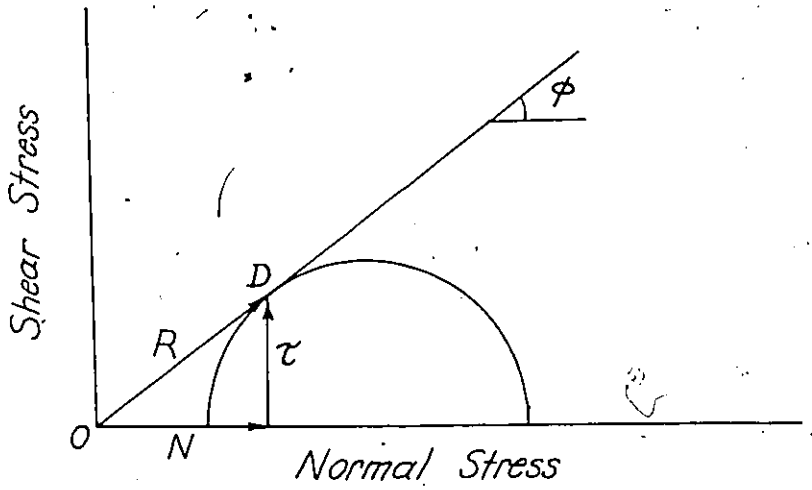

Fig. 2.2. The shearing of a non cohesive continuum.

It is important to realize that shear strength depends on effective stress and not total stress. Coulomb's equation must therefore be modified in terms of effective parameters and becomes

$$\tau = C' + \sigma'_n \tan\phi' \qquad (2.6.3)$$

The Mohr Coulomb theory has a fundamental meaning provided the assumption is made that no volume change occurs. With volume change included in the C-ϕ parameters, the theory is essentially a useful engineering tool, but nothing more. Since the volume changes depend on the principle stress system and since this differs between types of tests, one cannot expect to find universal C-ϕ values for a material independent of the method of testing.

Rowe's Theory. - When a system is stressed by two forces normal to each other Q and P as indicated in figure 2.3, slip will occur in general along a plane inclined at an angle β to the direction of the force P (Ref. 8). Assuming the material exhibits both cohesive and frictional components of shearing resistance, then the forces may be resolved to give

$$\frac{P - C_\mu x}{Q + C_\mu x \tan\beta} = \tan(\phi_\mu + \beta) \qquad (2.6.4)$$

where C_μ = a cohessive stress quantity

ϕ_μ = the angle of friction of the material.

Using this equation, the equations of state for a simple geometrical packing of spheres may be derived. Two such packings of spheres are the body centred cubic and the rhombic which correspond to the loosest and the most dense states respectively.

Consider a system of spheres in a body centred cubic packing as shown in figure 2.4(a). Movement of one sphere relative to another during

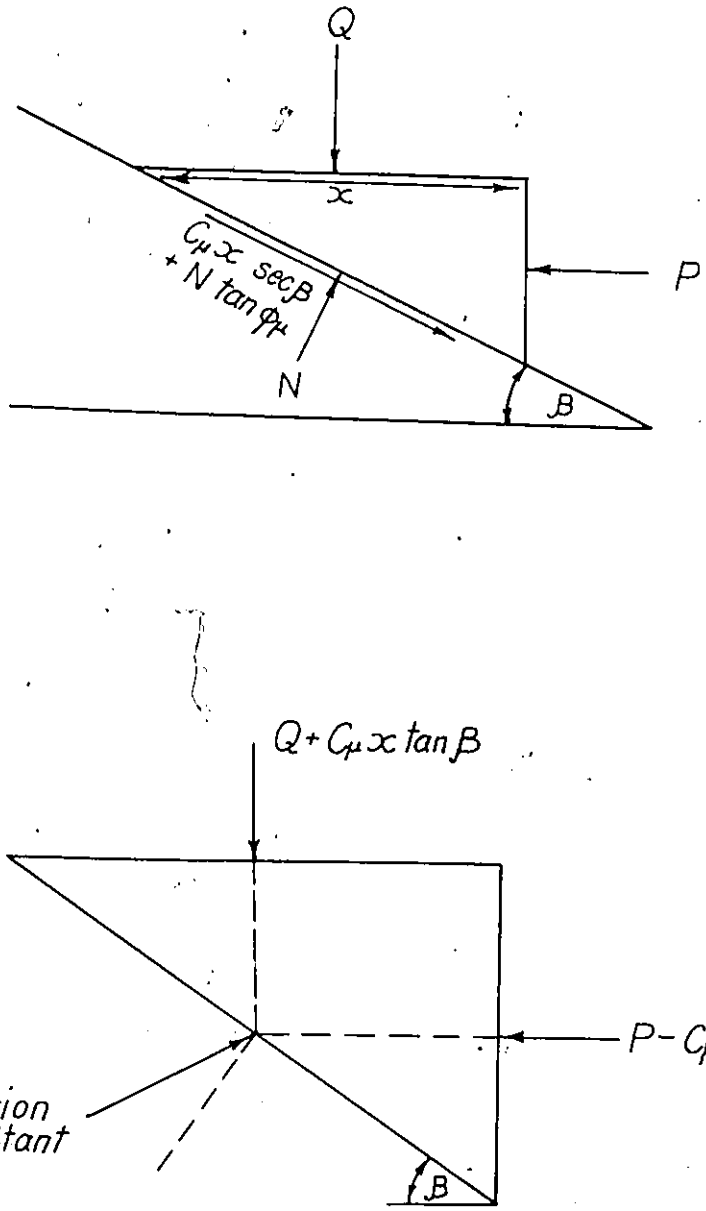

Fig. 2.3. The stressing of a system by two normal forces.

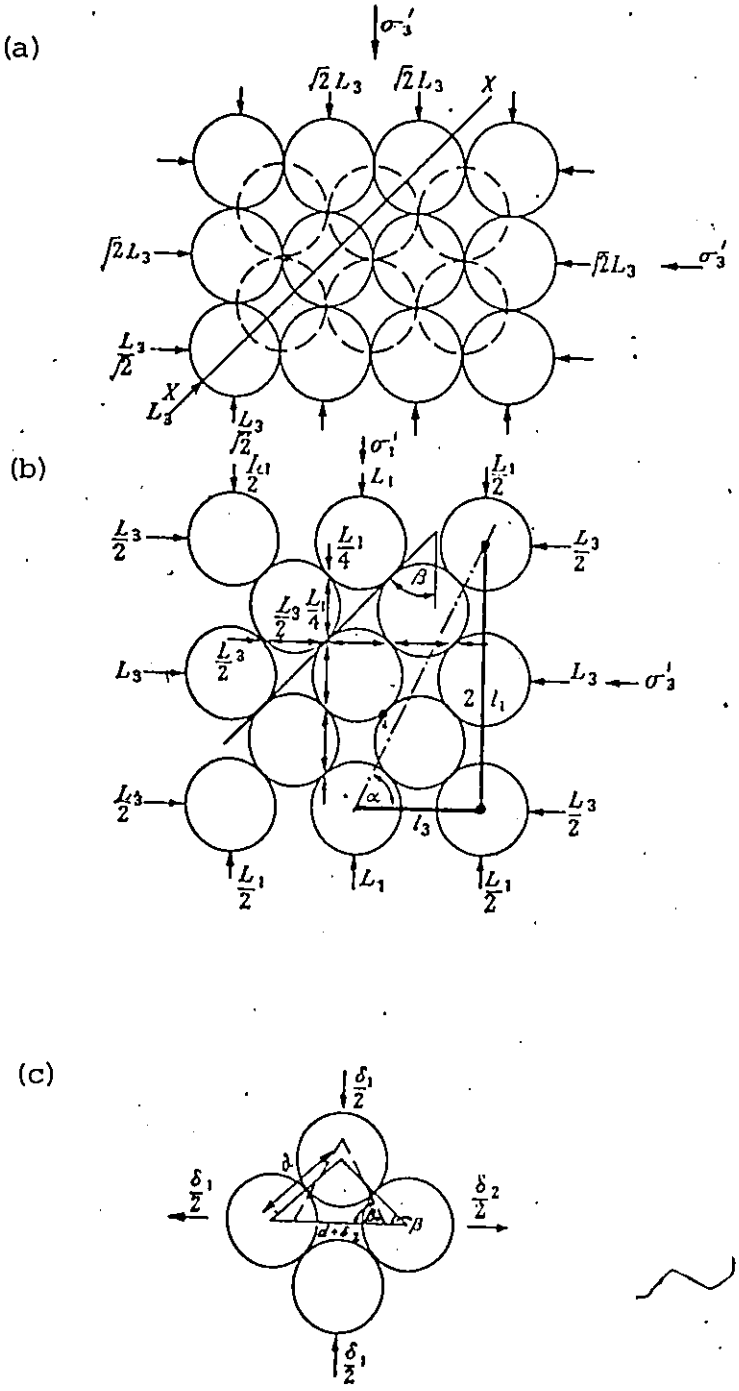

Fig. 2.4. The Body Centred Cubic Packing.

(a) Plan. (b) Elevation on X-X.

(c) Failure Mechanism.

the application of a deviatoric stress can only take place by sliding. Applying (2.6.4) at a point of contact of the spheres, the following condition of sliding is arrived at

$$\frac{L_1/4 - C'_\mu \ell_1}{L_3/2 + C'_\mu \ell_1 \tan(\beta)} = \tan(\phi'_\mu + \beta) \qquad (2.6.5)$$

Since $\sigma'_1 = L_1/\ell_3$ and $\sigma'_3 = L_3/\ell_1$, equation (2.6.5) may be rewritten in terms of effective principle stresses

$$\frac{\sigma'_1 \ell_3 - 4C'_\mu \ell_1}{2\sigma'_3 \ell_1 + 4C'_\mu \ell_1 \tan(\beta)} = \tan(\phi'_\mu + \beta) \qquad (2.6.6)$$

noting that $2\ell_1/\ell_3 = \tan(\alpha)$ and substituting into equation (2.6.6) we get

$$\sigma'_1 = \sigma'_3 \tan(\alpha)\tan(\phi'_\mu + \beta) + 2C'_\mu \tan(\alpha) \left[1 + \tan(\beta)\tan(\phi'_\mu + \beta) \right] . \qquad (2.6.7)$$

Figure 2.4 (b) shows the mechanism where by failure takes place. Note that the spheres move apart in the horizontal direction and move into the resultant space in the vertical direction. Considering δ'_1 and δ'_3 to be the deflections resulting from a change in load :

$$\delta_1 = 2d(\sin(\beta_o) - \sin(\beta))$$
$$\delta_3 = 2d(\cos(\beta) - \cos(\beta_o))$$

and

$$\delta'_1 = \frac{\partial \delta_1}{\partial \text{load}} = -2d\cos(\beta) \times \frac{\partial \beta}{\partial \text{load}}$$
$$\delta'_3 = \frac{\partial \delta_3}{\partial \text{load}} = -2d\sin(\beta) \times \frac{\partial \beta}{\partial \text{load}}$$

therefore

$$\frac{\delta'_3}{\delta'_1} = \tan(\beta)$$

Further in terms of strain

$$\frac{\epsilon'_3}{\epsilon'_1} = \frac{1}{2}\tan(\alpha)\tan(\beta) = \bar{\nu}' \qquad (2.6.8)$$

where $\bar{\nu}'$ is the instantaneous Poisson's ratio. The ratio of the work done per unit volume (RWD) on the assembly of spheres by the major principle stress to the work done on the minor principle stress by the assembly during an increment of expansion is given by

$$RWD = \frac{\sigma'_1\epsilon'_1}{2\sigma'_3\epsilon'_3} = \frac{\sigma'_1}{\sigma'_3}\frac{1}{2\bar{\nu}'}$$

and from (2.6.7) and (2.6.8)

$$RWD = \frac{\tan(\phi'_\mu + \beta)}{\tan(\beta)} + \frac{2C'_\mu}{\sigma'_3}\left[\frac{1}{\tan(\beta)} + \tan(\phi'_\mu + \beta)\right] \qquad (2.6.9)$$

Working through the same analysis for a rhombic packing of spheres will also give (2.6.9). Rowe demonstrated the validity of the theory by performing triaxial tests on cubic and rhombic packings of spheres made of steel.

The form of equation (2.6.9) which was derived for regular packings of uniform spheres may also be expected to apply to a mixture of packings of various sized particles. If such a particulate system is loaded, then the particles would slide past each other with the individual values of β being such as to minimize the rate of internal work done. This condition may be expressed as $\frac{\partial(RWD)}{\partial\beta} = 0$ for which $\beta = (45 - \frac{1}{2}\phi'_\mu)$. Substituting this value of β into (2.6.9) we have

$$\frac{\sigma'_1}{\sigma'_3}\frac{1}{2\bar{\nu}'} = \tan^2(45 + \frac{\phi'_\mu}{2}) + \frac{4C'_\mu}{\sigma'_3}\tan(45 + \frac{\phi'_\mu}{2}) \qquad (2.6.10)$$

All of the variables in (2.6.10) may be measured independently and the behaviour of the system predicted. In order to verify the applicability of (2.6.10), Rowe performed a large number of triaxial compression tests on cohesionless particles of loose and dense sands which showed good agreement between the experimental results and equation (2.6.10)

By rearranging, (2.6.10) may be put in a more usefull form for the purpose of analysis

$$\frac{\sigma_1'}{\sigma_3'} = K_1\sigma_3' + K_2$$

where $$K_1 = 2\tan^2(45 + \frac{\phi_\mu'}{2})$$

$$K_2 = 8C_\mu' \tan(45 + \frac{\phi_\mu'}{2})$$

CHAPTER III

Literature Review

A review of the technical literature reveals very few contributions concerning the shear strength properties of fresh concrete for the purpose of better understanding its workability and the pressure it develops in formwork.

In his research on the rheology of fresh concrete, L'Hermite (Ref. 3), used the triaxial cylinder torsion test to determine points on the Coulomb shear strength envelope for fresh concrete. For a concrete mix with a continuously graded aggregate, 300 kg of cement per cubic metre and a water/cement ratio of 0.65 he obtained the following load deformation curve for various values of normal load P;

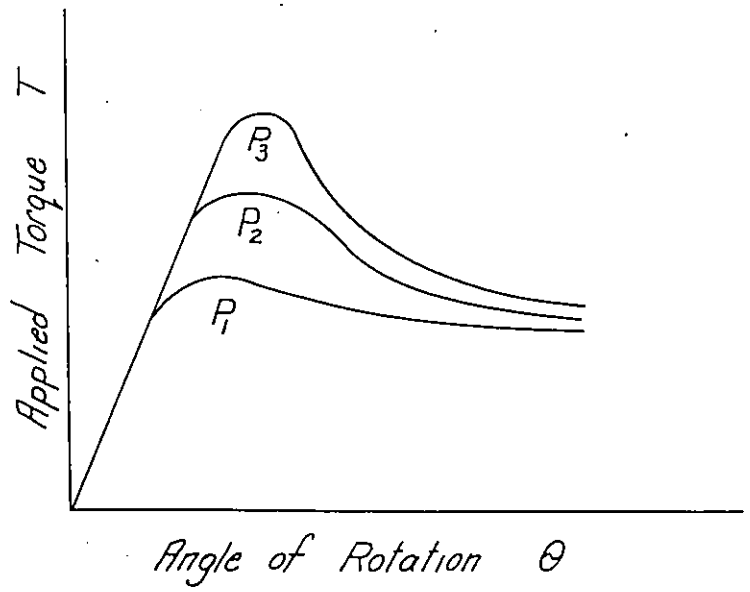

Fig. 3.1. L'Hermite's load deformation curve.

Analyzing the results using the Mohr Coulomb failure theory, L'Hermite obtained the following values of the coefficient of friction and the cohesion;

$\tan \phi = 0.70$

$\tan' \phi = 0.45$ (coefficient of friction with respect to the post peak strength)

Cohesion = $0.05\ kg/cm^2$

The cohesion was measured separately by means of a tensile test between two boxes. A more complete description of the test procedure however, was not included in the paper. L'Hermite also tested pure cement paste with the same quantity of water, and dry and saturated aggregate to evaluate their relative contributions to the shear strength of concrete. L'Hermite's results are tabulated below in table 3.2. It may be seen that concrete has a coefficient of friction between that of cement paste and saturated aggregate and a cohesion similar to that of cement paste.

Material	Tan ϕ	Tan'ϕ	Cohesion
Cement Paste	0.45	.06	.06 kgf/cm^2
Dry Aggregate	1.00	.71	0
Saturated Aggregate	0.80	.64	0

Table 3.2. L'Hermite's test results

In performing the tests, L'Hermite noticed that the maximum and post peak shear strength decreased with a decrease in the strain rate. For instance, in going from a speed of 0.5 to 0.25 mm per sec, no variation in maximum shear strength was observed. However, at a slow enough speed to be considered zero, the maximum shear strength decreased by 10 %. This was attributed to the viscosity of the mix.

From the investigation, L'Hermite concluded that:

(1) The rheological properties of fresh concrete can be measured by simple experiments, the results of which can be expressed in mechanical units

(2) The coefficient of friction tanØ, decreases as the quantity of mixing water increases, and

(3) The deformation at failure appears to depend on the grading of the aggregate.

In 1962, Ritchie (Ref. 6), published a paper on the triaxial testing of fresh concrete in which he stated that the workability of a concrete mix is a result of the fundamental rheological properties of the fresh mix. Further, Ritchie stated that workability can be subdivided into two fundamental properties:

(1) Compactibility, being the amount of useful internal work necessary to produce full compaction, and

(2) Mobility, being inversely proportional to the internal resistance of the mix to deformation.

In order to study the mobility effect and express it in fundamental terms, Ritchie measured directly the angle of internal friction of fresh concrete using the three dimensional stress system of the triaxial test. A variety of concrete mixes ranging from high to low workability were tested. Undrained triaxial tests were performed on 4 x 8 inch specimens at a strain rate of 2.1 % per minute until they were seen to fail or the strain exceeded 20 %. Cell pressures ranging from 5 to 60 psi were used. The corresponding Mohr circles were drawn along with the best line giving the angle of internal friction. Table 3.3 summarizes Ritchie's results.

Mix	Workability	Compacting factor	Water/cement ratio	Slump (in)	Vebe time (s)	Angle of internal friction (degrees)	Apparent cohesion (lb/in^2)
1:3	low	0.85	0.452	3¼	3.5	12	2.0
	medium	0.92	0.477	5	2.0	11	5.0
	high	0.95	0.485	5	1.5	8	4.0
1:4½	low	0.85	0.512	1¼	7.5	28	3.0
	medium	0.92	0.549	2	6.5	28	4.0
	high	0.95	0.561	2¾	4.0	25	7.0
1:6	low	0.85	0.557	zero	9.0	32	8.0
	medium	0.92	0.665	2¼	4.5	30	8.0
	high	0.95	0.690	2¼	2.5	*	*
1:7½	low	0.85	0.676	zero	10.0	34	10.00
	medium	0.92	0.775	¾	5.0	34	7.00
	high	0.95	0.805	1½	4.5	*	*

Table 3.3. Ritchie's Test Results.

From the results, the following generalized conclusions were made by Ritchie:

(1) For mixes having the same compacting factor, the angle of internal friction increases as the aggregate/cement ratio increases. This is a result of the paste layer becoming thinner and thinner giving rise to greater particle interaction, and

(2) As the water/cement ratio increases, the lubricating effect of the paste layer between the aggregate increases resulting in decreased values of internal friction.

In 1968, Olsen (Ref. 5), completed a study on the lateral pressures of

concrete on formwork in which he related the lateral pressure exerted by fresh concrete on formwork to the undrained shear strength of the concrete.

Olsen measured and recorded the variations in the undrained shear strength of fresh concrete with time using triaxial tests. He then proceeded to relate the stress-strain relationships of the concrete specimens from the triaxial tests to the strains and corresponding stresses existing in formwork. Olsen then compared his results to those obtained from recognized pressure formulae developed by the American Concrete Institute and the Civil Engineering Research Institute presently known as the Construction Industry Research and Information Association.

To evaluate the shear strength, Olsen performed undrained triaxial tests for set times ranging from 20 min to 180 min and confining pressures ranging from 20 psi to 80 psi. A standard mix having a ratio of cement to sand to coarse aggregate of 1.0 : 1.5 : 1.5 was used with a water cement ratio of 0.4. The results of the triaxial tests are summarized in table 3.4 below.

Set Time minutes	Cohesion psi	Internal Friction Angle degrees - minutes
20	2.8	1^0 34'
30	3.8	1^0 22'
45	3.8	1^0 47'
60	4.9	1^0 47'
75	5.0	3^0 02'
90	5.2	3^0 26'
120	6.6	3^0 18'
180	9.1	5^0 31'

Table 3.4. Olsen's Test Results.

From Olsen's results, the following generalized conclusions can be made:

(1) For low set times, the shear strength of fresh concrete consists mainly of cohesive bond in the cement paste

(2) As the setting continues, the cement paste becomes less plastic and the mobility of the aggregate particles decreases resulting in an increasing angle of internal friction, and

(3) Cohesion steadily increases with set time as cement combines with water to form the binding medium.

It should be emphasized that all three investigators performed undrained tests but neglected however to take pore pressure measurements. For instance, Ritchie assumed that the cement paste matrix having a gel structure of its own could not be considered to act in exactly the same manner as pore water. In what manner it would act however, he neglected to either state or investigate. Consequently, all of the test results are in terms of total stresses (except for L'Hermite's which would depend on the speed with which the fresh concrete was sheared). Therefore, an effective stress analysis cannot be carried out. Since the undrained values C and $\emptyset$ are pore pressure dependent, and the pore pressures developed under field conditions may differ significantly from those in the laboratory due to different drainage conditions such as length of drainage paths to a free draining surface, it is difficult to appreciate the applicability of their test results.

It is also evident from the discussion of the development of pressures in formwork that the stiffening of concrete is largely dependent on the temperature of the concrete. The effect of temperature on the shear strength of fresh concrete was not mentioned or investigated by any of the three investigators.

CHAPTER IV

Experimental Procedures and Test Results

4.1 Choice of Testing Procedure

As was previously discussed in chapter II, fourcommon test procedures exist for evaluating the shear strength of particulate masses. For this investigation, the triaxial compression test was chosen for the following reasons:

(1) The principle stresses imposed upon the test sample can be controlled by triaxial testing as opposed to the direct shear test, the torsional shear test or the vane shear test where the principle stresses are indeterminate,and

(2) During the stressing of the test sample, the pore water pressures can be measured by means of a pressure cell and transducer system making an effective stress analysis possible.

During the triaxial testing of a particulate mass such as fresh concrete two extreme conditions of drainage can exist:

(1) A drained condition where stresses are applied slowly with respect to the ability of the material to drain so that no excess pore pressures are developed, or

(2) An undrained condition where stresses are applied so rapidly that virtually no dissipation of pore pressures takes place.

These two extreme conditions of drainage are never likely to exist. However, because they represent limiting conditions and are easy to control,

they are valuable guides for understanding the behaviour of particulate masses.

Based upon the two extreme conditions of drainage, there are three types of triaxial tests which can be done:

(1) The Undrained Triaxial Test which allows no escape of pore water from the sample as it is compressed to failure

(2) The Consolidated Undrained Triaxial Test which allows the sample to initially consolidate or dissipate pore water pressure under a constant all around pressure. Subsequently, when the axial load is applied, no drainage is permitted, and

(3) The Drained Triaxial Test which allows the sample to consolidate prior to application of the axial load. Drainage is then permitted during the remainder of the test as the axial load is applied. To do this, the axial load is increased slowly so that development of significant pore water pressures are prevented.

When fresh concrete is placed in formwork, the impermeability of the form boards (with the exception of joints), permits little water to escape. Further, during mixing and placing, fresh concrete is continously manipulated and sheared and consequently it has little opportunity to consolidate or to dissipate pore water pressure by means of bleeding. For these reasons it was considered that undrained triaxial tests would best simulate the conditions of fresh concrete in formwork and the process of mixing and placing of fresh concrete.

4.2 Concrete Mix Characteristics

Two concrete mix proportions were used in this investigation corresponding to the following two groups of tests;

Triaxial Tests. - A single concrete mix was used throughout the triaxial testsing having ratios of cement to sand to coarse aggregate of 1.0:2.7:2.1 by weight and a water/cement ratio of 0.57. This resulted in a concrete with a 2 inch slump and an average 28 day compressive strength of 3,700 psi.

K_0 Tests. - For these tests, a mix having ratios of cement to sand to coarse aggregate of 1.0:1.5:3.0 by weight was used along with a water/cement ratio of 0.55. The resulting concrete had a 2.5 inch slump and a 28 day average compressive strength of 4,950 psi.

In all tests, Type 1 Normal Portland Cement was used and crushed air dried limestone gravel and quartz sand. The aggregate may be classified as angular in appearence. The grain size distributions of both aggregates are shown in figure 4.1. In an attempt to maintain temperature and humidity uniformity throughout the testing period, all materials were stored in containers prior to mixing and kept in the room where the testing was to be conducted.

4.3 Testing Procedures

Triaxial Compression Tests. - Figure 4.2 shows a sketch of the triaxial compression set up used during the investigation. Testing was done on 4 x 8 inch cylindrical concrete specimens. The sequence of steps in testing the samples of fresh concrete were as follows:

(1) The base of the triaxial cell was first cleaned and made free

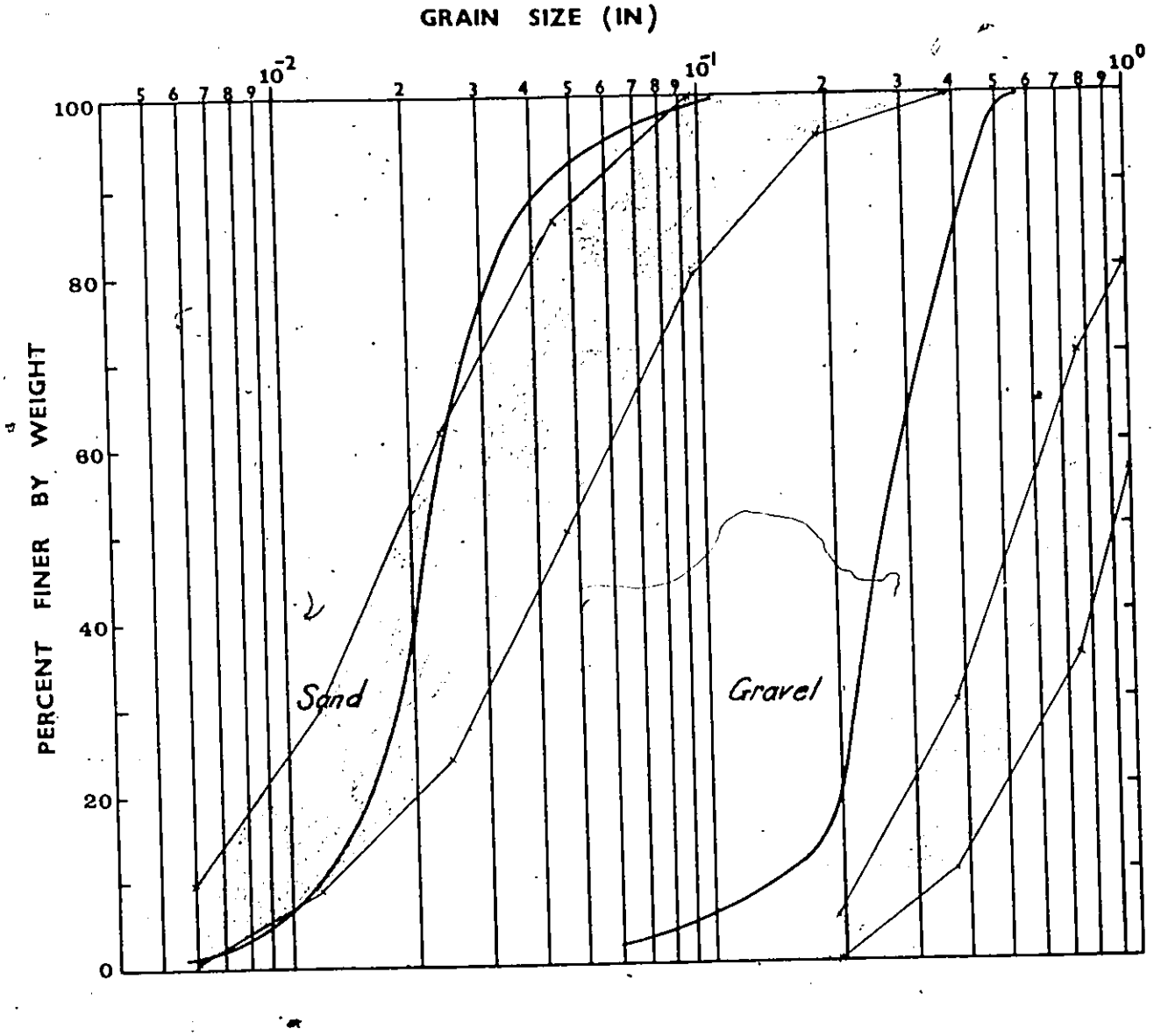

Fig 4.1. Grain size distribution and the limits specified in ASTM C33 for fine and coarse aggregate.

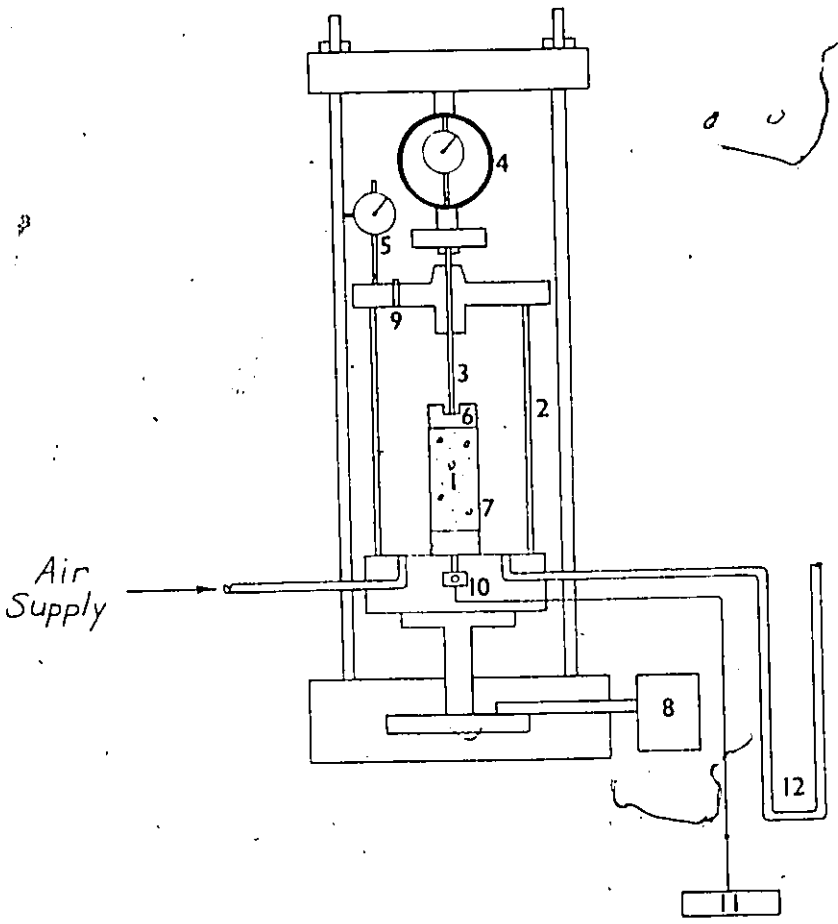

1 -Concrete Sample
2-Triaxial Cell
3-Triaxial Piston Rod
4-Proving Ring and Dial Gauge
5-Deflection Gauge
6-Top Cap
7-Rubber Membrane
8-Variable Speed Electric Motor
9-Pressure Regulating Valve
10-Pore Pressure Cell
11-Transducer
12-U-Tube Pressure Measuring Device

Fig. 4. 2. Triaxial Compression set up.

of any dried concrete from previous tests and the water channels were de-aired by flooding with water.

(2) A rubber membrane was attached and sealed to the pedestal by means of vacuum grease and rubber rings. A porous stone having been stored in water was then placed on the pedestal inside the rubber membrane.

(3) A cylindrical mold was placed so as to surround the rubber membrane and a vacuum was applied causing the membrane to take the same cylindrical shape as the mold. Moist filter paper was then placed along the inside of the membrane to allow the movement of water and therefore ensure uniform pore pressures throughout the sample during compression (see figure 4.3(a)).

(4) The appropriate proportions of gravel sand and cement were mixed. The water was then added and a timer recorded the set time. The set time was taken as the time following the addition of water to the mix to the instant when the axial load was applied.

(5) The mold was filled with fresh concrete in four successive layers, each layer receiving fifty tamps from a ½ inch diameter rod to achieve full compaction.

(6) The vacuum on the mold was removed and the concrete was sealed at the top with a metal top cap. The temperature of the air and the concrete were recorded and the test sample was then allowed to stand for a given set time (see figure 4.3(b)).

(7) Several minutes before the required set time elapsed, the

a)

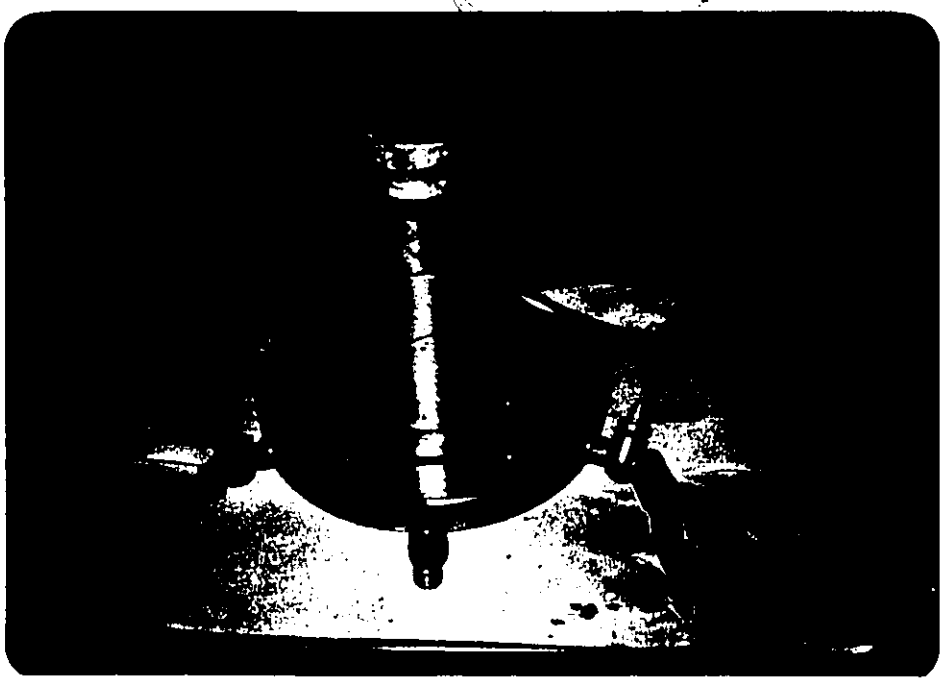

b)

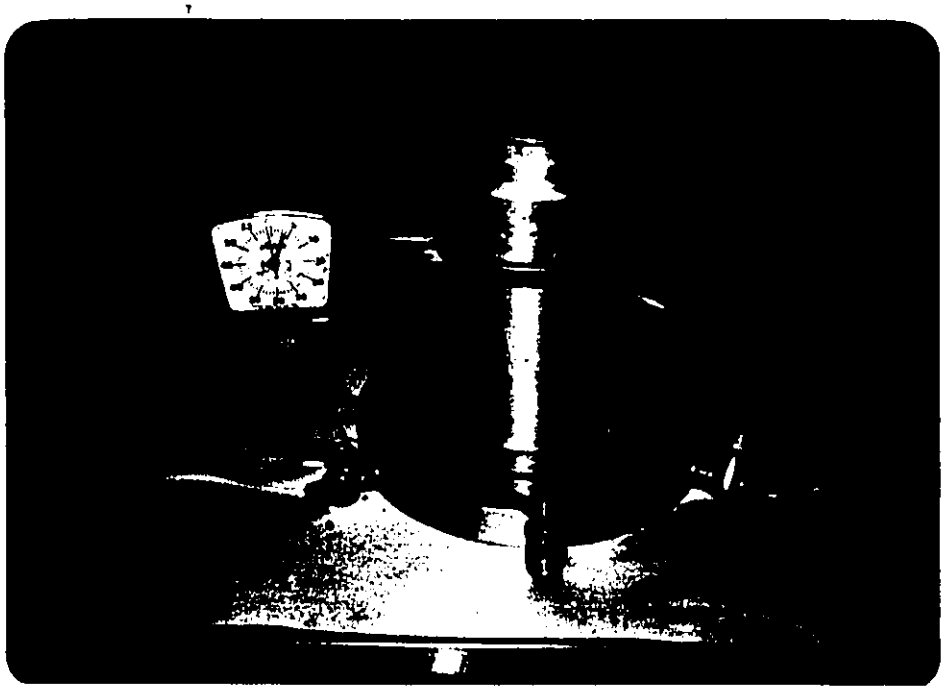

Fig. 4.3. a) Vacuum being applied to the membrane.

b) A test sample during its setting period.

mold was removed and a steel ring was placed around the midsection of the cylinder to monitor the lateral strains. The cell was then attached to the base and the entire assembly was mounted on the compression machine for testing (see figure 4.4(a)).

(8) When the desired cell pressure was reached, the deviator load was applied at a constant strain rate of .045 in/min and measurements of deviator load, longitudinal strain, lateral strain at the midsection of the sample and pore water pressures were taken. This implied that the sample was strained 20 % of its length in thirty five minutes. Although this period of time is relatively large in comparison to the set times of the samples, it ensures that uniform pore water pressures exist throughout the samples during compression.

Figure 4.4(b) shows several samples after having been tested. In all, forty undrained triaxial tests were successfully performed for set times of 40, 80, 120 and 160 minutes, cell pressures of 0, 5, 10, 15 and 20 psi and temperatures of 70^{o} F and 38^{o} F. Figure 4.5 shows a typical data sheet for one of the tests.

Unconfined Compression Tests. - During the triaxial testing it was discovered that the fresh concrete dilated during the application of the deviator load and that negative pore water pressures developed in the samples even though the cell pressure was set equal to zero. Consequently, it became impossible to perform an unconfined compression test for the purpose of getting a better estimation for the cohesion of fresh concrete as defined by the Mohr Coulomb failure theory. To overcome this, a series

a)

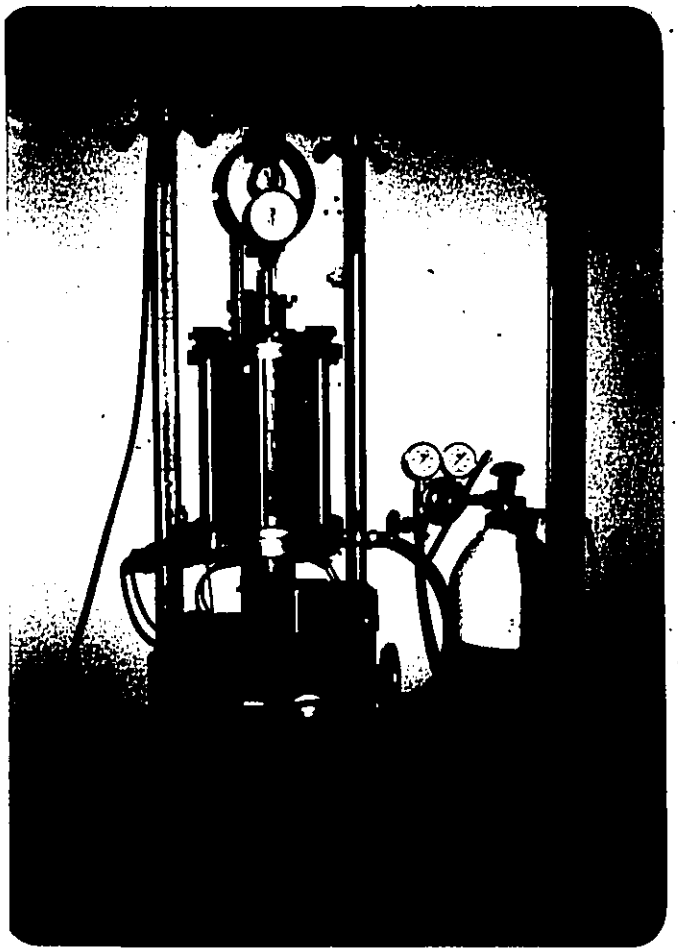

b)

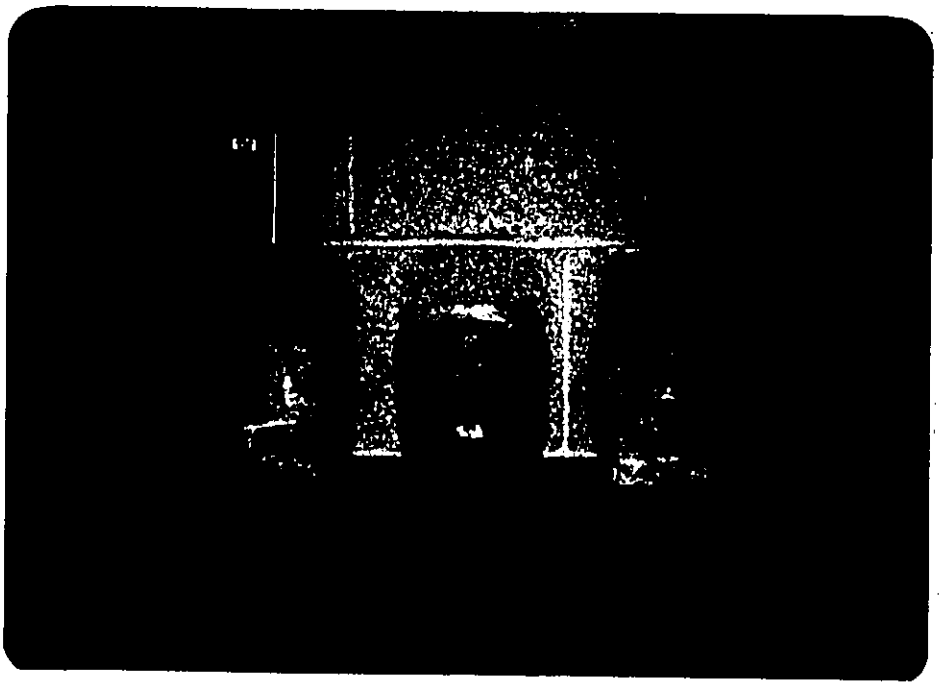

Fig. 4.4. (a) Entire triaxial assembly prior to testing.
(b) Samples after having been tested.

TRIAXIAL TEST

Date July 13 1978

Set Time 120 Min.

Cell Pressure 0 psi

Temperature 70°F

Strain Gauge x 10^{-3} in.	Load Dial x 10^{-4} in.	Transducer	Lateral Strain
0	0	0	32.9
100	56	-.2	33.2
200	105	-.8	33.6
300	156	-1.5	34.0
400	203	-2.1	34.5
500	242	-2.7	35.0
600	277	-3.1	35.4
700	304	-3.5	36.0
800	330	-3.8	36.4
900	350	-4.0	36.9
1000	367	-4.3	37.4
1100	389	-4.4	38.0
1200	405	-4.6	38.5
1300	420	-4.8	39.1
1400	431	-4.9	39.7
1500	442	-5.1	40.3
1600	463	-5.2	40.9

Fig. 4.5. Typical triaxial test data sheet

of drained unconfined compression tests were performed on unsupported cylindrical samples of fresh concrete.

The samples were formed by placing concrete in a plexiglass cylinder 3.22 inches in diameter and 7 inches high. The concrete was placed in four layers and each layer received fifty tamps as was done for the triaxial tests. The concrete was then allowed to set for the appropriate time period after which the cylinder was carefully slipped off and the sample compressed to failure at a strain rate of .045 inches per minute. To measure the lateral strain, a strip of wet paper marked off in inches was placed around the midsection of the sample. Figure 4.6 shows a cylindrical sample during its setting period in the plexiglass and just prior to testing in the compression machine.

Ko Tests. - Values of Ko for fresh concrete were obtained by applying vertical stresses through a piston in series with a loading ring onto fresh concrete samples 3.22 inches in diameter and 7 inches high. These samples were restrained from moving laterally by means of a plexiglass cylinder casing whose diameter was $\frac{1}{16}$ inches larger than that of the piston. This allowed water to drain out of the concrete during the application of vertical stresses. A circular sponge was placed between the piston and the concrete to prevent the loss of the finer sand and cement particles. The lateral strains and the corresponding stresses as a result of vertical loading were measured directly by means of two strain gauges on either side of the cylinder attached at its midheight. Two 'dummy' strain gauges were also used to offset the effects of temperature changes.

The cylinder was filled with concrete in four successive layers, each layer being tamped at least fifty times with a ½ inch diameter rod until no voids were evident when the concrete was viewed through the

Fig. 4.6. Unconfined compression test sample during its setting period and prior to testing.

plexiglass. The vertical load was applied in successive increments of 12.5 pounds and the corresponding strain gauge readings were taken only after the excess pore pressures had dissipated and the load dial gauge had stabilized.

The testing was performed within a period of approximately 30 minutes. In order to verify that fresh concrete is permeable to water, the water expelled from the cylinder top was collected and measured during increases in axial load. Figure 4.7 shows a typical data sheet for the Ko testing along with the water expelled during the vertical stressing. Figure 4.8 shows the Ko apparatus prior to and during the testing procedure.

The various tests and conditions of set time and temperature performed in this investigation are summarized in table 4.9.

4.4 Experimental Results

Triaxial Compression. - Figures 4.10 A to 4.17 A represent the stress-deformation characteristics of fresh concrete at 70^{o} F and 38^{o} F under confining pressures ranging from 0 psi to 20 psi and for set times ranging from 40 minutes to 160 minutes. The ordinate corresponds to the effective principle stress difference and was calculated using the area at the midsection of the test samples. It was assumed that failure occured predominantly at the midsection of the test samples as is evidenced by a bulging type of failure in figure 4.4(b). The cause of this type of failure can be explained by the increased strength at the sample ends as a result of friction developing between the concrete and the porous stone at the bottom of the sample and the concrete and the metal top cap at the top of

Ko TEST

Date Feb 1978

Set Time 160 Min.

Temperature 70°F

Load Dial x10^{-4} in.	Vertical Stress psi	Strain Gauge	Horizontal Stress psi	Water Expelled ml.	Ko
0				0	
100				8	
200				10	
300					
400	6.08	6	.24		.04
500				13	
600					
700					
800	12.1	32	.88		.07
900				16	
1000					
1100					
1200	18.0	46	1.84		.10
1300					
1400				18	
1500					
1600	24.0	47	1.88		.08
1700					
1800					
1900					
2000	30.0	65	2.60	20	.09

Fig. 4.7. Typical Ko test data sheet.

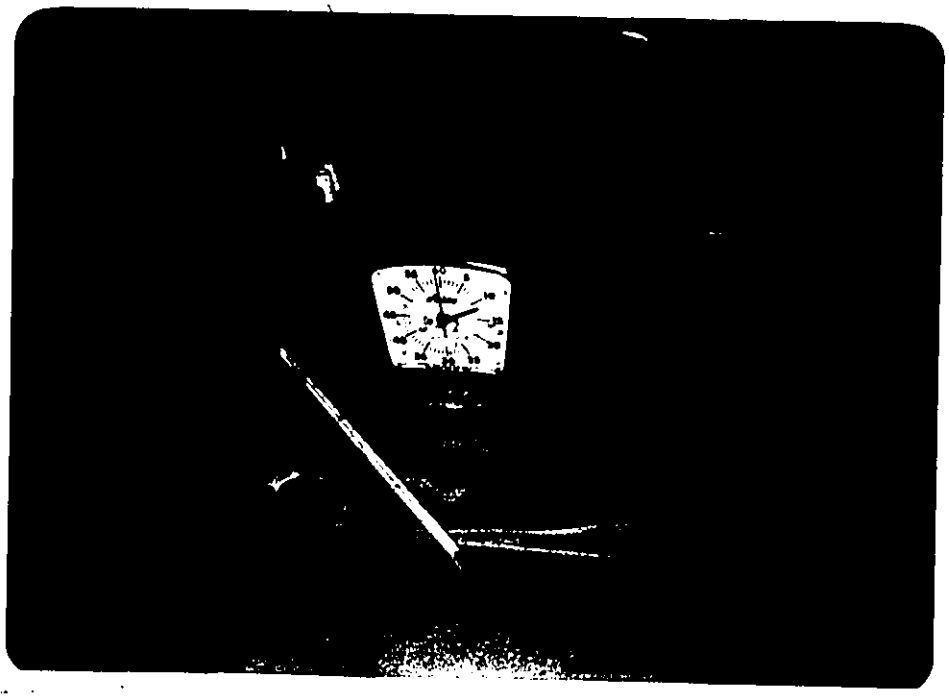

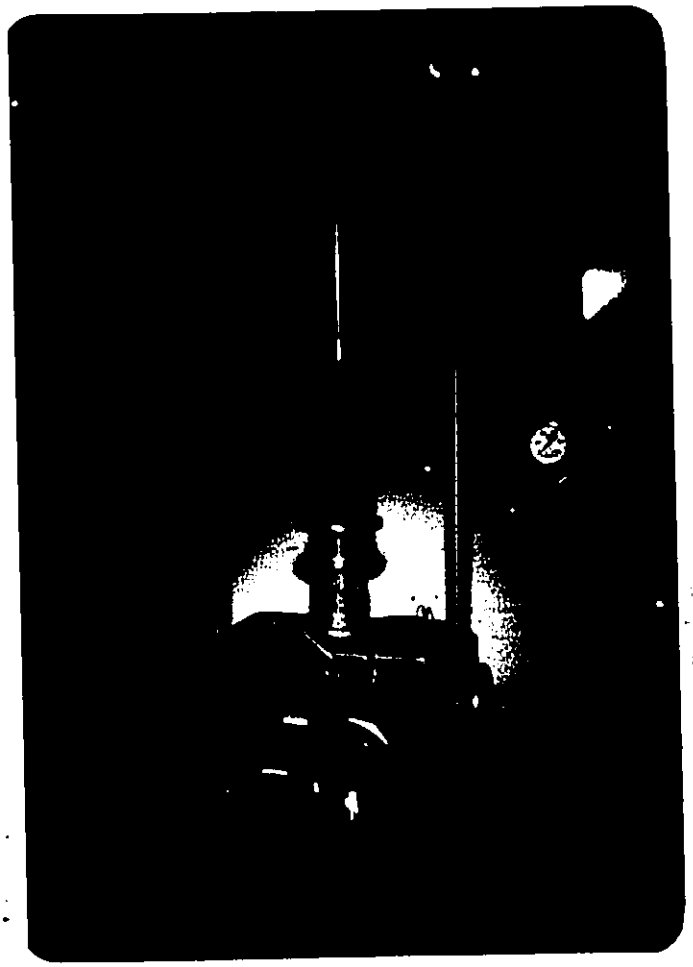

Fig. 4.8. K_0 apparatus prior to and during the testing procedure.

Test	Test Conditions		
	Set Time	Temperature	Confining Pressure
Triaxial Compression	40 min. 80 120 160	70^0F, 38^0F	0, 5, 10, 15, 20 psi
Unconfined Compression	40 min. 80 120 160	70^0 F, 38^0 F	0 psi
K_0	40 or 20 min. 80 120 160	70^0 F, 38^0 F	N.A.

Table 4.9 Summary of tests performed

the sample. The increase in strength due to the confining effects of the rubber membrane were neglected as several trial calculations indicated the rubber membrane correction to be in the order of 1 to 2 percent. This, it was felt, was less than the accuracy of the testing could warrant.

In figures 4.10 B to 4.17 B, the pore pressures developed during the triaxial testing have been plotted as a function of the axial deformation.

Unconfined Compression. - In figures 4.18 A and 4.18 B are plotted the results of the unconfined compression tests at 70^{o} F and 38^{o} F respectively in terms of effective compressive stress versus axial deformation. The compressive stresses were calculated using the area at the midsection of the sample as was done for the triaxial compression tests.

Ko Tests. - In figures 4.19 A and 4.19 B, Ko has been plotted as a function of the effective vertical stress and for set times ranging from 20 minutes to 160 minutes. The plots have been done for temperatures of 70^{o} F and 38^{o} F.

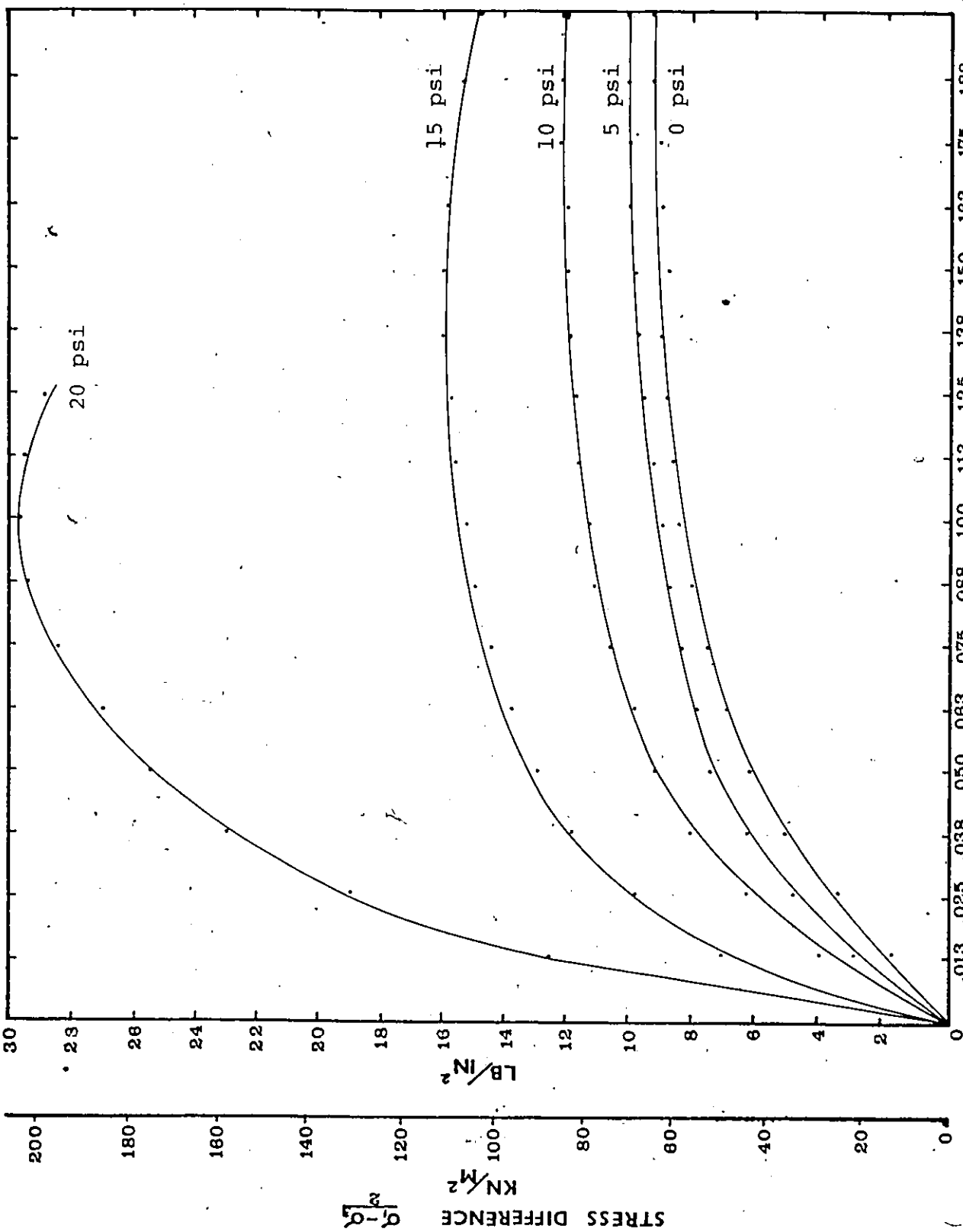

Fig. 4.10 A. Stress difference versus axial strain for 70°F and 160 min. set.

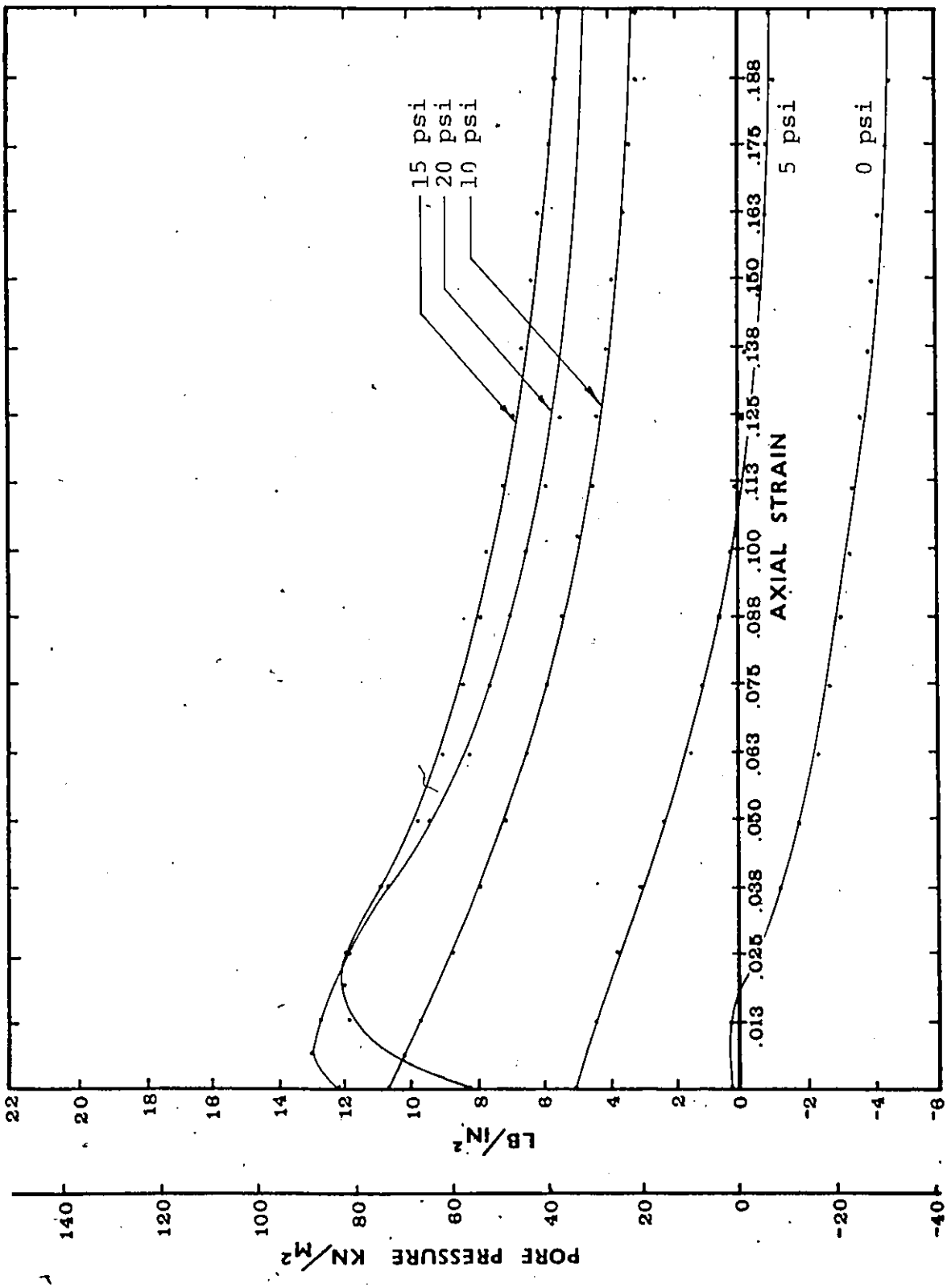

Fig. 4.10 B. Pore pressure versus axial strain for 70^0F and 160 min. set.

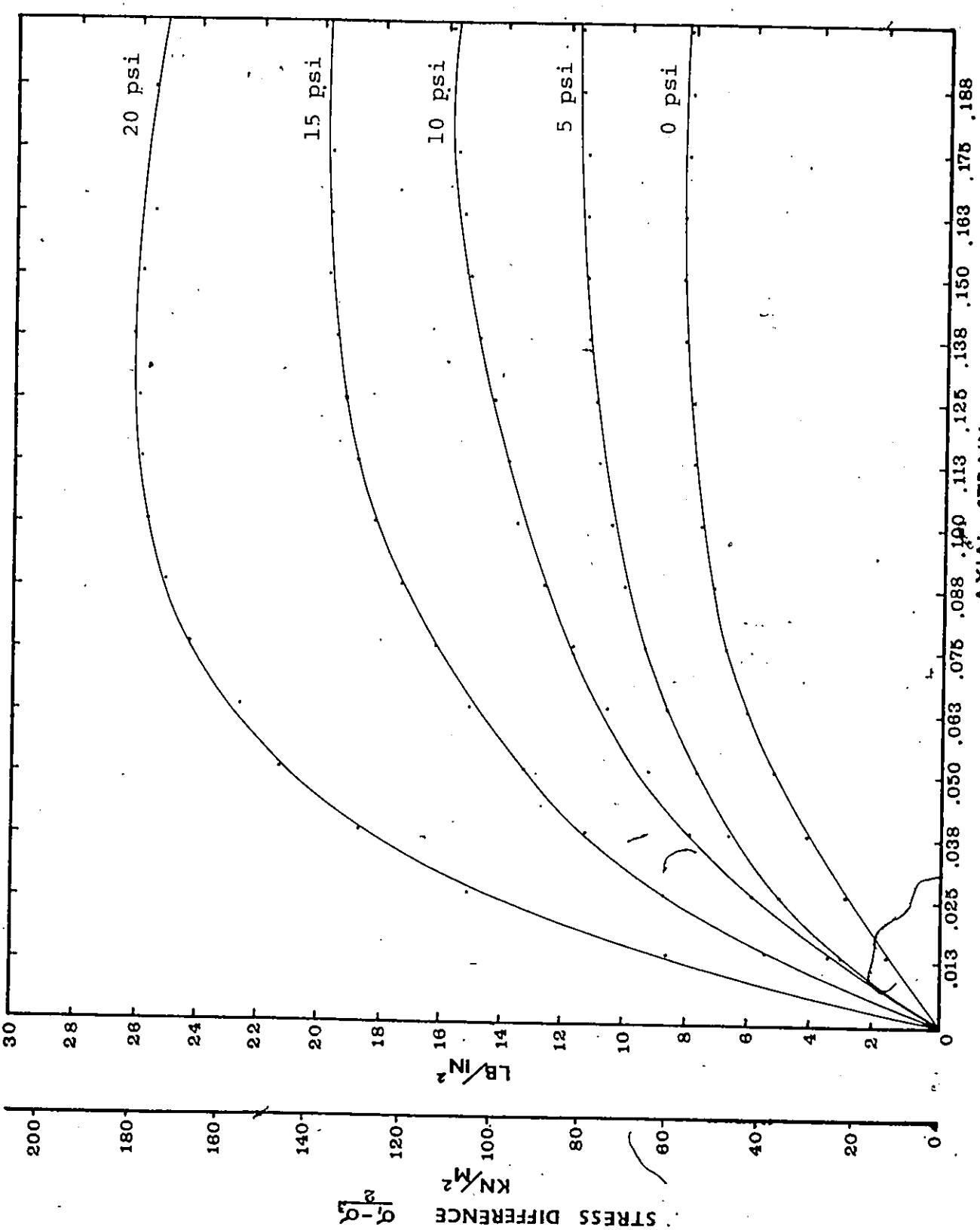

Fig. 4.11 A. Stress difference versus axial strain for 70°F and 120 min. set.

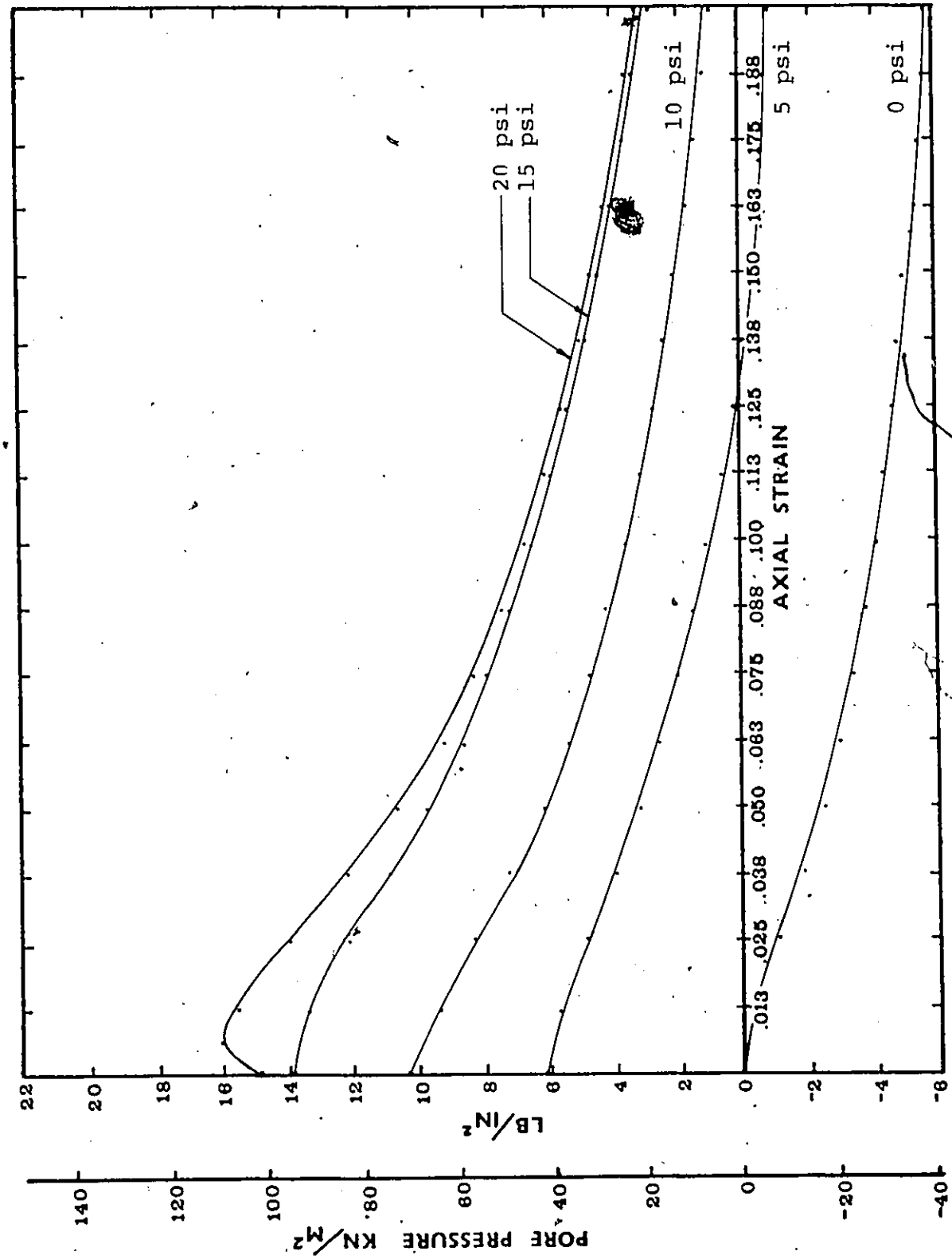

Fig. 4.11 B. Pore pressusre versus axial strain for 70^{0}F and 120 min. set.

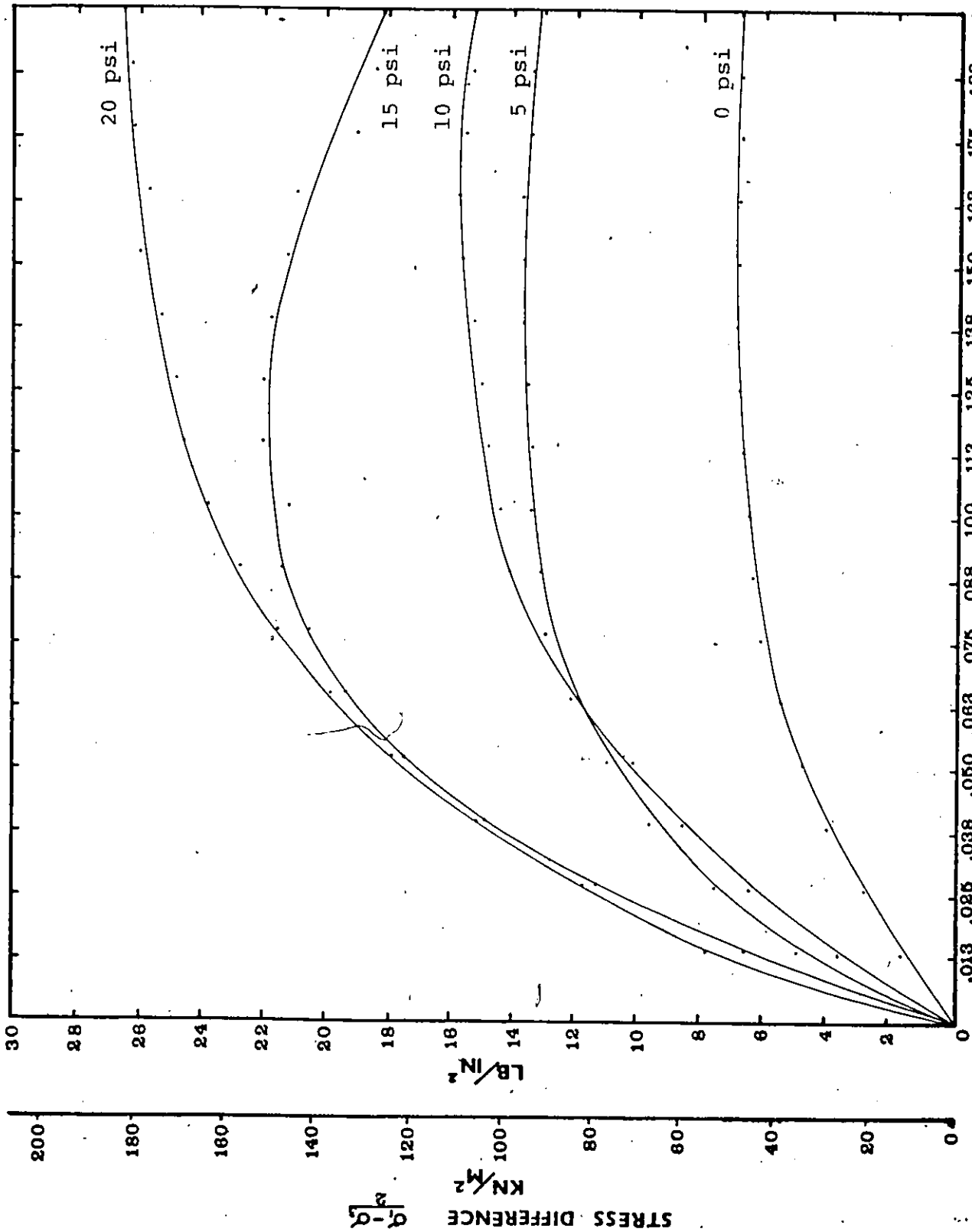

Fig. 4.12 A. Stress difference versus axial strain for 70°F and 80 min. set.

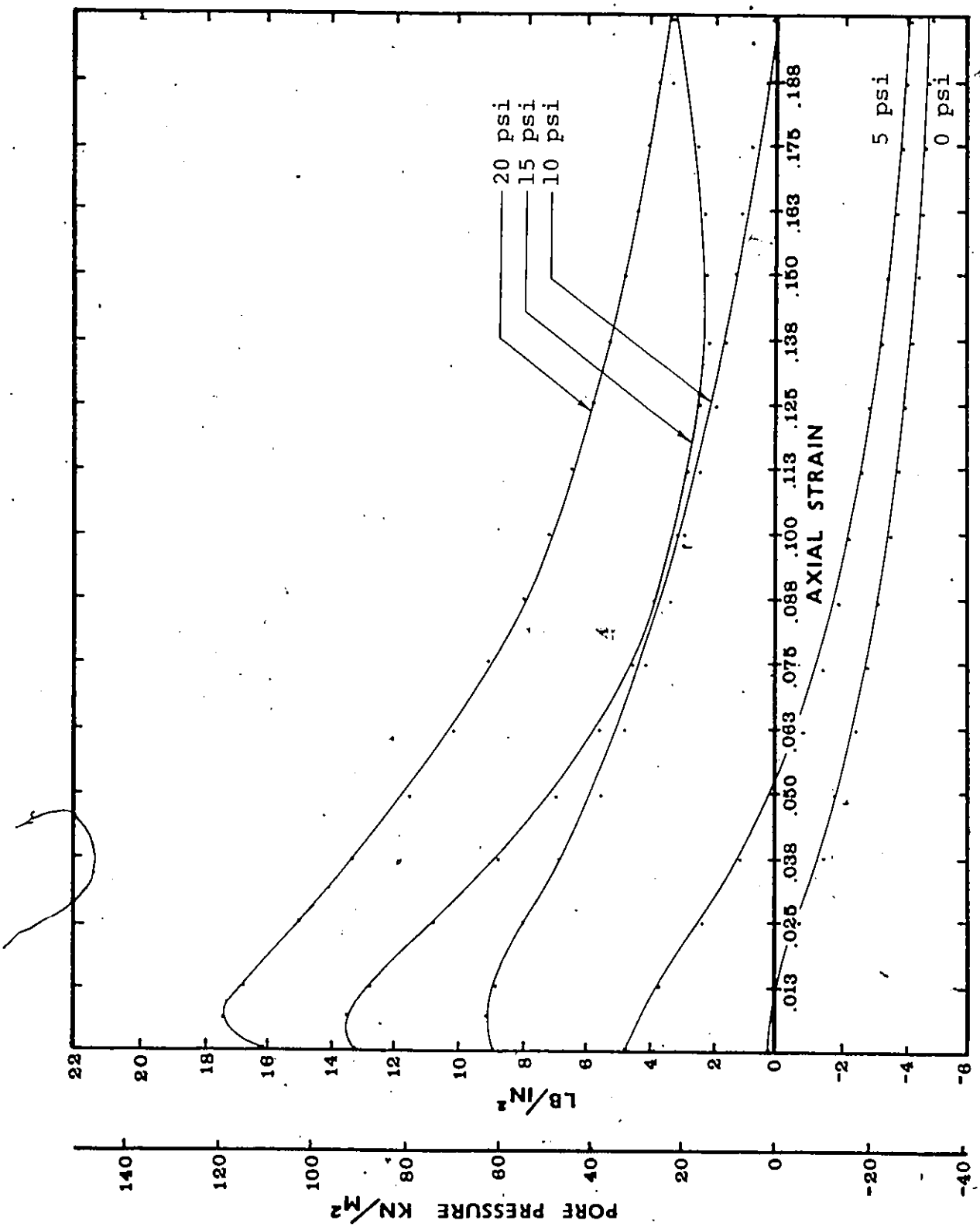

Fig. 4.12 B. Pore pressure versus axial strain for 70^0F and 80 min. set.

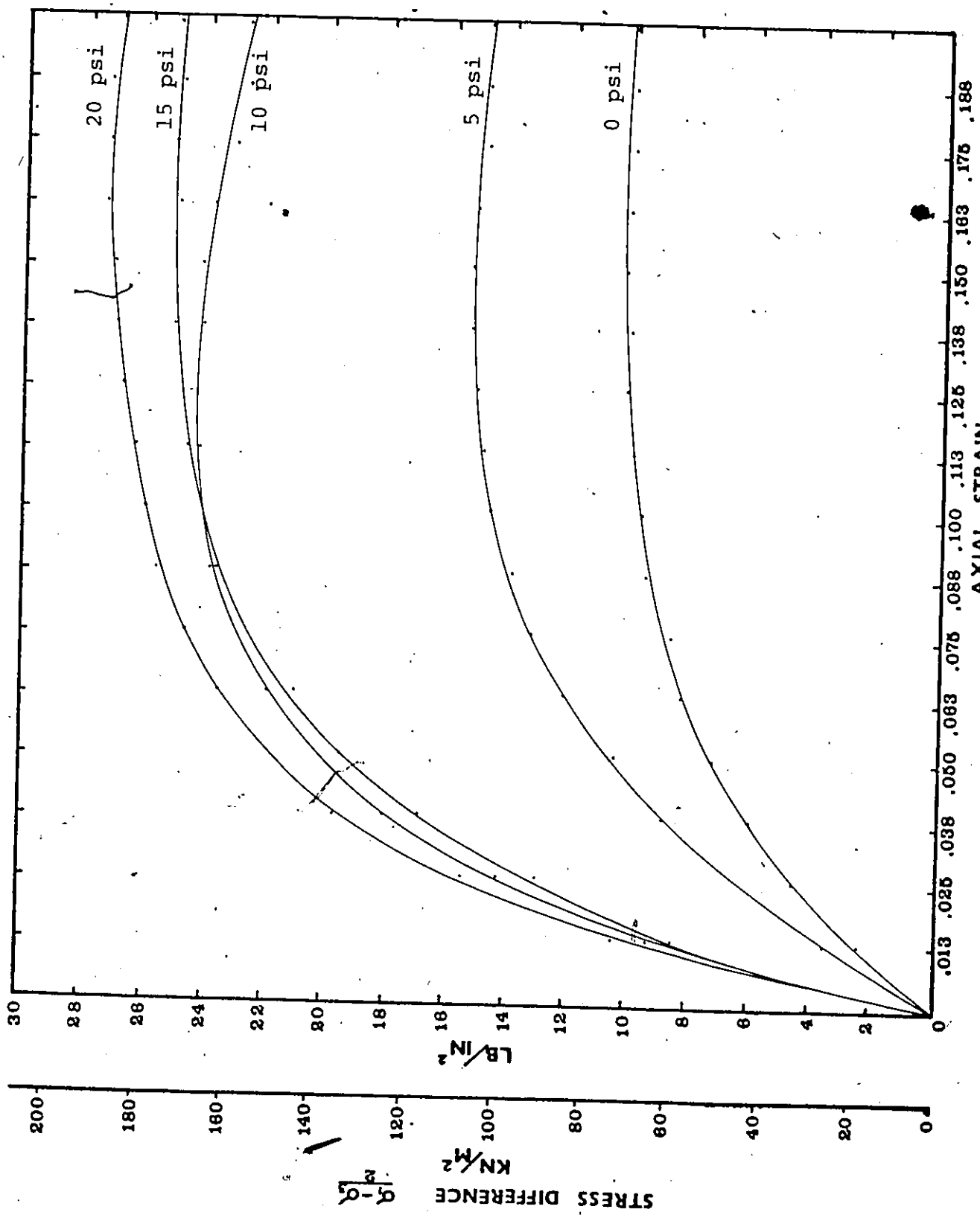

Fig. 4.13 A. Stress difference versus axial strain for 70°F and 40 min. set.

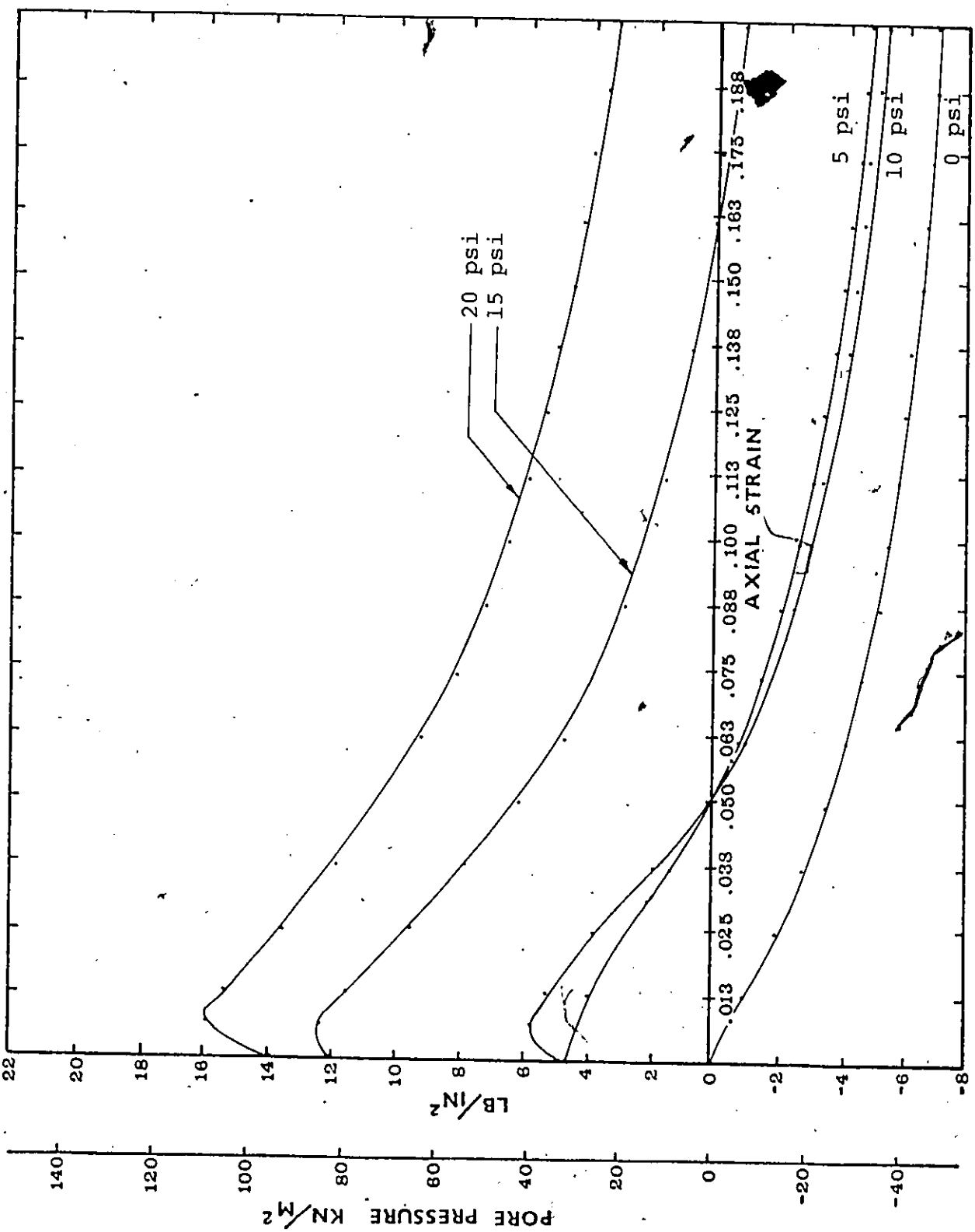

Fig. 4.13 B. Pore pressure versus axial strain for 70°F and 40 min. set.

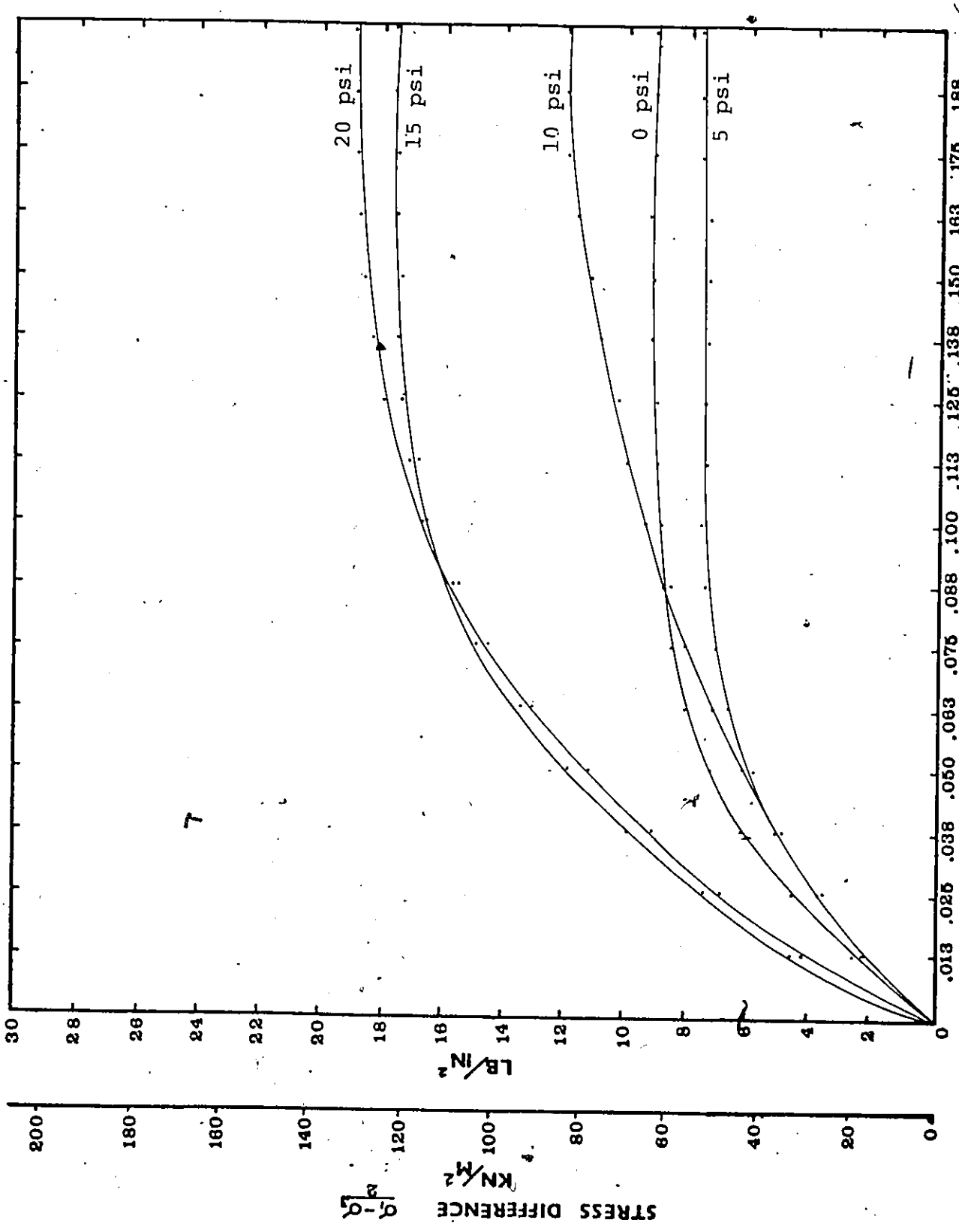

Fig. 4.14 A. Stress difference versus axial strain for 38°F and 160 min. set.

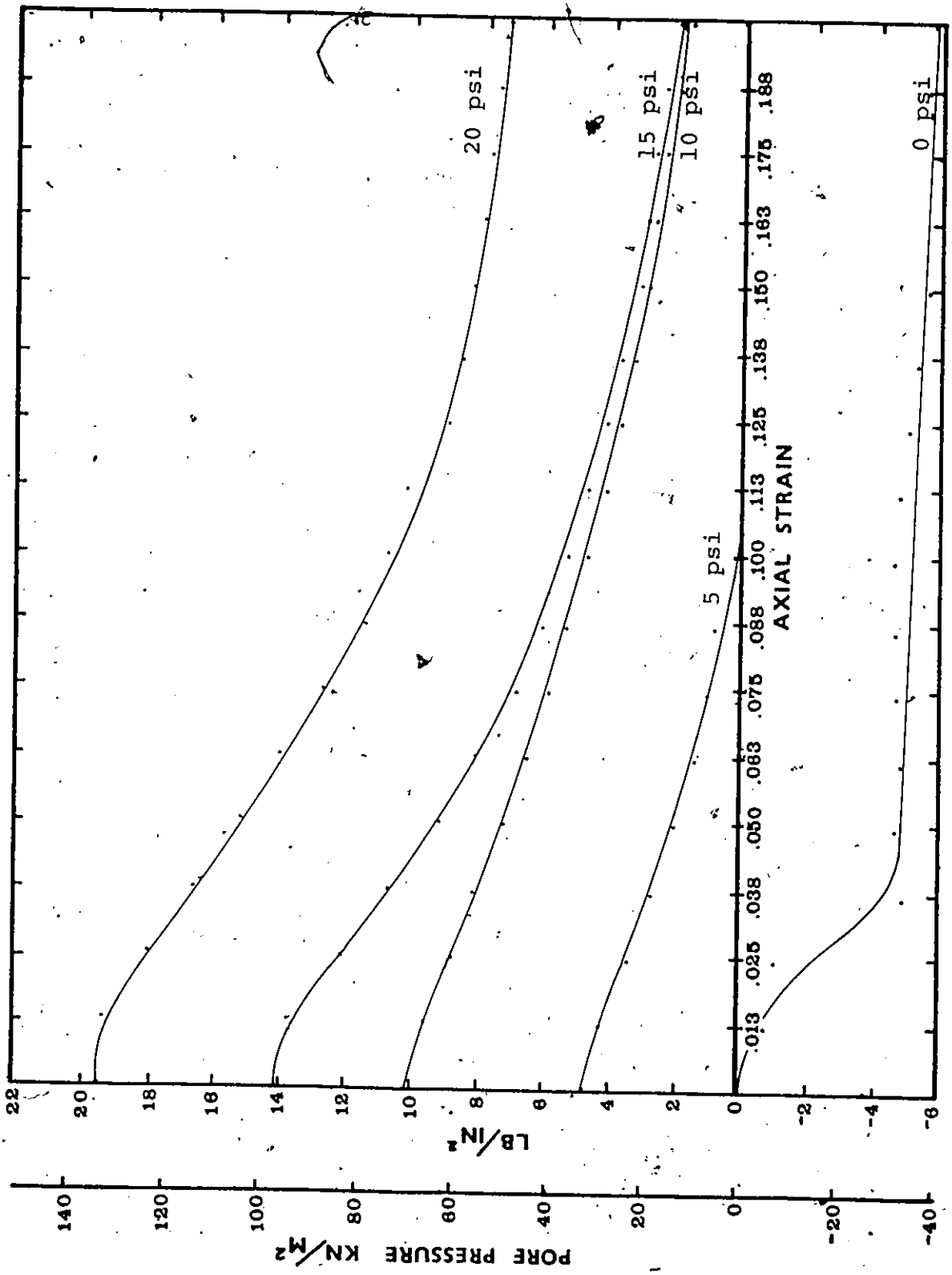

Fig. 4.14 B. Pore pressure versus axial strain for 38^0F and 160 min. set.

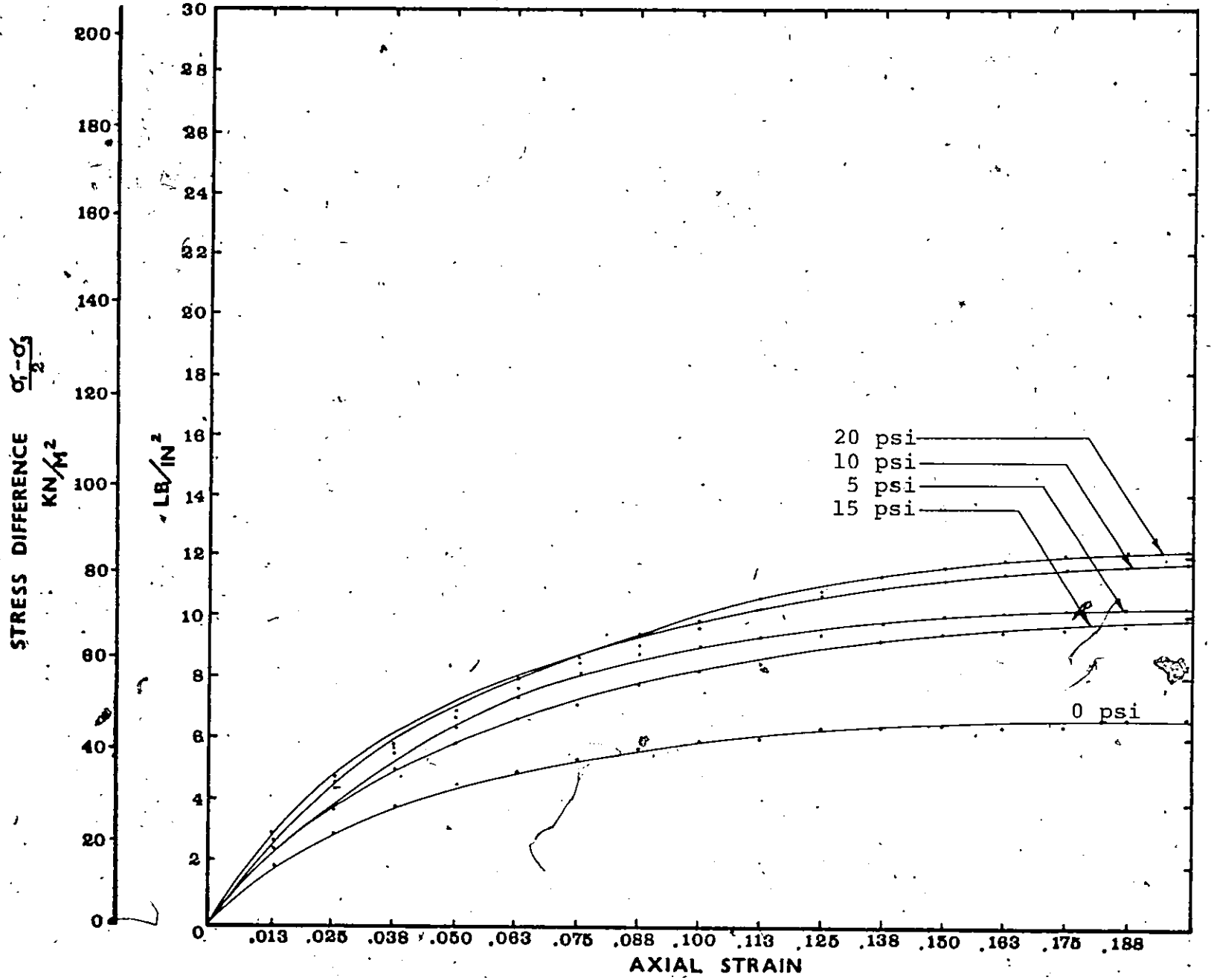

Fig. 4.15 A. Stress difference versus axial strain for 38°F and 120 min. set.

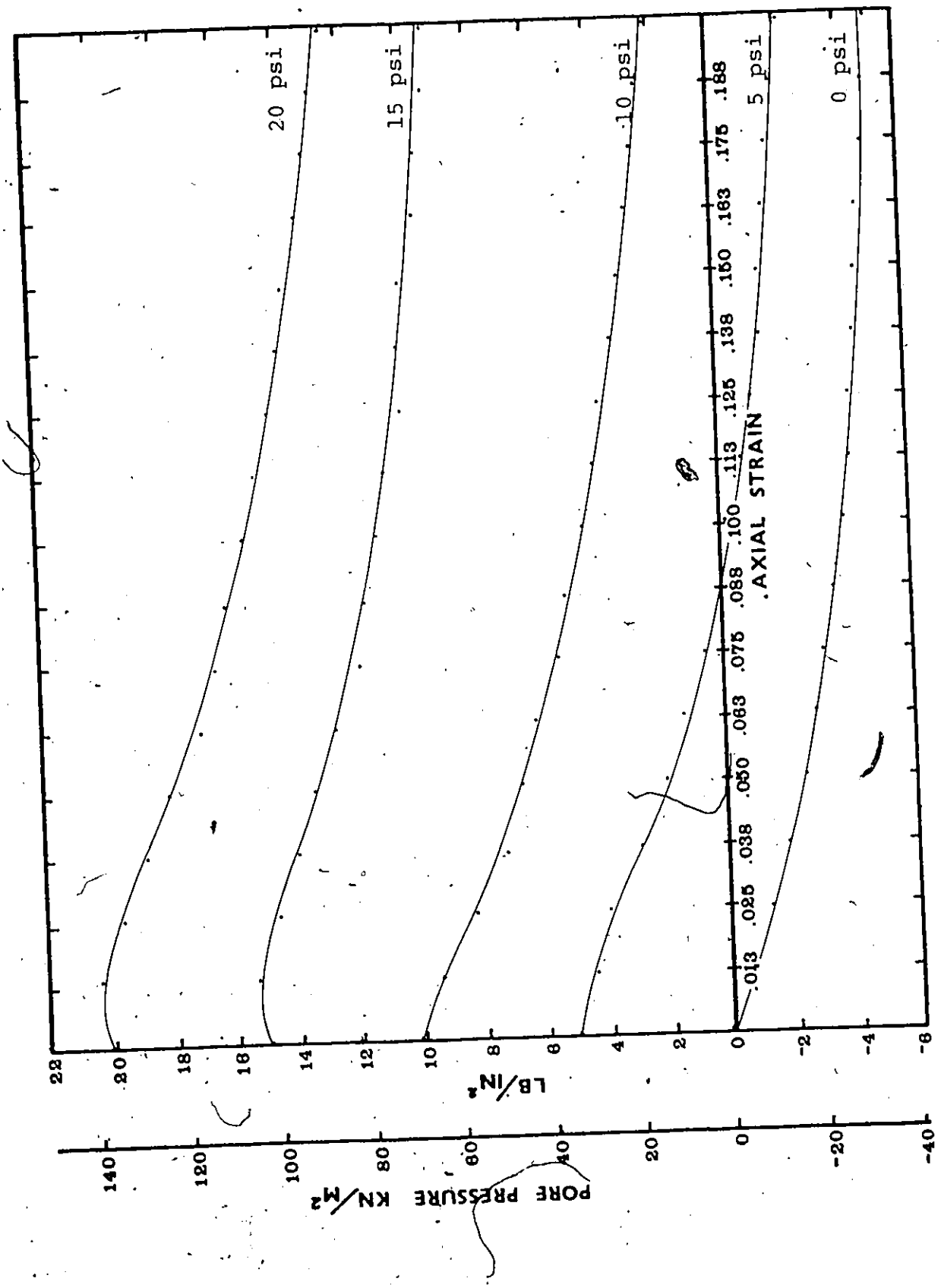

Fig. 4.15 B. Pore pressure versus axial strain for 38^{0}_{F} and 120 min. strain.

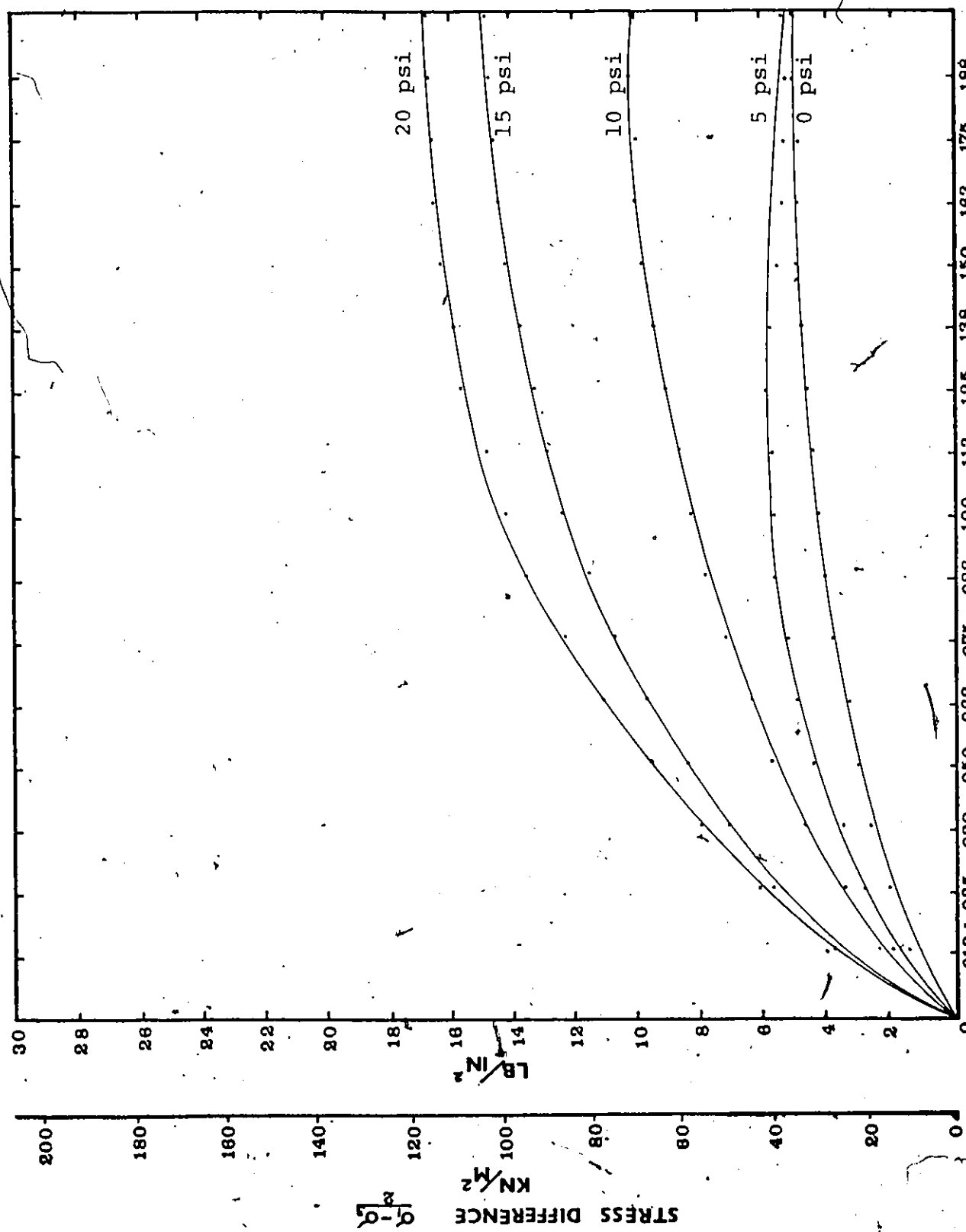

Fig. 4.16 A. Stress difference versus axial strain for 38°F and 80 min. set.

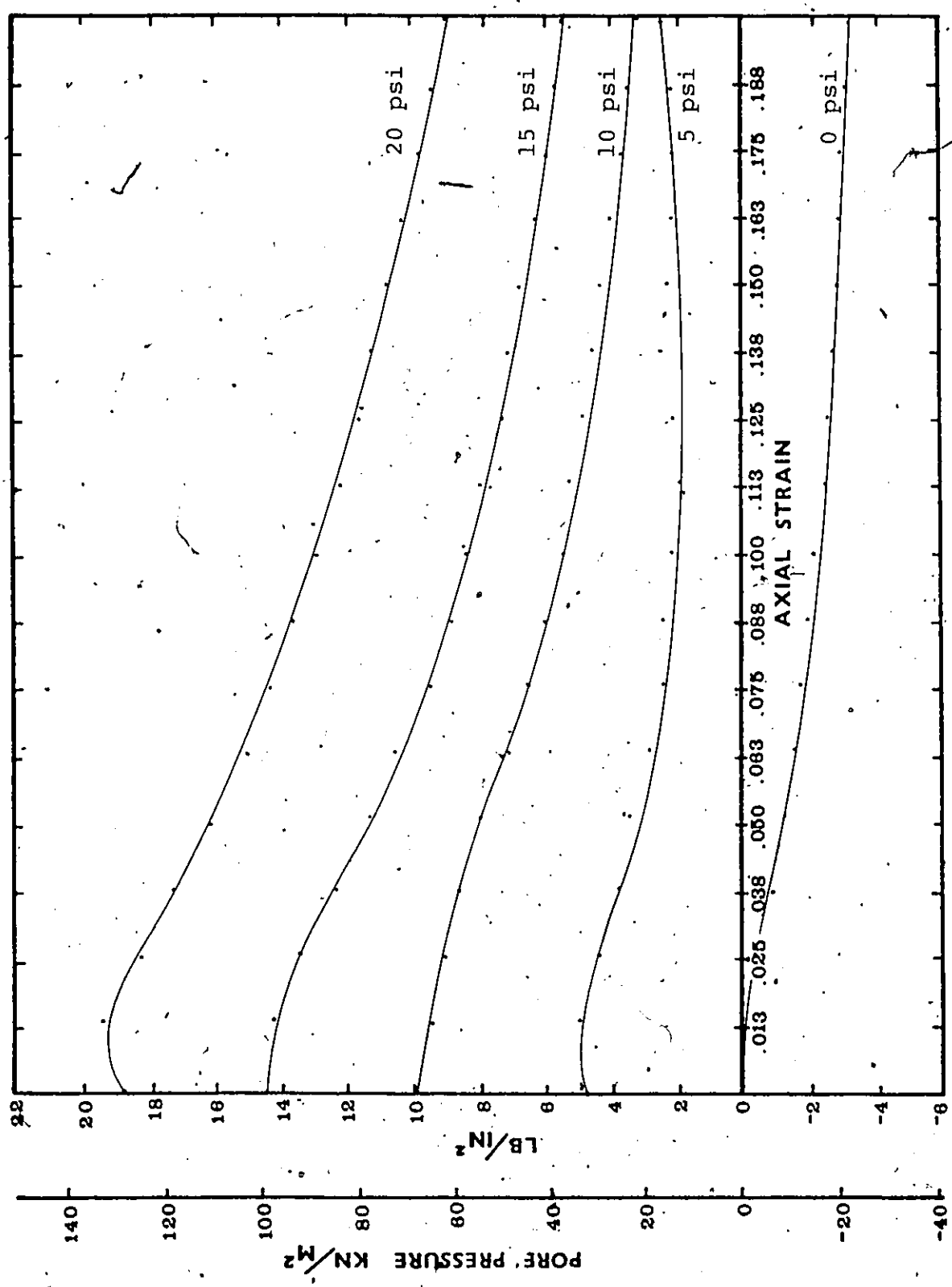

Fig. 4.16 B. Pore pressure versus axial strain for 38°F and 80 min. set.

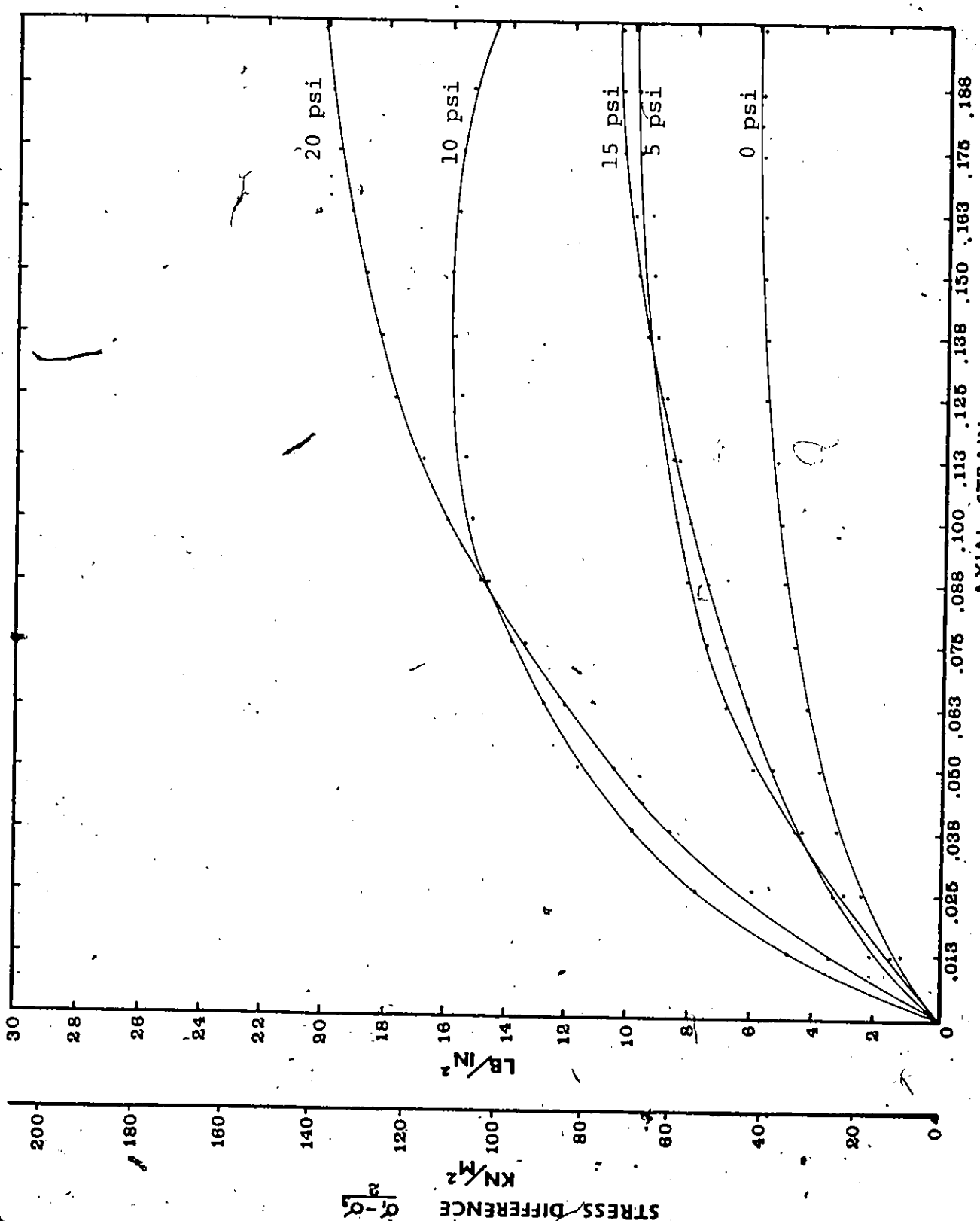

Fig. 4.17 A. Stress difference versus axial strain for 38°F and 40 min. set.

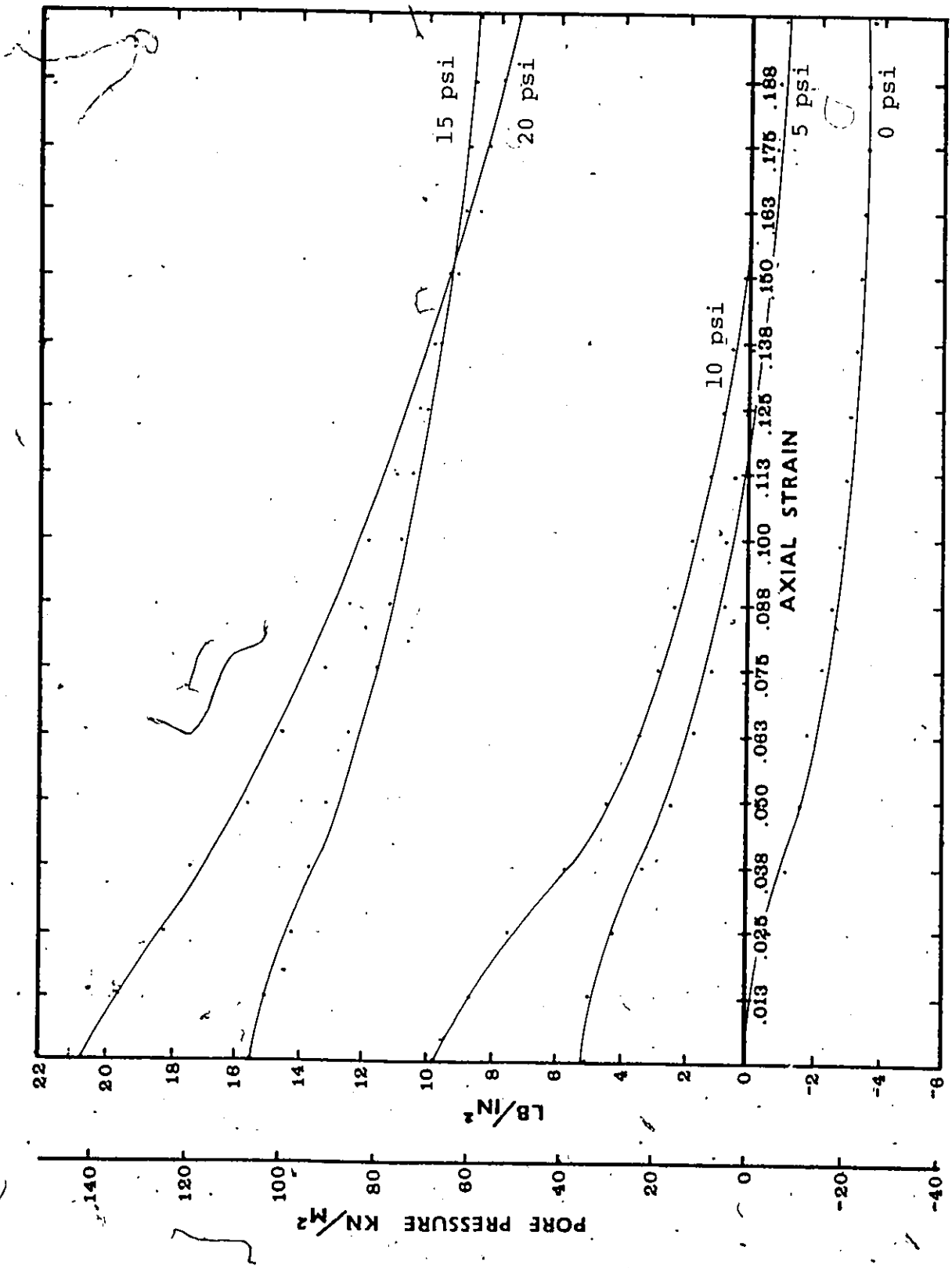

Fig. 4:17 B. Pore pressure versus axial strain for 38^0F and 40 min. set.

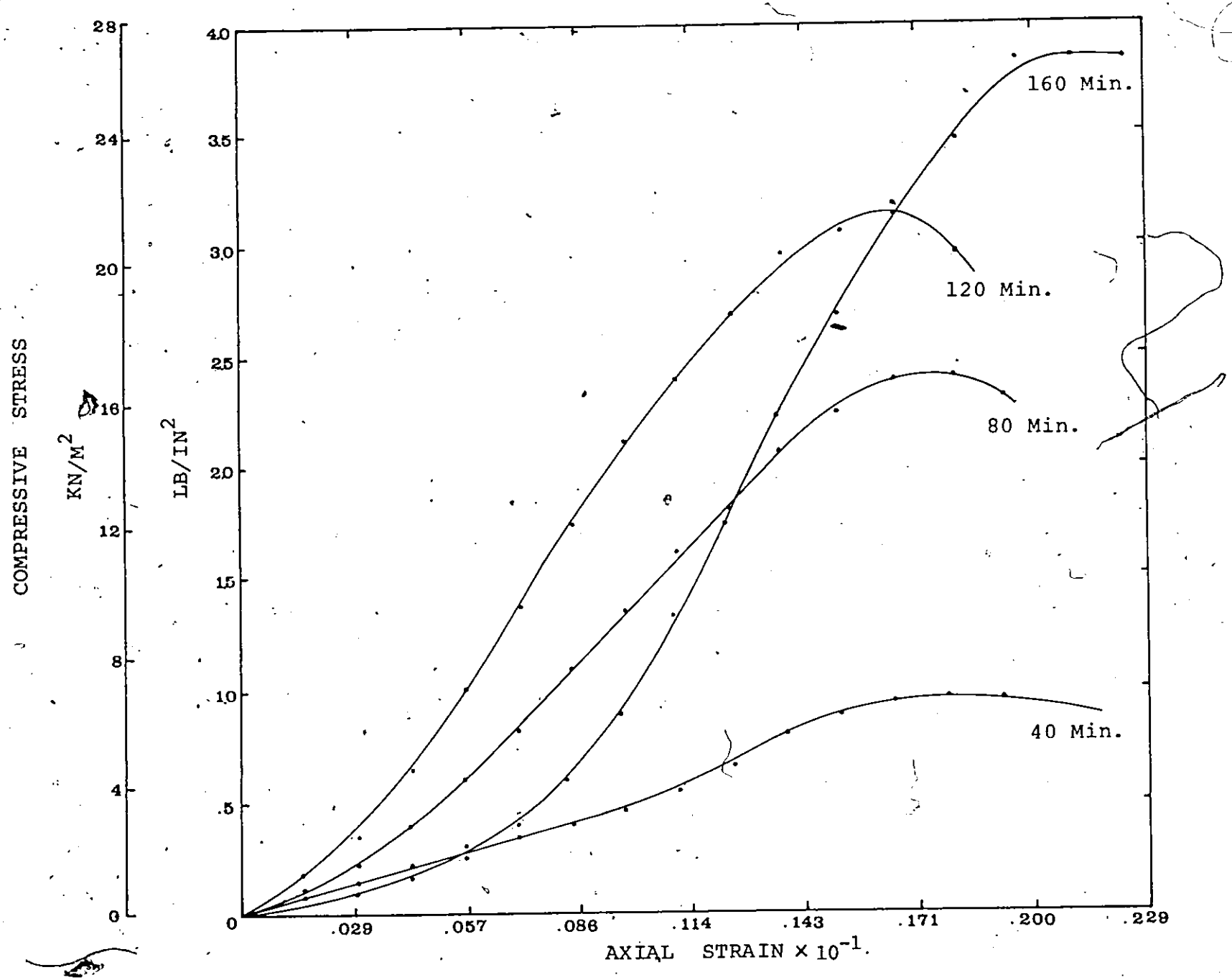

Fig. 4.18 A. Compressive stress versus axial strain at 70°F.

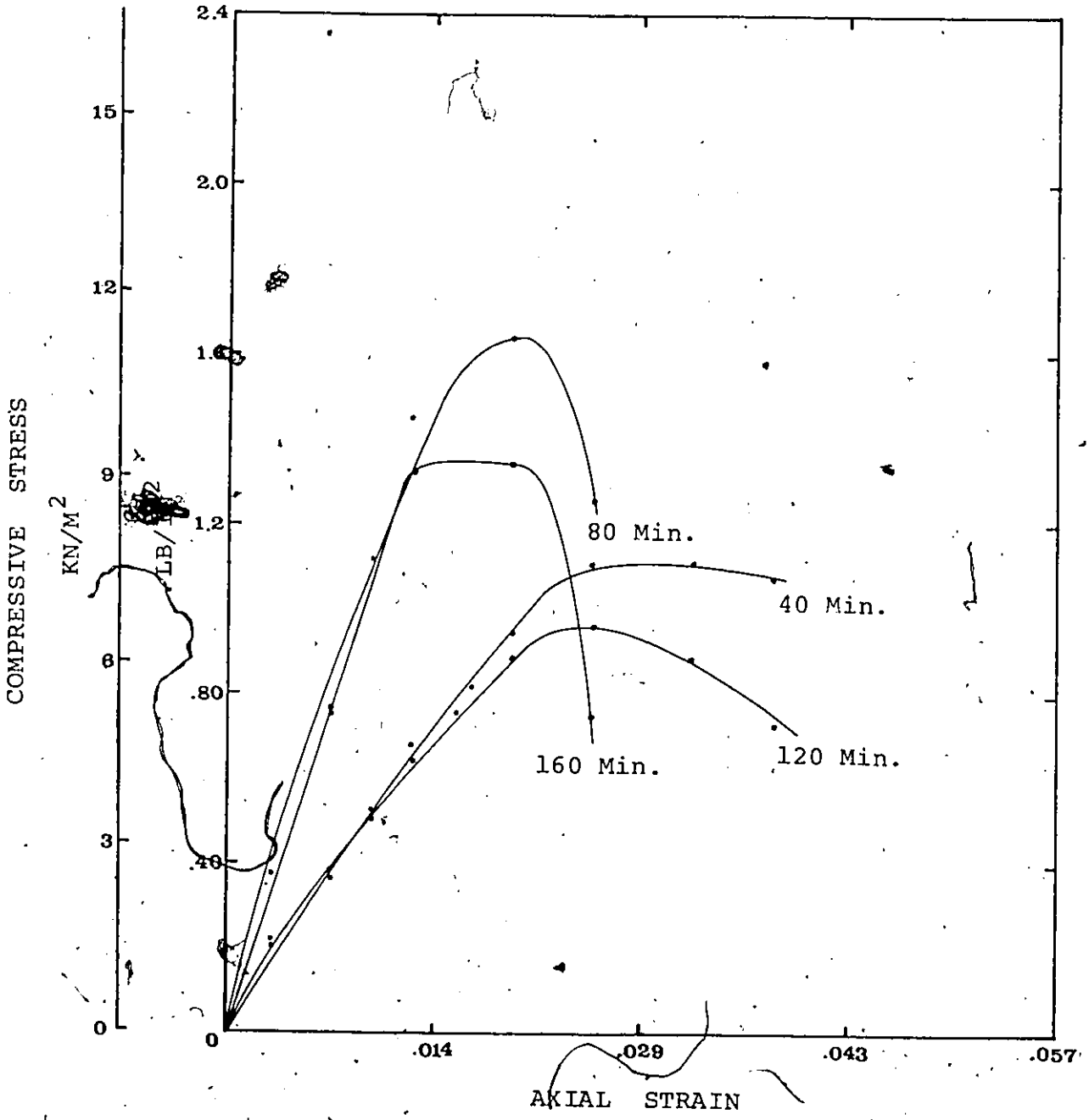

Fig. 4.18 B. Compressive stress versus axial strain at 38°F.

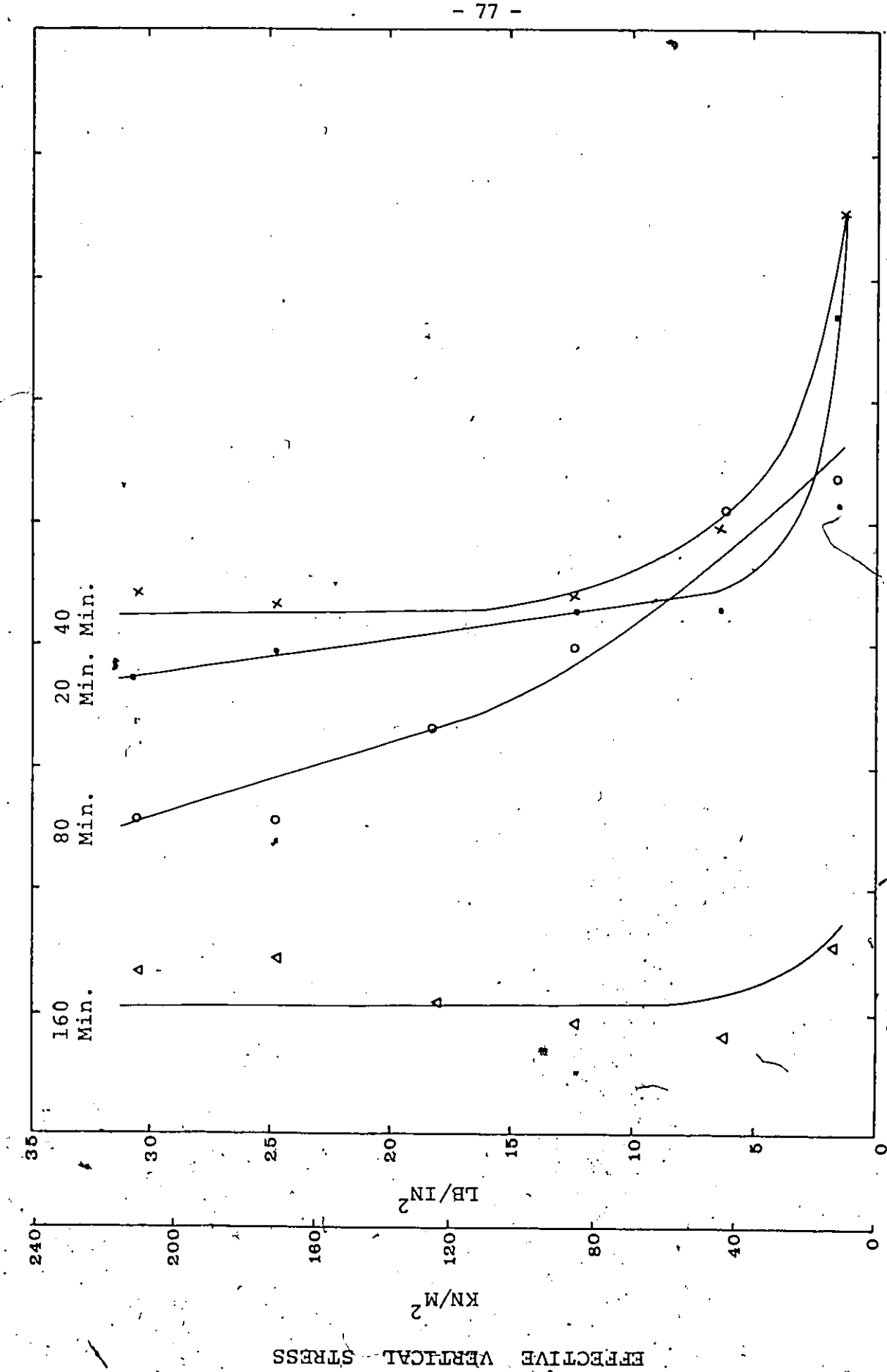

Fig. 4.19 A. K_o versus effective vertical stress at 70 F.

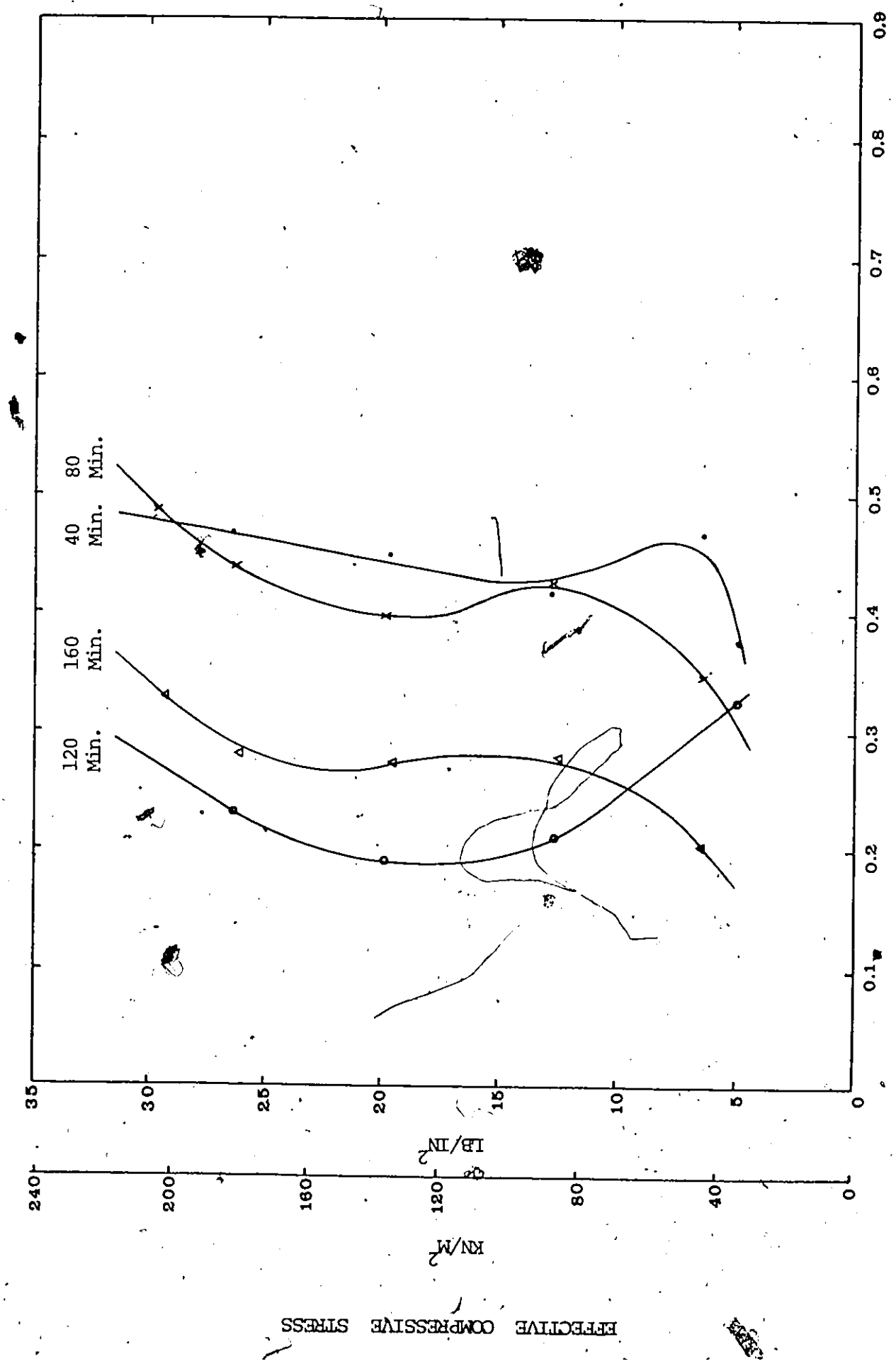

Fig. 4.19 B. K_0 versus effective vertical stress at 38^0F.

CHAPTER V

Analysis of Experimental Data

5.1 Choice of Shear Strength Theories

For the purpose of analysing and predicting the shear behaviour of fresh concrete, two shear strength theories were introduced in chapter II, namely the Mohr Coulomb theory and Rowe's theory. How useful these theories are depends on how well they satisfy the following two requirements (ref. 4.):

(1) The analytical requirement; the theory should be capable of summarizing the results of shear strength tests in the form of one or more fundamental strength parameters.

(2) The applicability requirement; the strength parameters should be directly applicable to the solution of problems dealing with shear strength such as lateral pressure calculations.

However, it is difficult to satisfy both of the above requirements simultaneously. For instance, the Mohr Coulomb theory describes the shear strength of a particulate mass in the form of two strength parameters; the effective cohesion and the effective friction angle. These however, are of a restricted analytical value because the Mohr Coulomb theory was derived for a continuum and cannot readily be applied to a dilatant particulate system. The strength parameters however, are easily applied to the evaluation of many common engineering problems dealing with the strength or stability of particulate systems. In comparison, the strength

parameters of Rowe's theory satisfy the analytical requirement allowing a more fundamental understanding of shear behaviour. However, Rowe's strength parameters do not satisfy the applicability requirement i. e. the parameters cannot be inserted into simple strength and stability equations because of the complex nature in which failure is assumed to occur.

In this investigation, both the Mohr Coulomb theory and Rowe's theory will be used to analyze the experimental results. Consequently, future investigators who may wish to apply the test results to workability and formwork pressure calculations will have a choice between two sets of strength parameters.

5.2 Choice of Failure Criteria

In the triaxial testing of soils it is generally accepted that a test sample has failed when the maximum stress difference $\sigma_1 - \sigma_3$ has been reached. For highly plastic materials, this condition of failure is sometimes not achieved until the test sample has undergone large axial strain. For this reason, failure has also come to be arbitrarily defined as the instant a test sample achieves 20 % axial strain. Intuitively, this definition of failure seems correct, since it not only imposes an upper limit to the stresses a soil will be subjected to in the field but also to the deformations wich are likely to occur.

For fresh concrete in formwork, it may be inappropriate to use 20 % axial strain as a failure criterion because such large strains are never likely to be encountered in real practice. However, it is difficult if not impossible to choose any single value of axial strain as a failure criterion since the deformations existing in formwork can vary significantly depending

on the formwork material, the quality of work in constructing the formwork, the spacing between ties etc. It was therefore decided to adopt two failure criteria for analyzing the test results:

(1) The maximum stress difference or 20 % axial strain.

(2) The maximum stress difference or 10 % axial strain.

5.3 Mohr Coulomb Analysis

In figures 5.1 to 5.4, the triaxial test results have been plotted on a p' - q plane. Each of the four lines corresponding to set times of 40, 80, 120 and 160 minutes represents a linear regression of five stress points for cell pressures of 0, 5, 10, 15 and 20 psi. Given such a plot, the angle α and intercept A' on the 'q' axis for any line may be related to the Mohr Coulomb strength parameters by means of the following two equations:

$$\sin \phi' = \tan \alpha'$$

$$C' = \frac{A'}{\cos \phi'}$$

The lines were first regressed through the origin to get an initial estimate of the friction angles. These friction angles were then used to estimate the cohesion C' for each of the four set times. The lines were then linearly regressed through their respective q' intercepts.

Figure 5.5 shows the relation between cohesion and set time at 70^0 F and 38^0 F. Each point represents the effective cohesion for a given set time and was evaluated using the results of the unconfined compression tests. The relation between the effective cohesion C' and the drained compressive strength qu is given by

$$C' = \frac{q_u}{2} \tan\left(45 - \frac{\phi'}{2}\right)$$

This relation was derived from (1.3.1) by setting $P_{HA} = 0$ and $\sigma_z = q_u$. A linear regression was performed on the points with the assumption that cohesion is initially zero and increases linearly with set time. Since the friction angle ϕ' depends on how failure is defined, two lines have been drawn for each temperature; one corresponding to a 10% failure strain and the other to a 20% failure strain. The results of the Mohr Coulomb analysis have been summarized in table 5.6.

5.4 Rowe's Analysis

Figures 5.7 to 5.10 represent plots of the triaxial test results on $\sigma_1'/\nu' - \sigma_3'$ planes. Four lines have been drawn in each figure for set times of 40, 80, 120 and 160 minutes. Each line has been linearly regressed through five points corresponding to 0, 10, 15 and 20 psi cell pressures. The slopes represent $K_1 = 2\tan^2(45 + \frac{\phi_\mu'}{2})$ in Rowe's equation corresponding to the set times for which the lines have been drawn. The σ_1'/ν' intercepts represent $K_2 = 8C_\mu' \tan(45 + \frac{\phi_\mu'}{2})$. Knowing the values of K_1 and K_2, the friction angle ϕ_μ' and the cohesion C_μ' corresponding to Rowe's theory may easily be evaluated. Initially it was assumed that the cohesion was negligably small and the lines were made to pass through the origin of the coordinate system. From the slopes, initial estimates of ϕ_μ' were made from which the cohesion C_μ' and subsequently K_2 were estimated for 70^0F. The lines were then linearly regressed a second time through their appropriate σ_1'/ν' intercepts to obtain more accurate values of ϕ_μ' at 70^0F. At 38^0F, accurate values of the instantaneous Poisson's ratio ν' could not be obtained because of the highly plastic nature of the concrete specimens.

Consequently, K_2 and correspondingly C'_μ could not be estimated. Therefore, a second linear regression was not possible at 38^0F. However, because the difference in ϕ'_μ at 70^0F between a linear regression through the origin and a linear regression through K_2 is in the order of 1^0 to 2^0, it was felt that the first estimates of ϕ'_μ at 38^0F adequately represented the true angles of internal friction.

Figure 5.11 shows the relation between cohesion and set time for a temperature of 70^0F. Each of the points was evaluated by applying Rowe's equation to the unconfined compressive strengths using the previously calculated friction angles corresponding to a 10% and a 20% failure strain. Again a straight line was regressed through the points on the assumption that cohesion is initially zero and increases in a linear fashion with set time. The results of Rowe's analysis have been summarized in table 5.12.

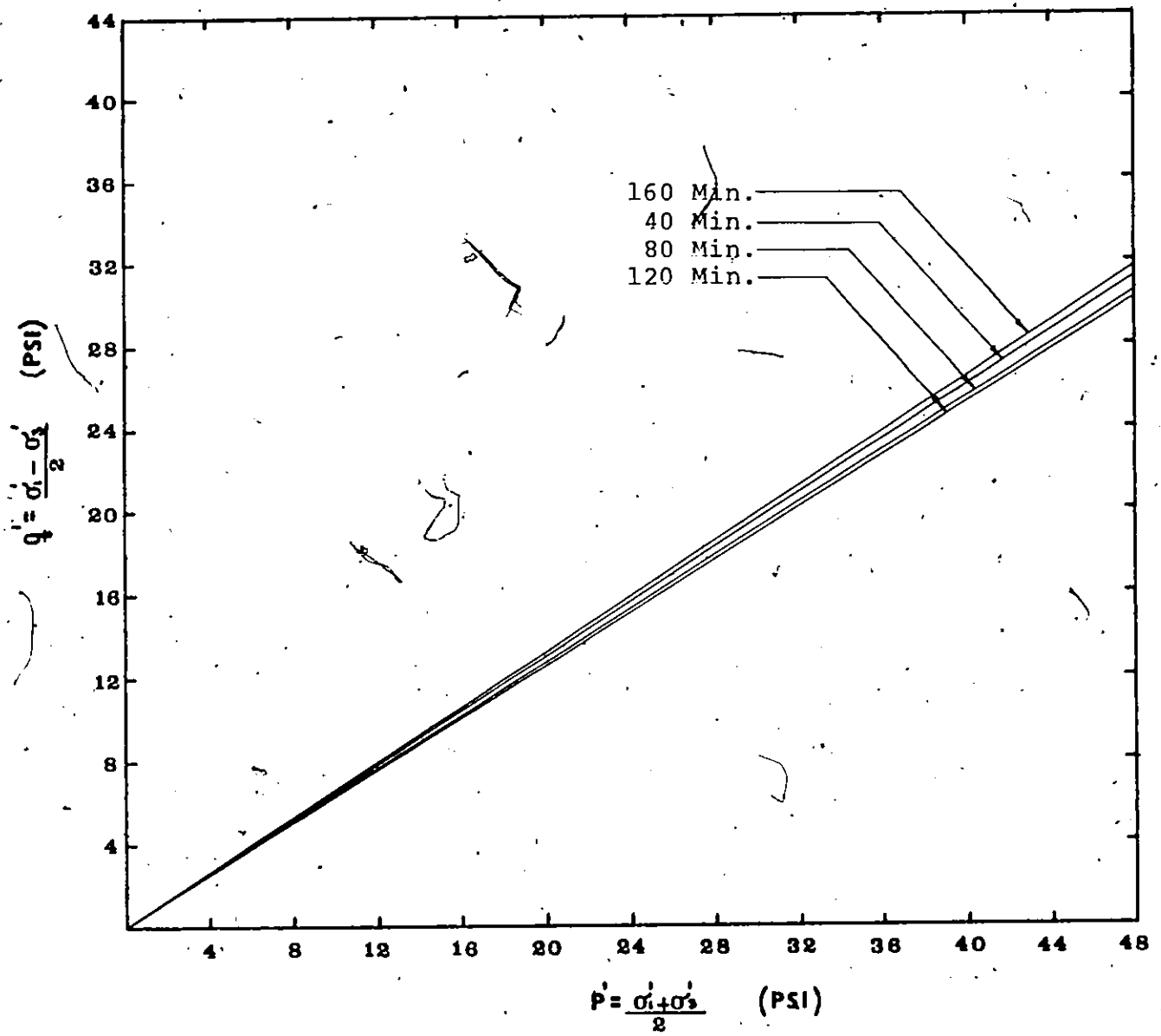

Fig 5.1. p' - q' plot for 70^{0}F and 10% failure strain

SET TIME	α'	σ_a'	ϕ'
160 MIN	33.3°	1.9°	41°
120 MIN	32.1°	1.2°	39°
80 MIN	32.4°	0.6°	39°
40 MIN	33.1°	1.6°	41°

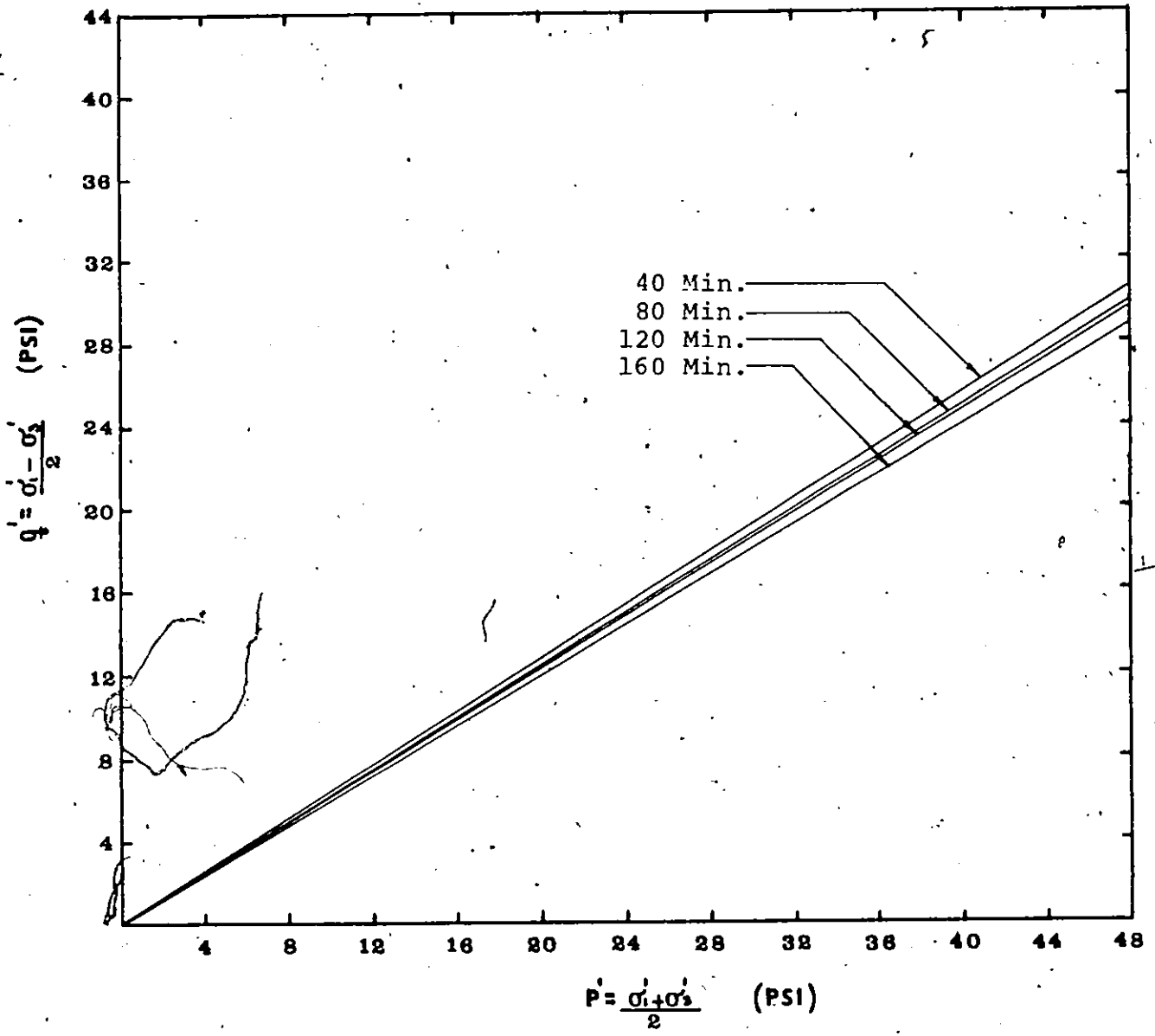

SET TIME	α'	$\sigma_n'^*$	ϕ'
160 MIN	31.1°	0.9°	37°
120 MIN	31.7°	1.7°	38°
80 MIN	31.9°	0.6°	39°
40 MIN	32.5°	0.4°	40°

Fig. 5.2. . p' - q' plot for 38°F and 10% failure strain.

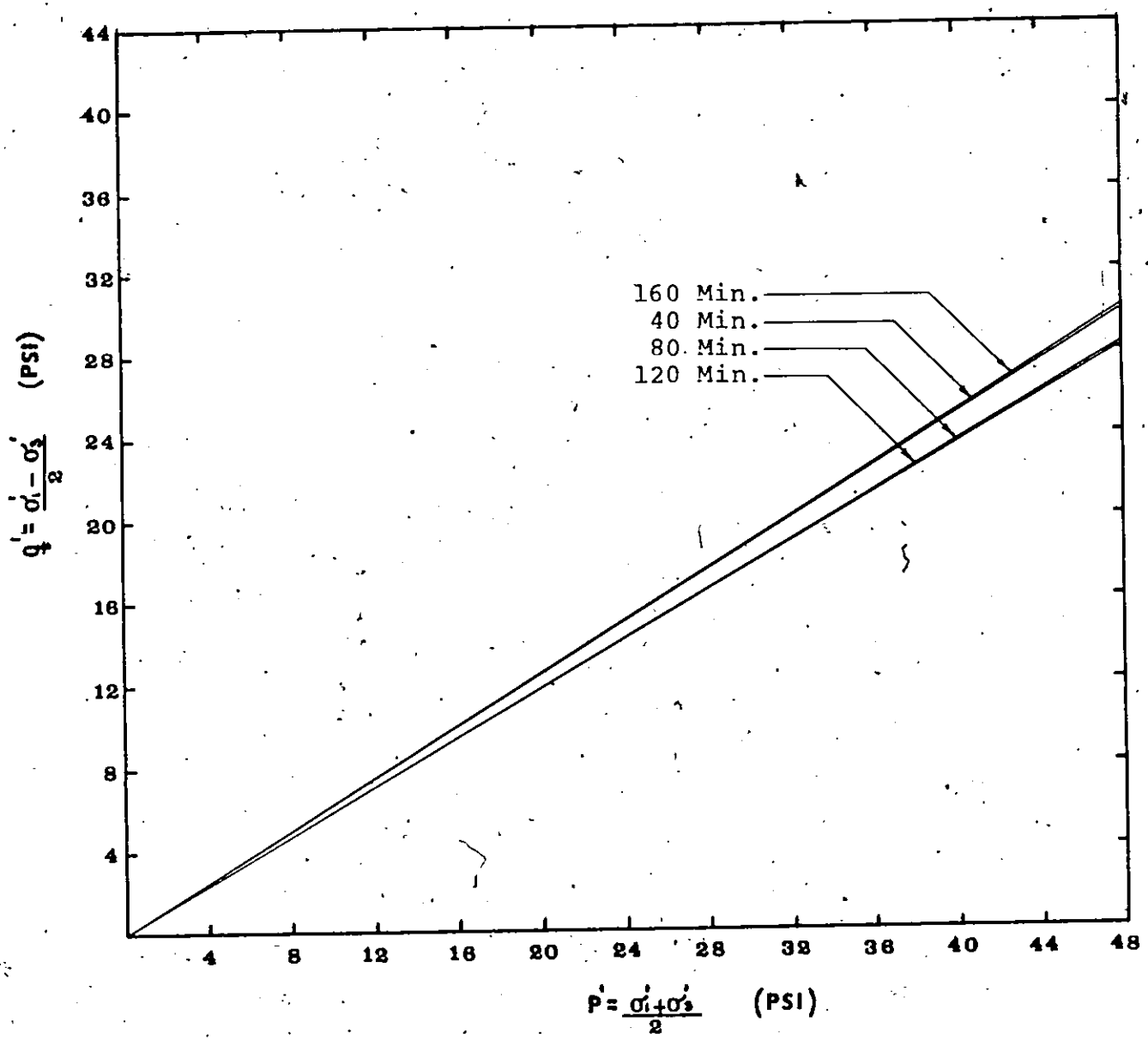

SET TIME	α'	$\sigma_n'^{\#}$	ϕ'
160 MIN	32°	2.7°	39°
120 MIN	30.2°	1.4°	36°
80 MIN	30.4°	1.7°	36°
40 MIN	31.9°	0.9°	38°

Fig. 5.3. p' - q' plot for 70^{0}F and 20% failure strain.

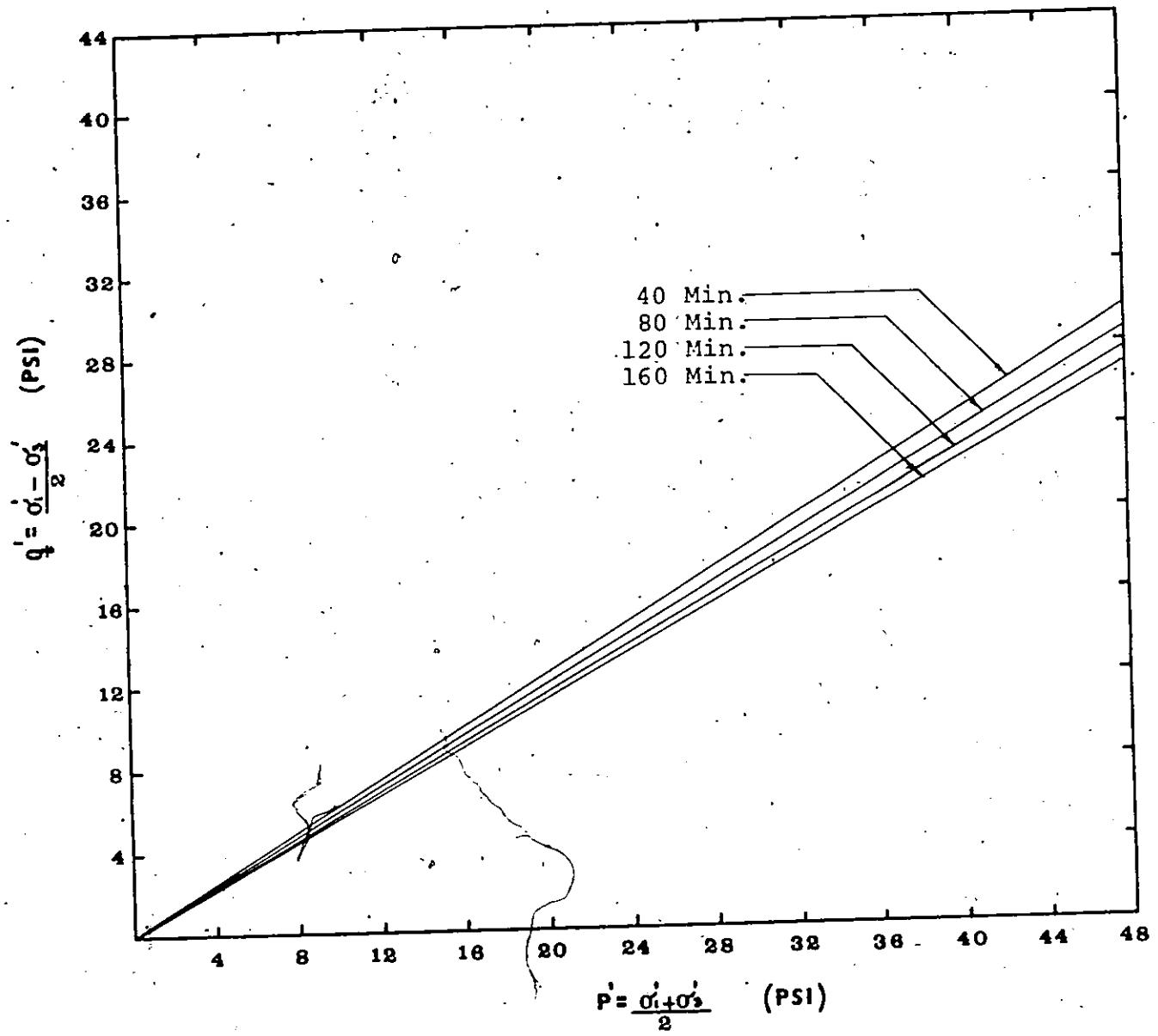

SET TIME	α'	σ_a'	ϕ'
160 MIN	29.3°	0.5°	34°
120 MIN	29.6°	1.1°	35°
80 MIN	30.7°	1.5°	36°
40 MIN	31.6°	1.1°	38°

Fig. 5.4. p' - q' plot for 38^0F and 20% failure strain.

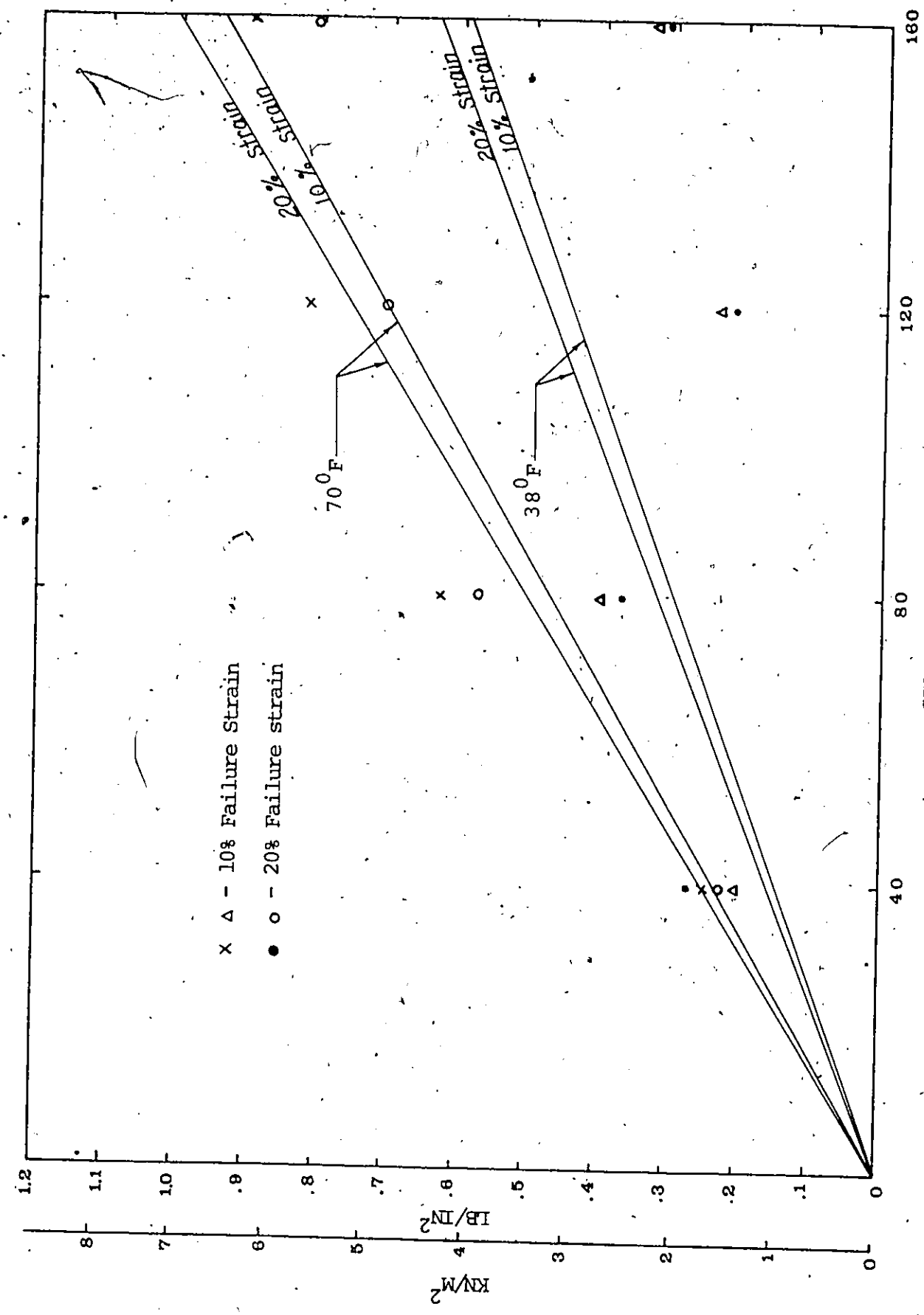

Fig. 5.5. Cohesion versus set time from Coulomb's analysis.

(a) Failure Criterion; Maximum Stress Difference or 10 % axial strain

Temperature	Set Time	Effective Friction Angle ϕ'	$\sigma_{\phi'}^*$	Cohesion C'	$\sigma_{c'}^*$
70^0 F	40 min.	41^0	0.4^0	.23 psi	.04 psi
	80	39^0	0.6^0	.46	.06
	120	39^0	1.2^0	.71	.10
	160	41^0	1.6^0	.95	.13
38^0 F	40	40^0	0.4^0	.16	.09
	80	39^0	0.6^0	.31	.17
	120	38^0	1.7^0	.47	.25
	160	37^0	0.9^0	.62	.38

(b) Failure Criterion; Maximum Stress or 20 % axial strain

Temperature	Set Time	Effective Friction Angle ϕ'	$\sigma_{\phi'}^*$	Cohesion C'	$\sigma_{c'}^*$
70^0 F	40 min.	38^0	0.9^0	.25 psi	.06 psi
	80	36^0	1.7^0	.50	.11
	120	36^0	1.4^0	.75	.15
	160	39^0	2.7^0	1.1	.21
38^0 F	40	38^0	1.1^0	.17	.09
	80	36^0	1.5^0	.33	.18
	120	35^0	1.1^0	.50	.28
	160	34^0	0.5^0	.66	.38

Table 5.6. Results of Mohr Coulomb Analysis.

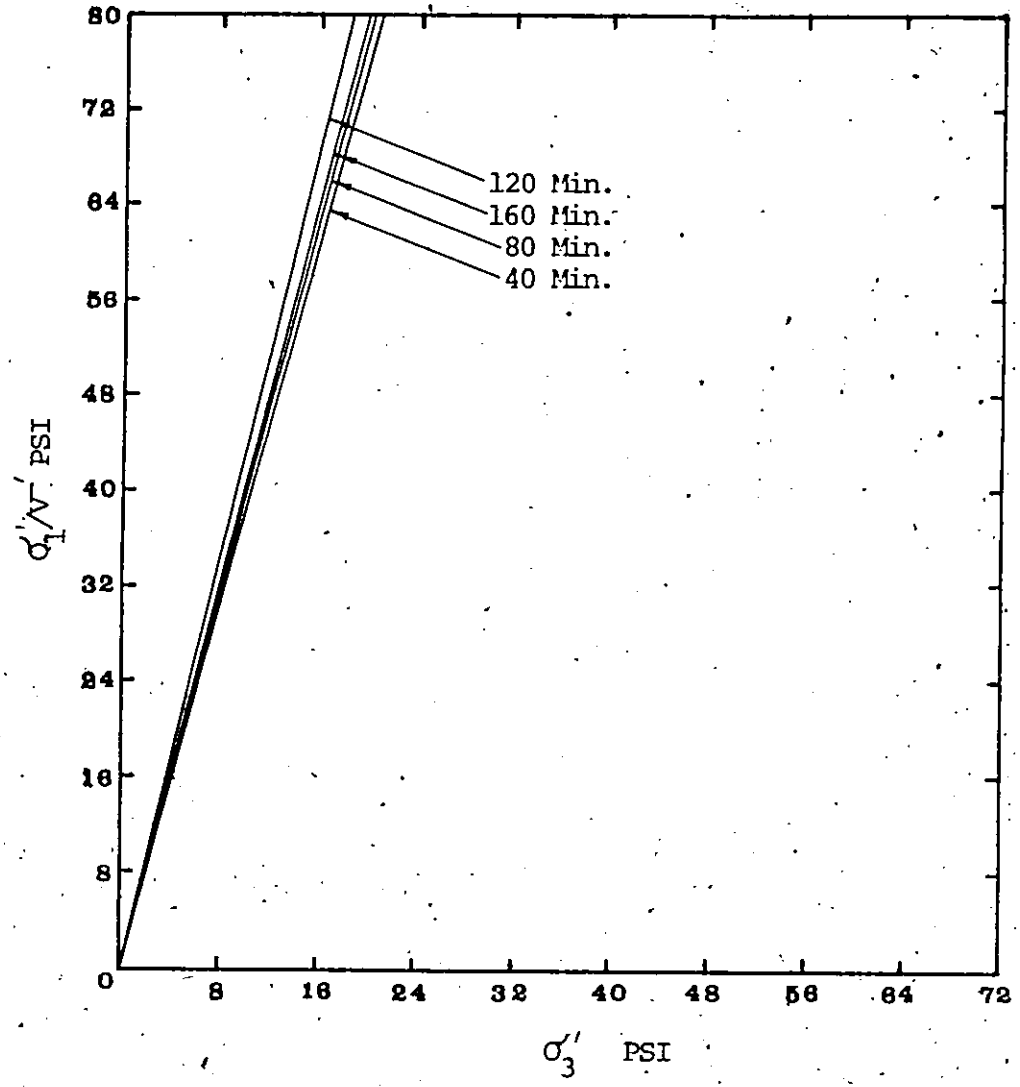

Fig. 5.7. σ_1' versus σ_3' for 70^{0}F and 10% failure strain.

SET TIME	K_1	$\sigma'^{*}_{K_1}$	ϕ'_μ
160 Min.	3.93	0.44	19°
120	4.12	0.38	20°
80	3.83	0.26	18°
40	3.74	0.28	18°

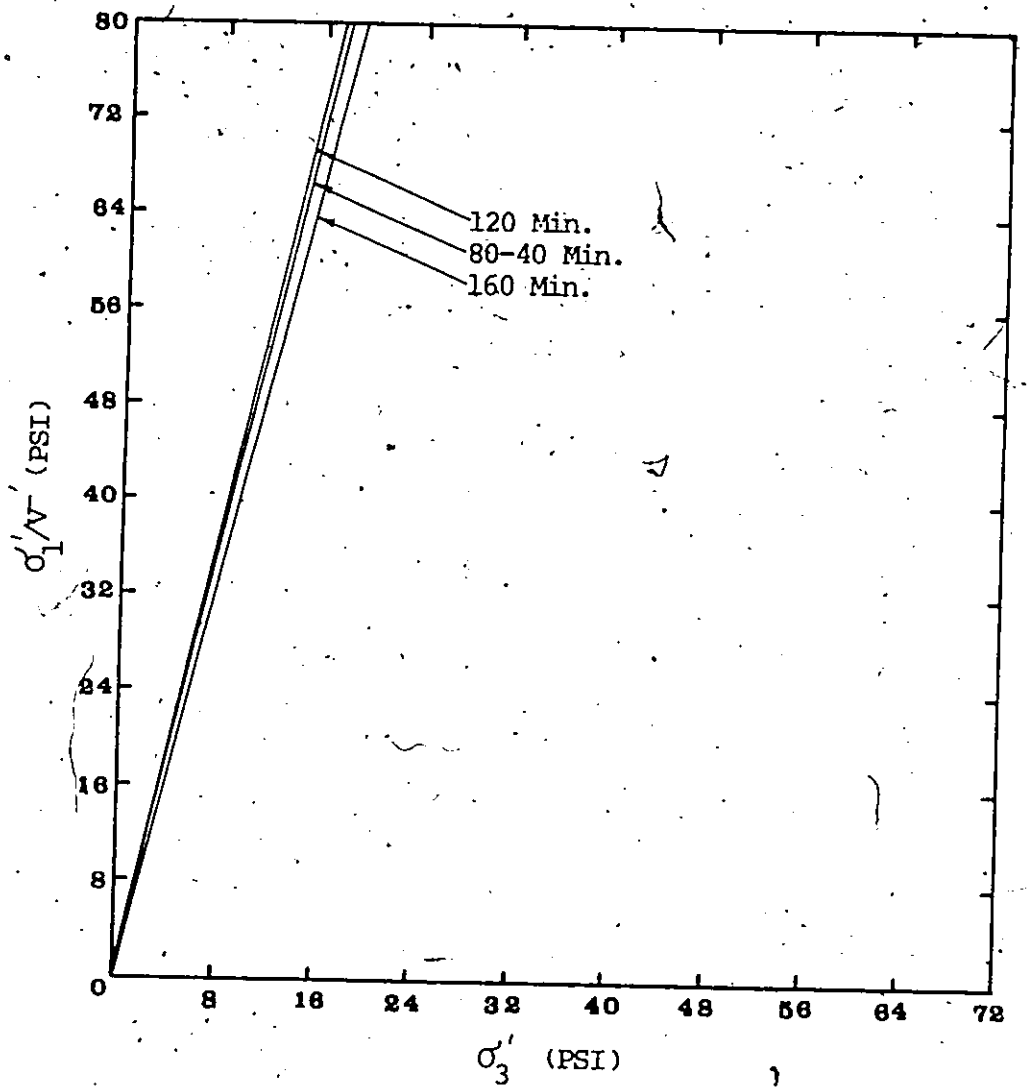

Fig. 5.8. $\frac{\sigma_1'}{V'}$ versus σ_3' for 38^0F and 10% failure strain.

SET TIME	K_f	σ'^{*}_{Kf}	ϕ'_μ
160 Min.	4.02	0.52	20°
120	4.61	1.29	23°
80	4.47	0.45	22°
40	4.47	0.50	22°

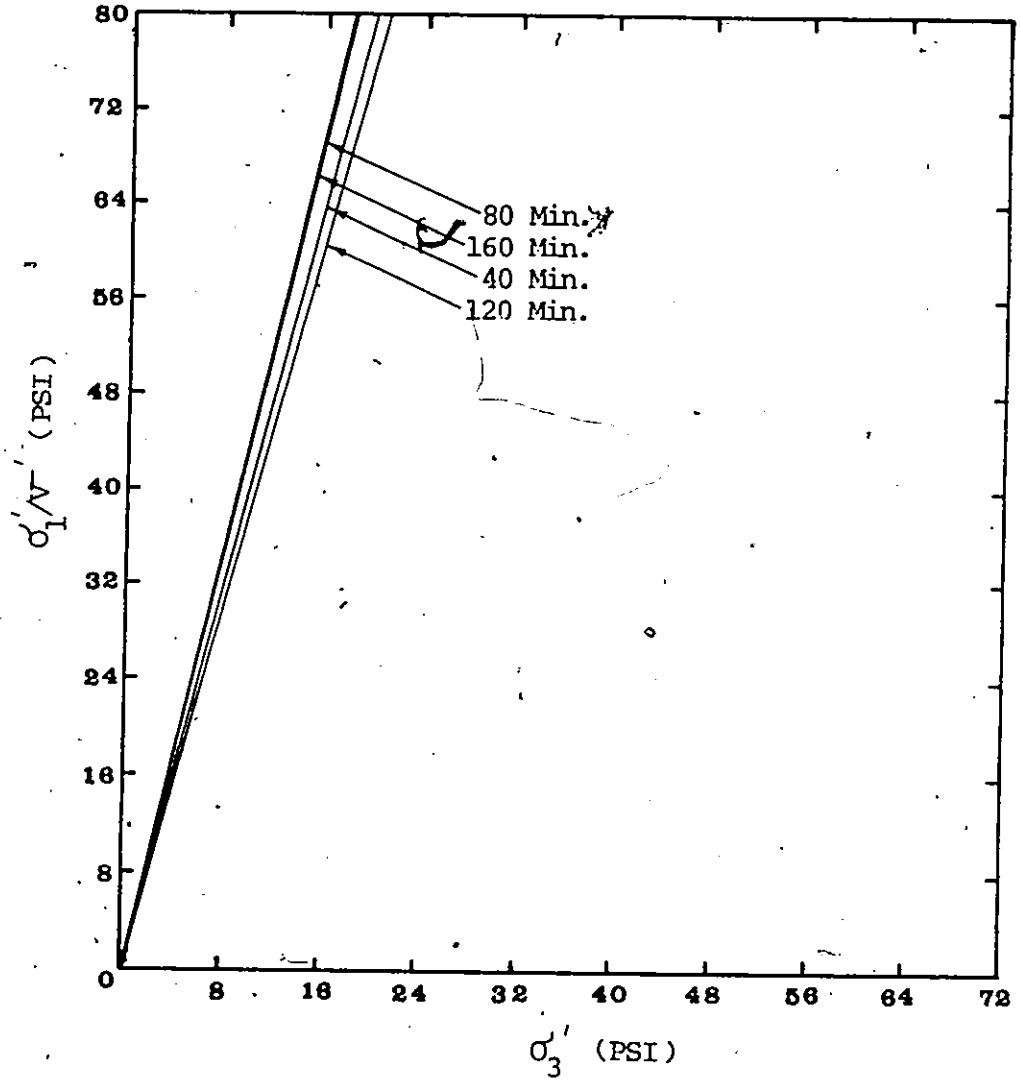

Fig. 5.9. $\frac{\sigma_1'}{V'}$ versus σ_3' for 70^0F and 20% failure strain.

SET TIME	K_1	$\sigma'^{*}_{K_1}$	ϕ'_μ
160 Min.	4.25	1.0	21°
120	3.73	0.66	18°
80	4.30	1.4	21°
40	3.95	0.37	19°

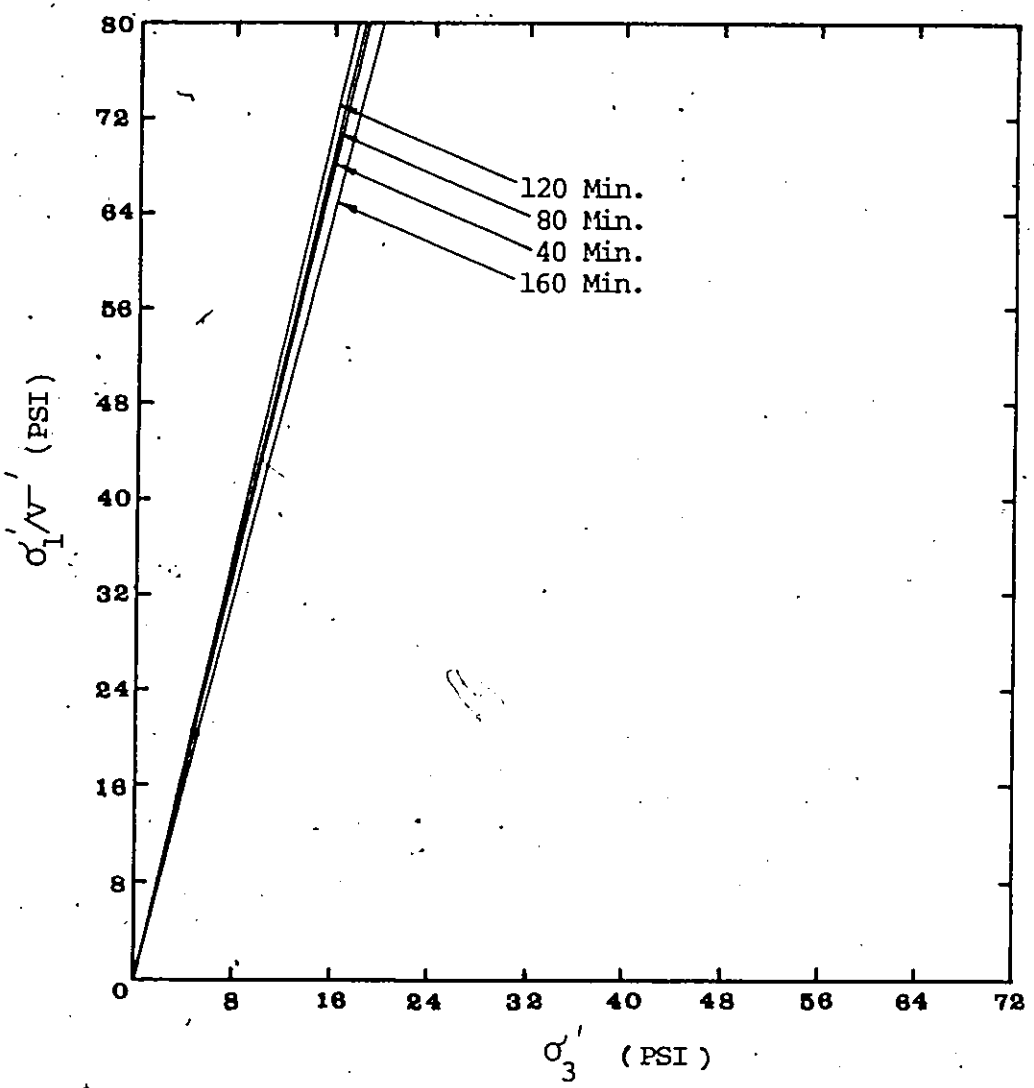

SET TIME	K_f	$\sigma'^{*}_{K_f}$	ϕ'_μ
160 Min.	3.96	0.35	19°
120	4.24	0.27	21°
80	4.10	0.59	20°
40	4.06	0.33	20°

Fig. 5.10. $\frac{\sigma_1'}{\sqrt{\ }'}$ versus σ_3' for 38^{0}F and 20% failure strain.

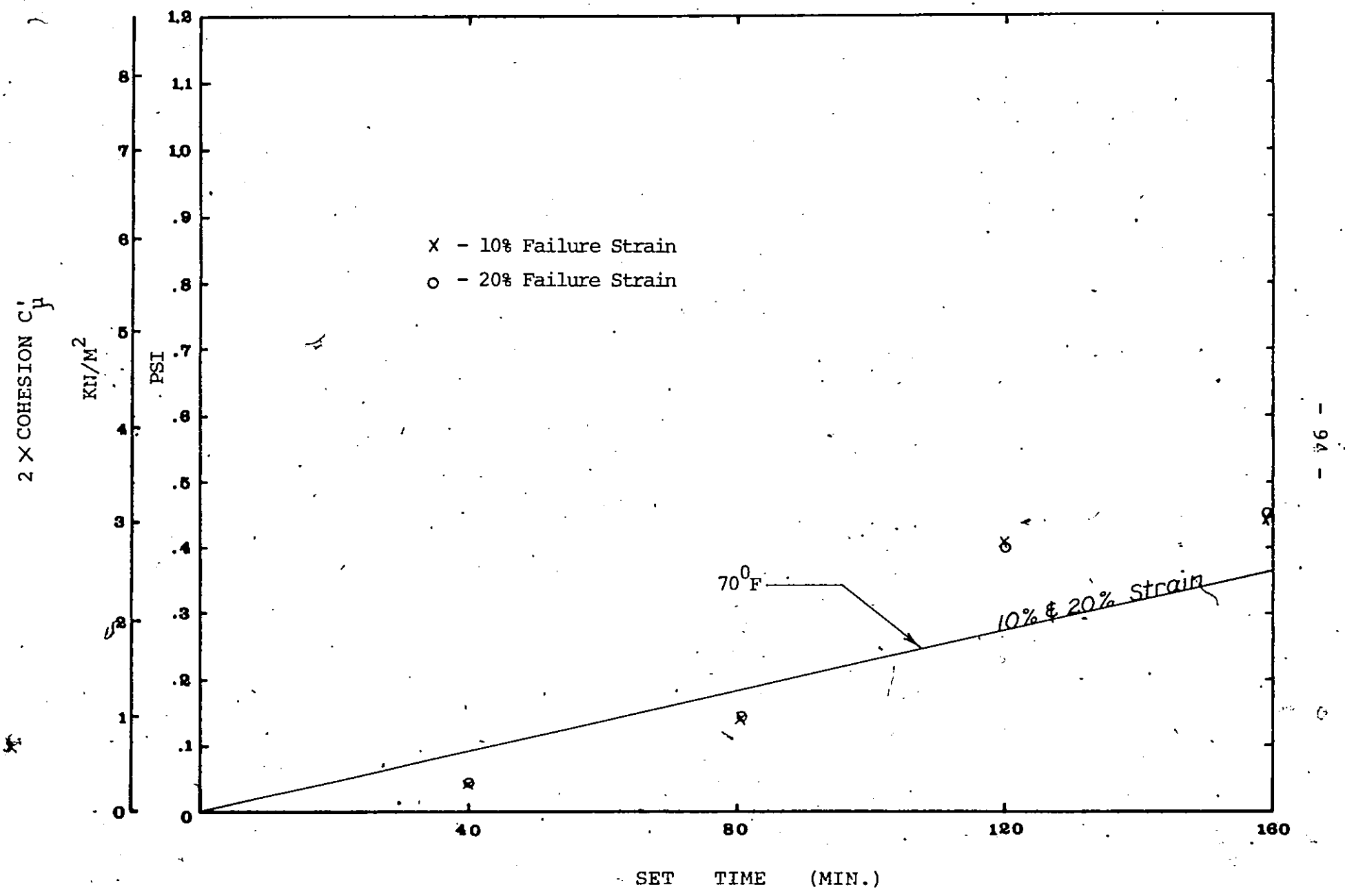

Fig. 5.11. Cohesion versus set time at 70° F from Rowe's analysis.

(a) Failure Criterion; Maximum stress difference or 10% axial strain.

Temperature	Set Time	Effective Friction Angle ϕ'_μ	$\sigma^*_{\phi'_\mu}$	Cohesion C'_μ	$\sigma^*_{C'_\mu}$
70^0F	40 min.	18^0	2.0^0	.046 psi	.02 psi
	80	18^0	1.8^0	.090	.04
	120	20^0	2.3^0	.13	.06
	160	19^0	2.8^0	.18	.08
38^0F	40	22^0	3.2^0	-	-
	80	22^0	3.0^0	-	-
	120	23^0	6.6^0	-	-
	160	20^0	2.8^0	-	-

(b) Failure Criterion; Maximum stress difference or 10% axial strain.

Temperature	Set Time	Effective friction Angle ϕ'_μ	$\sigma^*_{\phi'_\mu}$	Cohesion C'_μ	$\sigma^*_{C'_\mu}$
70^0F	40 min.	19^0	2.4^0	.045psi	.02 psi
	80	21^0	7.5^0	.090	.04
	120	18^0	4.3^0	.13	.06
	160	21^0	5.7^0	.18	.08
38^0F	40	20^0	2.0^0	-	-
	80	20^0	3.7^0	-	-
	120	21^0	1.7^0	-	-
	160	19^0	2.5^0	-	-

Table 5.12. Results of Rowe's Analysis.

CHAPTER VI

DISCUSSION

6.1 Discussion of Test Results

Figures 5.1 to 5.4 and figures 5.7 to 5.10 indicate that fresh concrete exhibits shear strength characteristics in accordance with both Coulomb's equation $\tau = C' + \sigma_n' \tan \phi'$ and Rowe's equation $\frac{\sigma_1'}{\sigma_3'} = K_1 \sigma_3' + K_2$ where K_1 and K_2 are functions of the effective friction angle and the effective cohesion. However, caution must be exercised when one interprets this statement with respect to Coulomb's theory. The decrease in pore pressure with axial strain as shown in figures 4.10 B to 4.17 B resulting from an applied deviator stress, implies that the concrete mix used in this investigation behaved in a dilatant fashion when being sheared. This tendency to dilate may be explained by the relatively small void ratios achieved due to a close packing of the aggregate particles as a result of the large range and uniform gradation of aggregate size and the tamping of the fresh concrete in an attempt to achieve full compaction. The test samples, therefore, could not be distorted without an increase in the distance between the particles unless the individual particles themselves were to break. Because of the dilatancy, only a portion of the work done by the applied stresses went into shearing the test samples. The remainder of the work went into rearranging the particles during dilatancy. Coulomb's strength parameters C' and ϕ' therefore, may not strictly represent the cohesion and the angle of internal friction respectively in the full sense of their definitions. Instead, the values assigned to C' and ϕ' are such as to make Coulomb's

straight line fit the test results. Dilatancy however, poses no problem with respect to Rowe's theory where Rowe's shear strength equation was derived for a particulate system as opposed to a continuum whose volume remains constant. The strength parameters C'_μ and ϕ'_μ correspond directly to the shearing resistance offered by cohesion and internal friction respectively.

From table 5.6 Coulomb's friction angle for the concrete mix lies in the range of 37^0 to 41^0 for a 10% failure strain and 34^0 to 39^0 for a 20% failure strain. These values correspond to a dense arrangement of particles and are supported by the fact that concrete aggregates tend to be closely packed and angular, achieving a high degree of particle interlock.

In table 5.12, Rowe's friction angle is seen to lie in the range of 18^0 to 21^0 for a 10% failure strain and 19^0 to 23^0 for a 20% failure strain. In the verification of his theory, Rowe evaluated the friction angles for clean sands and silts and found them to lie between 23^0 and 30^0; the lower friction angles corresponding to the coarser material. Since concrete is composed of aggregates in the coarse sand and gravel sizes, the friction angles obtained in this investigation are consistent with those in Rowe's investigation.

It may be seen that Rowe's friction angles are approximately half the value of Coulomb's friction angles. This supports the idea that Coulomb's friction angles not only include the effects of frictional resistance against shearing but also to resistance in expanding against the principle stresses acting on the test sample. A decrease of about 3^0 in Coulomb's friction angles at both 70^0F and 38^0F is observed to exist when the axial

failure strain is defined as 20 % as opposed to 10 %. A possible explanation for this decrease is that at the lower failure strain the majority of particles are interlocked and effectively resist the applied shear. For the higher failure strain however, only a portion of the particles are resisting the applied shear while the remainder of the particles are in a state of failure and offer less resistance to the applied shear. No general trend is evident for the observed changes in the friction angles for either an increasing set time or for temperature change. The reason is that the component of shear resistance resulting from the translation and frictional resistance between aggregate and cement particles which is included in the angle of internal friction, depends largely on the surface roughness and the load per particle. Since these are independent of temperature change and set time, so should be the angle of internal friction. Because of this, it may also be argued that Coulomb's friction angle does in fact include to some degree the effects of particle interaction.

Since the angle of internal friction is an inherent property of a concrete mix and remains essentially constant with time and temperature, it is the increase in cohesion as a result of the hydration process which allows fresh concrete to develop significant shear strength with time and solidify. This increase in cohesion with time is clearly depicted in figures 5.5 and 5.11 for both Coulomb's theory and Rowe's theory at 38^{0} F and 70^{0} F. Since hydration is a chemical reaction, the rate of increase in cohesion with time is seen to be significantly lower at 38^{0} F as compared to 70^{0} F.

In tables 5.6 and 5.12 it is seen that the standard deviations for the effective friction angles and effective cohesion are significantly smaller for Coulomb's analysis than for Rowe's analysis. For instance, the coefficient of variation is as high as 36% for the friction angle and 44% for the cohesion in Rowe's analysis while in the Coulomb analysis they are 7% and 19% respectively. This leads to the conclusion that although Coulomb's theory of shear strength is fundamentally incorrect when applied to systems consisting of individual grains it can more accurately express the results of shear strength tests performed on fresh concrete.

The lateral pressure corresponding to the at rest state may be evaluated when the coefficient K_o for fresh concrete is known. The variation of K_o for the given mix with set time, effective vertical stress and temperature can be seen in figures 4.19 A and 4.19 B. It may be seen that K_o is variable and highly dependent on set time at 70^0F and to a lesser degree at 38^0F. Initially, fresh concrete being in a highly plastic state behaves much like a liquid. Any vertical stresses are correspondingly transformed into lateral stresses. Consequently, K_o approaches unity. As the fresh concrete cures and hardens, lateral strains as a result of vertical stress become restricted and approach those of Poisson's ratio for cured concrete. The value of K_o therefore decreases significantly with set time. This decrease is of a smaller order at the colder temperature because of the hydration process being retarded.

6.2 Application of Test Results to Formwork Pressures

Concrete can be considered a free draining material. The ability of concrete to drain freely and dissipate excess pore pressure was demonstrated in the K_0 tests (see fig. 4.7). As much as 8 ml of water were found to be expelled from the test samples within a period of one minute following an increase in vertical stress. It was also found that no more than two minutes were necessary for the load dial gauge to stabilize following an increase in vertical load during which excess pore water pressures were dissipated. Because of this, it may be concluded that the lateral pressure existing in formwork is the sum of two pressures acting individually; the pore water pressure and the pressure exerted by the particles composing the concrete.

Pore Pressure. The lateral pressure exerted by the pore water on form walls is not necessarily hydrostatic. The leakage of water from cracks and joints creates a hydraulic gradient within the concrete mass resulting in seepage pressures as opposed to hydrostatic pressures. In addition, the free water is continuously taken up by the hydration process and eventually becomes capillary water. Therefore, the pressures due to the pore water with depth are something less than hydrostatic.

Particle Pressure. The lateral pressure exerted by the concrete particles is a function of the effective shear strength properties of the given concrete mix. The effect of shear strength is to reduce the lateral pressure exerted by the concrete particles by allowing vertical shear forces to develop between the concrete and the form walls resulting in a significant portion of the concrete weight being supported by the form walls and by restricting the lateral strains of the concrete during deflection of the form walls. In this study, it was found that the shear strength of fresh concrete has two

components; internal friction resulting from particle interaction and cohesion resulting from the hydration process.

Internal friction was found to be a constant property for a given mix and does not change with time or temperature. However, because it involves particle interaction, its value may vary to some degree with the shape, size gradation and proportioning of the aggregates in the mix. Internal friction requires strain to be mobilized. Vertical strains and consequently the development of vertical shear forces may always be assumed to exist in formwork because of the settlement of concrete due to shrinkage. Lateral strains however are highly variable and it is unreasonable to assume that internal friction with respect to lateral strains is fully mobilized particularly in rigid formwork and around form ties.

Cohesion refers to the ability of fresh concrete to change from a highly plastic material incapable of supporting itself to a rigid solid as a result of the development of a crystal structure within the cement paste bonding the particles of aggregate together. This study has shown that cohesion is highly dependent on the temperature of the concrete and the time during which the concrete is allowed to set.

Any factors which influence the values of the above two components of shear strength may also be expected to influence the particle pressures exerted on form walls. For instance, it was found that immediately following mixing, cohesion approached and was taken to be zero. This time dependency of cohesion implies that the initial deviation of the lateral pressure of concrete from the hydrostatic line of an equivalent fluid having the same density as concrete is due to the internal friction of the mix and also because the free water in the concrete exerts seepage pressures rather than

hydrostatic pressures. The time dependency also implies that the lateral pressures developed in formwork are inversely related to the rate of pour i.e. the higher the rate of pour, the less time the concrete has to develop cohesion before additional concrete head is added. Consequently a greater portion of the vertical pressure is transformed into lateral pressure. This is clearly depicted in figures 4.19 A and 4.19 B where K_0 representing the lateral particle pressure as a fraction of the applied vertical stess has been plotted for various set times. These plots represent predominantly the effects of cohesion on lateral pressure as the effects of internal friction have been minimized by restraining the samples laterally.

Temperature is a second factor influencing the development of cohesion. Table 5.6 indicates that for the mix used in this investigation, the cohesion developed at 38^0F is approximately 70% of the cohesion developed at 70^0F for any given set time. This difference in the development of cohesion has a significant effect on the lateral pressures exerted by fresh concrete. For instance the American Concrete Institute formulae predict an increase in the maximum pressure in wall forms from 793 psf at 70^0F to 1334 psf at 38^0F for a 5 ft per hr pour. This represents a 68% increase in the maximum pressure.

The concrete mix used in the triaxial testing is typical of most concretes to be found in practice. Although differences exist in aggregate sizes and proportions, almost all concretes contain aggregates in the sand and gravel sizes and tend to be well compacted as a result of the vibration or tamping in the placing procedure. It is reasonable to assume therefore, that large variations in the angle of internal friction do not exist between various concretes. In addition, it was previously stated that the internal friction of any mix may not be fully mobilized as a result of insufficient formwork deflections. Consequently the factors most likely to have the

greatest influence on formwork pressures are those influencing the development of cohesion in fresh concrete. Therefore, in addition to time and temperature, it is to be expected that the lateral pressures are strongly influenced by inhibiters and the fineness of the cement which govern the rate at which hydration proceeds and by vibration which could destroy the weak crystal structure of concrete at low set times.

CHAPTER V11

CONCLUSIONS AND RECOMMENDATIONS

This study has dealt with the mechanical properties of fresh concrete as they pertain to its shear strength behaviour in the nonflow condition. The shear strength characteristics of fresh concrete have been studied through the use of a triaxial compression set up. Tests were performed at warm and cold temperatures for different set times. The test results were subsequently analyzed by the shear strength theories of Mohr Coulomb and Rowe and expressed by two strength parameters corresponding to the internal friction and the cohesion components of shear strength for each set time - temperature combination.

In addition to shear testing, an attempt was made to evaluate the coefficient of lateral pressure at rest (K_0) by measuring the lateral pressure of vertically stressed concrete specimens restrained laterally by a plexiglass cylinder. These tests were also performed at 70^0F and 38^0F for different set times under what were considered to be drained conditions.

7.1 Conclusions

From this study the following conclusions can be made:

(1) The shear strength properties of fresh concrete may be expressed by either the Mohr Coulomb or Rowe's theory of shear strength. Although Coulomb's theory is fundamentally incorrect, it is able to adequately express the results of shear tests performed on fresh concrete.

(2) The shear strength of fresh concrete is both time and temperature dependent.

(3) Immediately following mixing, the shear strength of fresh concrete is due mainly to the internal friction resulting from particle interaction which remains constant with set time and temperature change.

(4) The hardening of concrete with set time is due mainly to the development of cohesion as a result of the hydration process. At lower temperatures, hydration is retarded and cohesion developes at a slower rate causing the fresh concrete to behave fluid like for a longer period of time.

(5) The coefficient K_0 for fresh concrete is highly variable and depends on set time, temperature and to a lesser degree on the applied vertical stress. Its value is lower at warm temperatures and decreases with set time.

7.2 Recommendations.

This investigation has been primarily concerned with the evaluation of the shear strength for a single concrete mix and its variation with set time and temperature. To supplement this study, further triaxial testing is necessary with other mix designs to establish a relation between shear strength and mix proportions. Subsequent studies are then required to relate the $\phi' - c'$ strength parameters of fresh concrete to such areas as lateral pressures in formwork, workability, compactibility, pumpability and the like.

It is also recommended that further studies into the shrinkage of fresh concrete with set time and the lateral deflections normally encountered in formwork take place so as to make our present understanding of the development of lateral pressures in formwork more complete.

REFERENCES

1. CERA Research Report: 1
"The pressure of Concrete on Formwork", Civil Engrg Research Association (Now: Construction Industry Research and Information Association - CIRIA), London, 1965.

2. Janssen, H. A.,"Versuche Uber Getreidedruck in Sillozellen", Zeitschrift, Verein Deutscher Ingenieure, Vol. 39, Aug. 31, 1895, pp. 1045-1049.

3. L'Hremite, R., "Vibration and the Rheology of Freshly Mixed Concrete". (In Revue des Materiaux de Construction. no. 405, 1949, pp. 179 - 187).

4. Meyerhof, G. G., "General Report on Theories". (In ASTM Special Technical Publication No. 361, Laboratory Shear testing of Soils - 1963, pp. 35 - 41).

5. Olsen, R. H., "Lateral Pressure of Concrete on Formwork", Ph.D. thesis, Oklahoma State University, Okla., U.S.A., 1968.

6. Ritchie, A. G. B., "The Triaxial Testing of Fresh Concrete", Magazine of Concrete Research, Vol. 14, no. 40, 1962.

7. Rodin, S., "Pressure of Concrete on Formwork", Proc.,Institute of Civil Engineering, London, Vol. 1, November 1952, pp. 709 - 745.

8. Rowe, P. W., "The Stress - Dilatancy Relation for Static Equilibrium of an Assembly of Particles in Contact", Proceedings of the Royal Society, A, Vol. 269, pp. 500 - 527, 1962.

9. Schodt, R., "Calculation of Pressure of Concrete on Forms", Proc., American Society of Civil Engineers, New York, Vol. 81, Paper 680, May 1955, pp. 1-16.

10. Sowers, G. F., "Strength Testing of Soils". (In ASTM Special Technical Publication No. 361, Laboratory Shear Testing of Soils - 1963, pp. 3-19.

ADDITIONAL REFERENCES

1. Craig, R.F., "Soil Mechanics", Van Nostrand Reinhold, pp. 83 - 114, 1978.

2. Neville, A. M., "Properties of Concrete", Pitman, pp. 181 - 231, 1973.

3. Powers, T. C., "The Properties of Fresh Concrete", Wiley, pp. 437 - 529, 1968.

4. Puerifoy, R. L., "Formwork for Concrete Structures", McGraw - Hill, pp. 17, 1964.

5. Terzaghi, K., and R. Peck, "Soil Mechanics in Engineering Practice", (Second Edition), Wiley, pp. 88 - 116, 1948.

TRIAXIAL COMPRESSION TEST

Air temperature = 40^0F
Concrete temperature = 44^0F
Height of sample = 8.0 inches
Time of set = 160 min.
Cell pressure = 0 psi
Strain rate = .045 inches / min.

Vertical Deformation (inches)	Diameter of Sample at Midheight (inches)	Pore Pressure (psi)	Deviator Load (Lbs)
0	4.03	0	0
.100	4.04	-.9	68
.200	4.08	-2.1	122
.300	4.13	-5.1	168
.400	4.20	-4.8	205
.500	4.24	-5.0	231
.600	4.30	-4.8	251
.700	4.34	-4.7	263
.800	4.45	-4.6	281
.900	4.47	-4.7	289
1.00	4.55	-5.0	301
1.10	4.61	-5.2	314
1.20	4.69	-5.7	326
1.30	4.73	-7.1	334
1.40	4.81	-6.0	342
1.50	4.90	-5.7	350
1.60	4.97	-5.8	362

TRIAXIAL COMPRESSION TEST

Air temperature = 70^0F
Concrete temperature = -
Height of sample = 8.0 inches
Time of set = 40 min.
Cell pressure = 0 psi
Strain rate = .045 inches / min.

Vertical Deformation (inches)	Diameter of Sample at Midheight (inches)	Pore Pressure (psi)	Deviator Load (Lbs)
0	4.01	0	0
.100	4.06	-1.0	68
.200	4.09	-2.0	124
.300	4.14	-2.8	169
.400	4.22	-3.5	210
.500	4.27	-4.2	244
.600	4.35	-4.7	266
.700	4.37	-5.2	293
.800	4.47	-5.5	311
.900	4.53	-5.8	330
1.00	4.61	-6.0	349
1.10	4.70	-6.2	360
1.20	4.75	-6.5	375
1.30	4.85	-6.6	390
1.40	4.94	-6.8	401
1.50	5.01	-6.9	412
1.60	5.10	6.9	424

TRIAXIAL COMPRESSION TEST

Air temperature = 70^0F
Concrete temperature = -
Height of sample = 8.0 inches
Time of set = 40 min.
Cell pressure = 5 psi
Strain rate = .045 inches / min.

Vertical Deformation (inches)	Diameter of Sample at Midheight (inches)	Pore Pressure (psi)	Deviator Load (Lbs)
0	4.02	4.6	0
.100	4.05	3.9	94
.200	4.10	2.0	210
.300	4.13	1.3	244
.400	4.22	0.0	300
.500	4.25	-0.8	352
.600	4.32	-1.5	397
.700	4.38	-2.1	429
.800	4.45	-2.7	461
.900	4.52	-3.1	488
1.00	4.59	-3.4	510
1.10	4.65	-3.8	532
1.20	4.73	-4.0	551
1.30	4.81	-4.3	564
1.40	4.92	-4.5	577
1.50	4.98	-4.6	594
1.60	5.05	-4.8	604

TRIAXIAL COMPRESSION TEST

Air temperature = 70^0F
Concrete temperature = -
Height of sample = 8.0 inches
Time of set = 40 min.
Cell pressure = 10 psi
Strain rate = .045 inches / min.

Vertical Deformation (inches)	Diameter of Sample at Midheight (inches)	Pore Pressure (psi)	Deviator Load (Lbs)
0	4.01	4.8	0
.100	4.03	5.3	244
.200	4.07	3.7	379
.300	4.12	1.8	488
.400	-	-	-
.500	4.27	-1.0	637
.600	-	-	-
.700	4.40	-2.5	733
.800	-	-	-
.900	4.56	-3.4	804
1.00	-	-	-
1.10	4.73	-4.2	860
1.20	4.80	-4.4	886
1.30	4.90	-4.6	907
1.40	4.98	-4.8	920
1.50	5.08	-5.1	935
1.60	5.15	-5.3	956

TRIAXIAL COMPRESSION TEST

Air temperature = 70^0F
Concrete temperature = -
Height of sample = 8.0 inches
Time of set = 40 min.
Cell pressure = 15 psi
Strain rate = .045 inches / min.

Vertical Deformation (inches)	Diameter of Sample at Midheight (inches)	Pore Pressure (psi)	Deviator Load (Lbs)
0	4.03	12.2	0
.100	4.03	11.6	221
.200	4.08	9.6	349
.300	4.13	7.8	458
.400	4.21	6.1	548
.500	4.28	4.7	614
.600	-	-	-
.700	4.40	2.8	726
.800	-	-	-
.900	4.55	1.6	812
1.00	-	-	-
1.10	4.69	0.7	879
1.20	-	-	-
1.30	4.88	0.0	946
1.40	4.95	-0.2	977
1.50	5.03	-0.3	1003
1.60	5.11	-0.9	1037

TRIAXIAL COMPRESSION TEST

Air temperature = 70^0F

Concrete temperature = -

Height of sample = 8.0 inches

Time of set = 40 min.

Cell pressure = 20 psi

Strain rate = .045 inches / min.

Vertical Deformation (inches)	Diameter of Sample at Midheight (inches)	Pore Pressure (psi)	Deviator Load (Lbs)
0	4.01	13.9	0
.100	4.01	15.4	270
.200	4.07	13.7	409
.300	4.12	11.9	517
.400	-	-	-
.500	4.25	9.2	673
.600	4.33	8.1	729
.700	4.38	7.3	778
.800	4.47	6.6	819
.900	4.54	5.9	864
1.00	4.62	5.4	905
1.10	4.69	5.0	942
1.20	4.77	4.5	979
1.30	4.86	4.2	1021
1.40	4.94	3.9	1058
1.50	5.02	3.5	1088
1.60	5.11	3.2	1115

TRIAXIAL COMPRESSION TEST

Air temperature = 70^0F
Concrete temperature = -
Height of sample = 8.0 inches
Time of set = 80 min.
Cell pressure = 0 psi
Strain rate = .045 inches / min.

Vertical Deformation (inches)	Diameter of Sample at Midheight (inches)	Pore Pressure (psi)	Deviator Load (Lbs)
0	4.06	0.2	0
.100	4.09	0.0	43
.200	4.14	-0.8	76
.300	4.19	-1.4	109
.400	4.24	-1.9	136
.500	4.31	-2.4	161
.600	4.36	-2.9	183
.700	4.43	-3.2	199
.800	4.50	-3.6	210
.900	4.56	-3.8	221
1.00	4.64	-4.0	234
1.10	4.70	-4.2	244
1.20	4.77	-4.4	253
1.30	4.86	-4.5	260
1.40	4.95	-4.6	269
1.50	5.01	-4.7	275
1.60	5.10	-4.8	287

TRIAXIAL COMPRESSION TEST

Air temperature = 70^0F
Concrete temperature = -
Height of sample = 8.0 inches
Time of set = 80 min.
Cell pressure = 5 psi
Strain rate = .045 inches / min.

Vertical Deformation (inches)	Diameter of Sample at Midheight (inches)	Pore Pressure (psi)	Deviator Load (Lbs)
0	4.05	4.7	0
.100	4.07	3.8	116
.200	4.13	2.4	202
.300	4.19	1.2	266
.400	4.27	0.0	315
.500	4.33	-0.8	359
.600	4.36	-1.4	390
.700	4.46	-1.9	416
.800	4.53	-2.3	439
.900	4.62	-2.6	458
1.00	4.69	-2.9	480
1.10	4.77	-3.2	499
1.20	4.86	-3.4	517
1.30	4.93	-3.7	536
1.40	5.02	-3.8	551
1.50	5.11	-4.0	562
1.60	5.17	-4.1	577

TRIAXIAL COMPRESSION TEST

Air temperature = 70^0F
Concrete temperature = -
Height of sample = 8.0 inches
Time of set = 80 min.
Cell pressure = 10 psi
Strain rate = .045 inches / min.

Vertical Deformation (inches)	Diameter of Sample at Midheight (inches)	Pore Pressure (psi)	Deviator Load (Lbs)
0	4.00	8.9	0
.100	4.01	8.9	90
.200	4.06	8.0	165
.300	4.11	6.8	229
.400	4.17	5.6	281
.500	4.23	4.7	334
.600	4.30	4.0	379
.700	4.34	3.3	416
.800	4.43	2.8	446
.900	4.50	2.4	476
1.00	4.58	1.9	502
1.10	4.64	1.6	525
1.20	4.70	1.3	547
1.30	4.76	1.1	570
1.40	4.88	0.8	592
1.50	4.97	0.3	606
1.60	5.04	0.0	621

TRIAXIAL COMPRESSION TEST

Air temperature = 70^0F
Concrete temperature = -
Height of sample = 8.0 inches
Time of set = 80 min.
Cell pressure = 15 psi
Strain rate = .045 inches / min.

Vertical Deformation (inches)	Diameter of Sample at Midheight (inches)	Pore Pressure (psi)	Deviator Load (Lbs)
0	4.01	13.4	0
.100	4.01	12.8	165
.200	4.05	10.8	293
.300	4.11	8.8	398
.400	4.16	7.0	480
.500	4.23	5.6	547
.600	4.30	4.5	599
.700	4.35	3.8	640
.800	4.44	3.0	662
.900	4.51	2.8	711
1.00	4.59	2.4	733
1.10	4.66	2.1	748
1.20	4.73	2.3	757
1.30	4.81	2.3	769
1.40	4.98	2.6	755
1.50	5.03	3.3	748
1.60	5.10	3.3	755

TRIAXIAL COMPRESSION TEST

Air temperature = 70^0F
Concrete temperature = -
Height of sample = 8.0 inches
Time of set = 80 min.
Cell pressure = 20 psi
Strain rate = .045 inches / min.

Vertical Deformation (inches)	Diameter of Sample at Midheight (inches)	Pore Pressure (psi)	Deviator Load (Lbs)
0	4.03	16.3	0
.100	4.03	16.9	199
.200	4.08	15.1	307
.300	4.14	13.3	409
.400	4.20	11.5	495
.500	4.27	10.1	569
.600	4.33	8.9	634
.700	4.40	7.9	696
.800	4.47	7.1	752
.900	4.54	6.4	800
1.00	4.62	5.7	838
1.10	4.68	5.2	875
1.20	4.74	4.7	920
1.30	4.81	4.3	946
1.40	4.84	4.0	976
1.50	4.90	3.7	1000
1.60	4.93	3.4	1025

TRIAXIAL COMPRESSION TEST

Air temperature = 70^0F
Concrete temperature = -
Height of sample = 8.0 inches
Time of set = 120 min.
Cell pressure = 0 psi
Strain rate = .045 inches / min.

Vertical Deformation (inches)	Diameter of Sample at Midheight (inches)	Pore Pressure (psi)	Deviator Load (Lbs)
0	4.01	0.0	0
.100	4.06	-.3	43
.200	4.10	-1.1	79
.300	4.16	-1.8	117
.400	4.23	-2.5	152
.500	4.30	-3.1	182
.600	4.35	-3.6	207
.700	4.43	-4.0	228
.800	4.49	-4.3	248
.900	4.55	-4.5	263
1.00	4.64	-4.8	275
1.10	4.70	-5.0	292
1.20	4.77	-5.2	304
1.30	4.86	-5.4	315
1.40	4.94	-5.5	323
1.50	5.03	-5.7	332
1.60	5.11	-5.8	347

TRIAXIAL COMPRESSION TEST

Air temperature = 70^0F
Concrete temperature = -
Height of sample = 8.0 inches
Time of set = 120 min.
Cell pressure = 5 psi
Strain rate = .045 inches / min.

Vertical Deformation (inches)	Diameter of Sample at Midheight (inches)	Pore Pressure (psi)	Deviator Load (Lbs)
0	4.00	6.0	0
.100	4.05	5.7	82
.200	4.09	4.8	135
.300	4.15	3.9	184
.400	4.22	3.1	221
.500	4.29	2.5	225
.600	4.34	1.8	285
.700	4.41	1.3	315
.800	4.49	.9	338
.900	4.56	.4	362
1.00	4.63	0.0	380
1.10	4.69	0.0	400
1.20	4.75	-.1	413
1.30	4.84	-.4	428
1.40	4.92	-.5	443
1.50	5.00	-.9	465
1.60	5.08	-1.1	484

TRIAXIAL COMPRESSION TEST

Air temperature = 70^0F
Concrete temperature = -
Height of sample = 8.0 inches
Time of set = 120 min.
Cell pressure = 10 psi
Strain rate = .045 inches / min.

Vertical Deformation (inches)	Diameter of Sample at Midheight (inches)	Pore Pressure (psi)	Deviator Load (Lbs)
0	4.03	10.4	0
.100	4.05	9.4	94
.200	4.07	8.3	157
.300	4.10	7.2	214
.400	4.16	6.1	259
.500	4.22	5.3	304
.600	4.27	4.6	341
.700	4.32	4.0	377
.800	4.36	3.4	409
.900	4.45	2.9	435
1.00	4.50	2.5	465
1.10	4.55	2.1	491
1.20	4.63	1.8	517
1.30	4.69	1.5	540
1.40	4.75	1.2	559
1.50	4.81	.9	587
1.60	4.90	.6	605

TRIAXIAL COMPRESSION TEST

Air temperature = 70^0F
Concrete temperature = -
Height of sample = 8.0 inches
Time of set = 120 min.
Cell pressure = 15 psi
Strain rate = .045 inches / min.

Vertical Deformation (inches)	Diameter of Sample at Midheight (inches)	Pore Pressure (psi)	Deviator Load (Lbs)
0	3.99	13.8	0
.100	4.01	13.5	143
.200	4.06	12.2	229
.300	4.10	10.9	304
.400	4.16	9.7	368
.500	4.22	8.6	424
.600	4.29	7.8	473
.700	4.35	7.0	520
.800	4.42	6.3	563
.900	4.49	5.7	600
1.00	4.54	5.2	628
1.10	4.62	4.6	662
1.20	4.68	4.2	688
1.30	4.76	3.9	711
1.40	4.85	3.4	737
1.50	4.90	3.2	763

TRIAXIAL COMPRESSION TEST

Air temperature = 70^0F
Concrete temperature = 9
Height of sample = 8.0 inches
Time of set = 120 min.
Cell pressure = 20 psi
Strain rate = .045 inches / min.

Vertical Deformation (inches)	Diameter of Sample at Midheight (inches)	Pore Pressure (psi)	Deviator Load (Lbs)
0	4.02	14.6	0
.100	4.03	15.7	225
.200	4.07	14.0	398
.300	4.14	12.2	510
.400	4.21	10.6	598
.500	4.29	9.1	669
.600	4.35	8.1	731
.700	4.41	7.1	774
.800	4.49	6.4	818
.900	4.57	5.8	856
1.00	4.64	5.3	886
1.10	4.70	4.8	916
1.20	4.80	4.3	945
1.30	4.89	4.0	972
1.40	-	-	-
1.50	5.04	3.3	1025

TRIAXIAL COMPRESSION TEST

Air temperature = 70^0F
Concrete temperature = -
Height of sample = 8.0 inches
Time of set = 160 min.
Cell pressure = 0 psi
Strain rate = .045 inches / min.

Vertical Deformation (inches)	Diameter of Sample at Midheight (inches)	Pore Pressure (psi)	Deviator Load (Lbs)
0	4.05	0.2	0
.100	4.05	0.2	46
.200	4.15	-0.4	90
.300	4.20	-1.3	127
.400	4.30	-1.9	157
.500	4.35	-2.4	176
.600	4.40	-2.8	195
.700	4.45	-3.1	210
.800	4.50	-3.4	225
.900	4.60	-3.6	236
1.00	4.70	-3.8	247
1.10	4.8	-4.0	259
1.20	4.9	-4.1	262
1.30	5.0	-4.3	277
1.40	5.1	-4.4	285
1.50	5.1	-4.5	300
1.60	5.2	-4.6	307

TRIAXIAL COMPRESSION TEST

Air temperature = 70^0F
Concrete temperature = -
Height of sample = 8.0 inches
Time of set = 160 min.
Cell pressure = 5 psi
Strain rate = .045 inches / min.

Vertical Deformation (inches)	Diameter of Sample at Midheight (inches)	Pore Pressure (psi)	Deviator Load (Lbs)
0	4.01	5.0	0
.100	4.02	4.5	75
.200	4.07	3.8	131
.300	4.10	3.0	173
.400	4.18	2.3	210
.500	4.25	1.6	233
.600	4.32	1.2	255
.700	4.37	0.8	270
.800	4.45	0.3	289
.900	4.51	0.0	308
1.00	4.59	0.0	323
1.10	4.66	0.0	341
1.20	4.73	-0.3	356
1.30	4.80	-0.7	371
1.40	4.87	-0.8	386
1.50	4.97	-1.0	401
1.60	5.04	-1.2	413

TRIAXIAL COMPRESSION TEST

Air temperature = 70^0F
Concrete temperature = -
Height of sample = 8.0 inches
Time of set = 160 min.
Cell pressure = 10 psi
Strain rate = .045 inches / min.

Vertical Deformation (inches)	Diameter of Sample at Midheight (inches)	Pore Pressure (psi)	Deviator Load (Lbs)
0	4.03	10.5	0
.100	4.06	9.6	105
.200	4.11	8.6	176
.300	4.16	7.8	229
.400	4.25	7.0	270
.500	4.31	6.4	300
.600	4.37	5.8	329
.700	4.45	5.4	355
.800	4.54	5.0	381
.900	4.59	4.6	396
1.00	4.66	4.4	411
1.10	4.75	4.2	434
1.20	4.79	4.0	452
1.30	4.87	3.7	467
1.40	4.92	3.5	479
1.50	5.02	3.3	501
1.60	5.07	3.2	509

TRIAXIAL COMPRESSION TEST

Air temperature = 70^0F
Concrete temperature = -
Height of sample = 8.0 inches
Time of set = 160 min.
Cell pressure = 15 psi
Strain rate = .045 inches / min.

Vertical Deformation (inches)	Diameter of Sample at Midheight (inches)	Pore Pressure (psi)	Deviator Load (Lbs)
0	4.03	12.4	0
.100	4.04	12.9	161
.200	4.08	11.9	247
.300	4.16	10.8	307
.400	4.23	9.9	356
.500	4.29	9.2	390
.600	4.35	8.6	424
.700	4.45	8.0	450
.800	4.51	7.8	476
.900	4.59	7.3	502
1.00	4.66	7.0	530
1.10	4.73	6.8	550
1.20	4.80	6.5	576
1.30	4.90	6.2	595
1.40	4.98	5.9	615
1.50	5.09	5.7	636

TRIAXIAL COMPRESSION TEST

Air temperature = 70^0F

Concrete temperature = –

Height of sample = 8.0 inches

Time of set = 160 min.

Cell pressure = 20 psi

Strain rate = .045 inches / min.

Vertical Deformation (inches)	Diameter of Sample at Midheight (inches)	Pore Pressure (psi)	Deviator Load (Lbs)
0	3.99	8.3	0
.100	3.99	12.1	326
.200	4.03	12.1	499
.300	4.09	10.8	621
.400	4.15	9.6	703
.500	4.24	8.5	782
.600	4.30	7.7	845
.700	4.35	7.0	894
.800	4.42	6.4	931
.900	4.51	6.0	961
1.00	4.61	5.6	990

TRIAXIAL COMPRESSION TEST

Air temperature = 38^0F

Concrete temperature = 38^0F

Height of sample = 8.0 inches

Time of set = 160 min.

Cell pressure = 5 psi

Strain rate = .045 inches / min.

Vertical Deformation (inches)	Diameter of Sample at Midheight (inches)	Pore Pressure (psi)	Deviator Load (Lbs)
0	4.05	4.7	0
.100	4.06	4.2	61
.200	4.10	3.4	98
.300	4.13	2.7	134
.400	4.20	2.0	164
.500	4.25	1.4	191
.600	4.31	1.0	210
.700	4.36	.8	226
.800	4.42	.2	236
.900	4.50	0.0	244
1.00	4.58	0.0	253
1.10	4.65	0.0	260
1.20	4.70	0.0	263
1.30	4.80	0.0	273
1.40	4.85	0.0	286
1.50	4.95	0.0	297
1.60	5.00	0.0	308

TRIAXIAL COMPRESSION TEST

Air temperature = 38^0F

Concrete temperature = -

Height of sample = 8.0 inches

Time of set = 160 min.

Cell pressure = 10 psi

Strain rate = .045 inches / min.

Vertical Deformation (inches)	Diameter of Sample at Midheight (inches)	Pore Pressure (psi)	Deviator Load (Lbs)
0	4.03	10.1	0
.100	4.05	9.6	59
.200	4.06	8.8	96
.300	4.10	8.2	135
.400	4.16	7.3	171
.500	4.23	6.6	206
.600	4.27	5.9	234
.700	4.33	5.4	257
.800	4.37	4.8	288
.900	4.45	4.2	316
1.00	4.51	3.9	335
1.10	4.58	3.4	365
1.20	4.64	3.1	385
1.30	4.70	2.8	409
1.40	4.76	2.5	433
1.50	4.84	2.1	451
1.60	4.92	1.7	464

TRIAXIAL COMPRESSION TEST

Air temperature = 36^0F

Concrete temperature = -

Height of sample = 8.0 inches

Time of set = 160 min.

Cell pressure = 15 psi

Strain rate = .045 inches / min.

Vertical Deformation (inches)	Diameter of Sample at Midheight (inches)	Pore Pressure (psi)	Deviator Load (Lbs)
0	4.05	14.1	0
.100	4.05	13.7	122
.200	4.09	12.1	200
.300	4.12	10.7	268
.400	4.20	9.3	332
.500	4.26	8.1	386
.600	4.32	6.9	438
.700	4.38	6.1	478
.800	4.45	5.5	518
.900	4.53	4.8	548
1.00	4.60	4.3	584
1.10	4.67	3.8	605
1.20	4.75	3.3	623
1.30	4.83	3.0	648
1.40	4.93	2.8	676
1.50	5.02	2.6	703
1.60	5.09	2.1	722

TRIAXIAL COMPRESSION TEST

Air temperature = 38^0F

Concrete temperature = -

Height of sample = 8.0 inches

Time of set = 160 min.

Cell pressure = 20 psi

Strain rate = .045 inches / min.

Vertical Deformation (inches)	Diameter of Sample at Midheight (inches)	Pore Pressure (psi)	Deviator Load (Lbs)
0	4.03	19.6	0
.100	4.03	19.4	109
.200	4.06	18.0	180
.300	4.12	16.7	248
.400	4.18	15.3	312
.500	4.25	14.1	377
.600	4.30	12.8	430
.700	4.35	11.6	468
.800	4.43	11.0	518
.900	4.50	10.4	552
1.00	4.63	9.2	614
1.10	4.69	8.8	644
1.20	4.76	8.5	669
1.30	4.83	8.2	696
1.40	4.91	7.9	722
1.50	4.98	7.7	746
1.60	5.05	7.5	766

TRIAXIAL COMPRESSION TEST

Air temperature = 36^0F
Concrete temperature = 40^0F
Height of sample = 8.0 inches
Time of set = 120 min.
Cell pressure = 0 psi
Strain rate = .045 inches / min.

Vertical Deformation (inches)	Diameter of Sample at Midheight (inches)	Pore Pressure (psi)	Deviator Load (Lbs)
0	4.05	0	0
.100	4.07	-0.6	50
.200	4.12	-1.3	79
.300	4.19	-2.0	105
.400	4.25	-2.5	128
.500	4.31	-3.0	146
.600	4.36	-3.3	164
.700	4.43	-3.7	179
.800	4.50	-4.0	191
.900	4.58	-4.2	205
1.00	4.63	-4.3	217
1.10	4.69	-4.5	225
1.20	4.78	-4.6	236
1.30	4.86	-4.7	243
1.40	4.94	-5.0	253
1.50	5.01	-5.1	263
1.60	5.06	-5.2	273

TRIAXIAL COMPRESSION TEST

Air temperature = 40^0F
Concrete temperature = 38^0F
Height of sample = 8.0 inches
Time of set = 120 min.
Cell pressure = 5 psi
Strain rate = .045 inches / min.

Vertical Deformation (inches)	Diameter of Sample at Midheight (inches)	Pore Pressure (psi)	Deviator Load (Lbs)
0	4.05	5.0	0
.100	4.06	4.5	60
.200	4.09	3.9	104
.300	4.16	2.8	148
.400	4.23	1.9	185
.500	4.29	1.3	221
.600	4.36	0.6	248
.700	4.40	0	272
.800	4.49	-0.2	290
.900	4.54	-0.8	308
1.00	4.61	-1.2	323
1.10	4.67	-1.5	340
1.20	4.75	-1.5	362
1.30	4.81	-1.7	377
1.40	4.91	-1.9	390
1.50	4.95	-2.1	402
1.60	5.04	-2.3	415

TRIAXIAL COMPRESSION TEST

Air temperature = 38^0F
Concrete temperature = 38^0F
Height of sample = 8.0 inches
Time of set = 120 min.
Cell pressure = 10 psi
Strain rate = .045 inches / min.

Vertical Deformation (inches)	Diameter of Sample at Midheight (inches)	Pore Pressure (psi)	Deviator Load (Lbs)
0	4.05	10.1	0
.100	4.07	9.4	77
.200	4.10	8.4	119
.300	4.14	7.3	158
.400	4.21	6.7	198
.500	4.24	6.2	230
.600	4.32	5.4	257
.700	4.37	5.1	285
.800	4.43	4.5	304
.900	4.49	4.0	329
1.00	4.54	3.8	354
1.10	4.61	3.3	373
1.20	4.68	3.0	392
1.30	4.75	2.7	413
1.40	4.83	2.5	432
1.50	4.91	2.3	450
1.60	4.98	2.0	466

TRIAXIAL COMPRESSION TEST

Air temperature = 36^0F
Concrete temperature = 40^0F
Height of sample = 8.0 inches
Time of set = 120 min.
Cell pressure = 15 psi
Strain rate = .045 inches / min.

Vertical Deformation (inches)	Diameter of Sample at Midheight (inches)	Pore Pressure (psi)	Deviator Load (Lbs)
0	4.05	15.0	0
.100	4.05	15.4	63
.200	4.08	14.6	98
.300	4.12	14.0	134
.400	4.20	13.4	164
.500	4.26	12.7	191
.600	4.31	11.8	212
.700	4.37	11.6	238
.800	4.43	11.2	259
.900	4.51	10.8	276
1.00	-	10.2	-
1.10	4.63	10.2	315
1.20	4.68	10.0	330
1.30	4.76	9.6	344
1.40	4.85	9.5	363
1.50	4.91	9.2	375
1.60	5.00	9.1	397

TRIAXIAL COMPRESSION TEST

Air temperature = 36^0F
Concrete temperature = 38^0F
Height of sample = 8.0 inches
Time of set = 120 min.
Cell pressure = 20 psi
Strain rate = .045 inches / min.

Vertical Deformation (inches)	Diameter of Sample at Midheight (inches)	Pore Pressure (psi)	Deviator Load (Lbs)
0	4.05	20.3	0
.100	4.05	20.5	72
.200	4.08	19.7	116
.300	4.13	18.8	153
.400	4.17	18.0	190
.500	4.22	17.0	220
.600	4.29	16.5	251
.700	4.35	16.1	279
.800	4.40	15.6	308
.900	4.45	15.1	335
1.00	4.54	14.5	356
1.10	4.60	14.2	382
1.20	4.65	13.9	403
1.30	4.71	13.4	421
1.40	4.78	13.1	440
1.50	4.86	12.8	458
1.60	4.94	12.5	473

TRIAXIAL COMPRESSION TEST

Air temperature = 42^0F
Concrete temperature = -
Height of sample = 8.0 inches
Time of set = 80 min.
Cell pressure = 0 psi
Strain rate = .045 inches / min.

Vertical Deformation (inches)	Diameter of Sample at Midheight (inches)	Pore Pressure (psi)	Deviator Load (Lbs)
0	4.05	0	0
.100	4.08	0	38
.200	4.13	-0.2	58
.300	4.21	-0.8	74
.400	4.26	-1.2	86
.500	4.33	-1.5	99
.600	4.36	-1.7	112
.700	4.45	-1.9	125
.800	4.50	-2.1	137
.900	4.57	-2.4	146
1.00	4.63	-2.5	156
1.10	4.70	-2.7	164
1.20	4.76	-2.8	176
1.30	4.85	-2.9	183
1.40	4.94	-3.0	191
1.50	5.01	-3.2	202
1.60	5.07	-3.3	211

TRIAXIAL COMPRESSION TEST

Air temperature = 38^0F

Concrete temperature = 38^0F

Height of sample = 8.0 inches

Time of set = 80 min.

Cell pressure = 5 psi

Strain rate = .045 inches / min.

Vertical Deformation (inches)	Diameter of Sample at Midheight (inches)	Pore Pressure (psi)	Deviator Load (Lbs)
0	4.03	4.8	0
.100	4.05	5.0	47
.200	4.08	4.3	71
.300	4.12	3.7	95
.400	4.18	3.4	122
.500	4.22	2.8	140
.600	4.28	2.4	153
.700	4.34	2.4	168
.800	4.40	2.1	176
.900	4.47	1.9	184
1.00	4.54	2.1	194
1.10	4.61	2.5	197
1.20	4.67	2.3	194
1.30	4.73	2.1	194
1.40	4.81	2.1	199
1.50	4.89	2.1	199
1.60	4.95	2.4	210

TRIAXIAL COMPRESSION TEST

Air temperature = 38^0F
Concrete temperature = 42^0F
Height of sample = 8.0 inches
Time of set = 80 min.
Cell pressure = 10 psi
Strain rate = .045 inches / min.

Vertical Deformation (inches)	Diameter of Sample at Midheight (inches)	Pore Pressure (psi)	Deviator Load (Lbs)
0	4.06	9.8	0
.100	4.07	9.6	59
.200	4.09	9.1	92
.300	4.14	8.6	128
.400	4.21	8.0	161
.500	4.26	7.0	189
.600	4.31	6.4	215
.700	4.35	5.9	239
.800	4.41	5.4	258
.900	4.49	5.2	280
1.00	4.55	4.8	303
1.10	4.63	4.4	322
1.20	4.69	4.2	347
1.30	4.76	3.9	363
1.40	4.86	3.5	377
1.50	4.95	3.3	400
1.60	5.01	3.0	408

TRIAXIAL COMPRESSION TEST

Air temperature = 38^0F

Concrete temperature = 40^0F

Height of sample = 8.0 inches

Time of set = 80 min.

Cell pressure = 15 psi

Strain rate = .045 inches / min.

Vertical Deformation (inches)	Diameter of Sample at Midheight (inches)	Pore Pressure (psi)	Deviator Load (Lbs)
0	4.05	14.5	0
.100	4.06	14.3	96
.200	4.09	13.4	150
.300	4.14	12.2	194
.400	4.21	11.3	239
.500	4.27	10.6	282
.600	4.33	9.5	320
.700	4.38	8.8	354
.800	4.45	8.3	391
.900	4.51	7.8	419
1.00	4.57	7.2	444
1.10	4.64	7.0	471
1.20	4.70	6.6	500
1.30	4.76	6.1	521
1.40	4.85	5.8	546
1.50	4.94	5.5	572
1.60	5.02	5.3	595

TRIAXIAL COMPRESSION TEST

Air temperature = 40^0F
Concrete temperature = 42^0F
Height of sample = 8.0 inches
Time of set = 80 min.
Cell pressure = 20 psi
Strain rate = .045 inches / min.

Vertical Deformation (inches)	Diameter of Sample at Midheight (inches)	Pore Pressure (psi)	Deviator Load (Lbs)
0	4.03	18.7	0
.100	4.04	19.4	103
.200	4.08	18.3	164
.300	4.13	17.2	220
.400	4.19	16.1	269
.500	4.23	15.0	318
.600	4.31	14.3	368
.700	4.36	13.5	410
.800	4.44	12.7	446
.900	4.50	12.0	479
1.00	4.57	11.5	518
1.10	4.64	11.0	545
1.20	4.71	10.6	578
1.30	4.80	10.1	605
1.40	4.89	9.6	631
1.50	4.97	9.2	656
1.60	5.06	8.8	681

TRIAXIAL COMPRESSION TEST

Air temperature = 38^0F

Concrete temperature = 40^0F

Height of sample = 8.0 inches

Time of set = 40 min.

Cell pressure = 20 psi

Strain rate = .045 inches / min.

Vertical Deformation (inches)	Diameter of Sample at Midheight (inches)	Pore Pressure (psi)	Deviator Load (Lbs)
0	4.05	20.7	0
.100	4.06	19.6	90
.200	4.10	18.2	160
.300	4.14	17.3	233
.400	4.20	15.6	292
.500	4.26	14.6	349
.600	4.31	.3.2	397
.700	4.36	12.5	449
.800	4.43	11.8	494
.900	4.49	10.9	534
1.00	4.55	10.2	579
1.10	4.63	9.7	616
1.20	4.69	9.2	653
1.30	4.76	8.5	688
1.40	4.86	8.2	730
1.50	4.92	7.7	758
1.60	5.00	7.3	790

TRIAXIAL COMPRESSION TEST

Air temperature = 38^0F
Concrete temperature = 40^0F
Height of sample = 8.0 inches
Time of set = 40 min.
Cell pressure = 15 psi
Strain rate = .045 inches / min.

Vertical Deformation (inches)	Diameter of Sample at Midheight (inches)	Pore Pressure (psi)	Deviator Load (Lbs)
0	4.11	15.6	0
.100	4.13	15.0	59
.200	4.16	14.2	92
.300	4.22	13.6	126
.400	4.29	13.1	156
.500	4.33	12.5	185
.600	4.39	11.6	210
.700	4.46	11.2	234
.800	4.51	10.8	260
.900	4.59	10.5	283
1.00	4.65	9.9	307
1.10	4.70	9.6	328
1.20	4.76	9.3	353
1.30	4.85	8.9	371
1.40	4.93	8.7	398
1.50	5.01	8.5	418
1.60	5.09	8.3	430

TRIAXIAL COMPRESSION TEST

Air temperature = 40^0F
Concrete temperature = 42^0F
Height of sample = 8.0 inches
Time of set = 40 min.
Cell pressure = 10 psi
Strain rate = .045 inches / min.

Vertical Deformation (inches)	Diameter of Sample at Midheight (inches)	Pore Pressure (psi)	Deviator Load (Lbs)
0	4.05	9.7	0
.100	4.06	8.7	115
.200	4.09	7.5	206
.300	4.16	5.7	270
.400	4.23	4.4	329
.500	4.29	3.4	372
.600	4.35	2.8	417
.700	4.42	2.3	454
.800	4.49	1.7	482
.900	4.57	1.2	506
1.00	4.63	0.8	526
1.10	4.68	0.5	545
1.20	4.75	0	566
1.30	4.84	0	583
1.40	4.91	0	590
1.50	4.99	0	600
1.60	5.07	0	600

TRIAXIAL COMPRESSION TEST

Air temperature = 38^0F
Concrete temperature = 40^0F
Height of sample = 8.0 inches
Time of set = 40 min.
Cell pressure = 5 psi
Strain rate = .045 inches / min.

Vertical Deformation (inches)	Diameter of Sample at Midheight (inches)	Pore Pressure (psi)	Deviator Load (Lbs)
0	4.07	5.1	0
.100	4.07	5.0	33
.200	4.10	4.3	79
.300	4.18	3.3	128
.400	4.22	2.4	168
.500	4.30	1.6	201
.600	4.35	1.1	227
.700	4.41	0.7	252
.800	4.49	0.7	272
.900	4.55	0.5	285
1.00	4.63	0.1	306
1.10	4.69	-0.1	323
1.20	4.75	-0.5	333
1.30	4.84	-0.7	350
1.40	4.92	-0.8	371
1.50	5.00	-1.0	386
1.60	5.07	-1.1	407

TRIAXIAL COMPRESSION TEST

Air temperature = 40^0F
Concrete temperature = 40^0F
Height of sample = 8.0 inches
Time of set = 40 min.
Cell pressure = 0 psi
Strain rate = .045 inches / min.

Vertical Deformation (inches)	Diameter of Sample at Midheight (inches)	Pore Pressure (psi)	Deviator Load (Lbs)
0	4.03	0	0
.100	4.06	0	38
.200	4.09	-0.5	65
.300	4.13	-1.2	89
.400	4.19	-1.6	108
.500	4.22	-3.0	125
.600	4.30	-2.4	139
.700	4.35	-2.6	151
.800	4.41	-2.8	161
.900	4.46	-3.0	170
1.00	4.51	-3.1	180
1.10	4.57	-3.3	188
1.20	4.64	-3.4	197
1.30	4.71	-3.5	203
1.40	4.77	-3.7	210
1.50	4.84	-3.7	218
1.60	4.91	-3.9	224

UNCONFINED COMPRESSION TEST

Air temperature = 70^0F

Concrete temperature = -

Height of sample = 7 inches

Time of set = 160 min.

Strain rate = .045 inches/min.

Vertical Deformation (inches)	Diameter of Sample at Midheight (inches)	Axial Load (lbs)
0	3.22	0
.0100	-	.62
.0200	-	.87
.0300	-	1.24
.0400	-	1.86
.0500	-	2.98
.0600	-	4.96
.0700	-	7.44
.0800	-	11.16
.0900	-	14.65
.1000	-	18.60
.1100	-	21.70
.1200	-	26.04
.1300	-	28.52
.1400	-	31.62
.1500	3.23	32.24
.1600	-	32.24
.1700	3.25	31.87

UNCONFINED COMPRESSION TEST

Air temperature = 70^0F

Concrete temperature = -

Height of sample = 7 inches

Time of set = 120 min.

Strain rate = .045 inches/ min.

Vertical Deformation (inches)	Diameter of Sample at Midheight (inches)	Axial Load (lbs)
0	3.22	0
.0100	-	1.24
.0200	-	2.48
.0300	-	4.96
.0400	-	8.18
.0500	-	11.16
.0600	-	14.26
.0700	-	17.36
.0800	-	19.84
.0900	-	22.32
.1000	3.23	24.80
.1100	-	25.42
.1200	-	26.04
.1300	3.25	24.80

UNCONFINED COMPRESSION TEST

Air temperature = 70^0F
Concrete temperature = -
Height of sample = 7 inches
Time of set = 80 min.
Strain rate = .045 inches/min.

Vertical Deformation (inches)	Diameter of Sample at Midheight (inches)	Axial Load (lbs)
0	3.18	0
.0100	-	.87
.0200	-	1.36
.0300	-	2.48
.0400	-	4.22
.0500	-	6.20
.0600	-	8.43
.0700	-	lo.54
.0800	-	12.90
.0900	-	14.76
.1000	3.25	17.11
.1100	3.22	18.60
.1200	-	19.84
.1300	3.23	20.21
.1400	3.25	19.22
.1500	-	18.23
.1600	3.26	16.12

UNCONFINED COMPRESSION TEST

Air temperature = 70^0F

Concrete temperature = -

Height of sample = 7 inches

Time of set = 40 min.

Strain rate = .045 inches/min.

Vertical Deformation (inches)	Diameter of Sample at Midheight (inches)	Axial Load (lbs)
0	3.25	0
.0100	-	.62
.0200	-	1.24
.0300	-	1.86
.0400	-	2.61
.0500	-	2.98
.0600	-	3.48
.0700	-	3.98
.0800	3.25	4.72
.0900	3.26	5.59
.1000	-	6.83
.1100	-	7.46
.1200	3.26	8.08
.1300	3.28	8.45
.1400	3.31	8.45
.1500	3.33	7.95
.1600	3.34	7.21

UNCONFINED COMPRESSION TEST

Air temperature = 38^0F
Concrete temperature = 40^0F
Height of sample = 7 inches
Time of set = 160 min.
Strain rate = .045 inches/min.

Vertical Deformation (inches)	Diameter of Sample at Midheight (inches)	Axial Load (lbs)
0	3.22	0
.0500	-	2.38
.0900	-	4.13
.1400	-	4.13
.1800	-	2.38
.2300	-	0.25
.2700	3.22	-

UNCONFINED COMPRESSION TEST

Air temperature = 38^{0}F
Concrete temperature = 40^{0}F
Height of sample = 7 inches
Time of set = 120 min.
Strain rate = .045 inches/min.

Vertical Deformation (inches)	Diameter of Sample at Midheight (inches)	Axial Load (lbs)
0	3.22	0
.0200	-	.63
.0500	-	1.13
.0700	-	1.63
.0900	-	2.13
.1100	-	2.38
.1400	-	2.75
.1800	-	3.00
.2300	-	2.75
.2700	3.22	2.25

UNCONFINED COMPRESSION TEST

Air temperature = 38^0F
Concrete temperature = 40^0F
Height of sample = 7 inches
Time of set = 80 min.
Strain rate = .045 inches/min.

Vertical Deformation (inches)	Diameter of Sample at Midheight (inches)	Axial Load (lbs)
0	3.22	0
.0200	-	1.13
.0500	-	2.38
.0700	-	3.50
.0900	-	4.50
.1400	-	4.88
.1800	3.22	3.88

UNCONFINED COMPRESSION TEST

Air temperature = 38^0F
Concrete temperature = 40^0F
Height of sample = 7 inches
Time of set = 40 min.
Strain rate = .045 inches/min.

Vertical Deformation (inches)	Diameter of Sample at Midheight (inches)	Axial Load (lbs)
0	3.22	0
.0200	–	.63
.0500	–	1.13
.0700	–	1.63
.0900	–	2.00
.1100	–	2.50
.1400	–	2.88
.1800	–	3.50
.2300	–	3.50
.2700	3.22	3.38

About The Author

Name;	Angelos Alexandridis
Born;	Almiros, Greece, 1955
Nationality;	Canadian Citizen
Education:	
Elementary;	Percy Street School, Ottawa, Ontario, 1961-1967
Primary;	Glashan Public School, Ottawa, Ontario, 1967-1969
Secondary;	Ridgemont High School, Ottawa, Ontario, 1969-1973
University;	University Of Ottawa, Ottawa, Ontario, 1973-1979
Degrees;	B.A.Sc. (Civil Engineering) May, 1977 M.A.Sc. (Civil Engineering) June, 1979